THESIS FOR THE DEGREE OF DOCTOR OF PHILOSOPHY

Aggregation, Propagation and Pathological Implications of α-synuclein Amyloid Fibrils in Parkinson's Disease

FRITJOF HAVEMEISTER

Department of Life Sciences

CHALMERS UNIVERSITY OF TECHNOLOGY

Gothenburg, Sweden 2026

Aggregation, Propagation and Pathological Implications of α-synuclein Amyloid Fibrils in Parkinson's Disease

FRITJOF HAVEMEISTER
ISBN 978-91-8103-460-8

Doktorsavhandling vid Chalmers tekniska högskola
Ny serie nr 5917
ISSN 0346-718X
https://doi.org/10.63959/chalmers.dt/5917

Department of Life Sciences
Chalmers University of Technology
SE-412 96 Gothenburg
Sweden
Telephone + 46 (0)31-772 1000

Cover:

The image shows a confocal fluorescence micrograph of rat neurons acquired in collaboration with Cellectricon. Neuronal cell bodies are labeled with NeuN (green), and the dendritic network with MAP2 (orange). Rat neurons are widely used as cellular models in neurodegenerative disease research and were used in this thesis to investigate key steps in the prion-like propagation pathway, including uptake, seeding of endogenous α-syn, and inclusion formation.

Printed by Chalmers Digitaltryck

Gothenburg, Sweden 2026

Aggregation, Propagation and Pathological Implications of α-synuclein Amyloid Fibrils in Parkinson's Disease

FRITJOF HAVEMEISTER

Department of Life Sciences

Chalmers University of Technology

ABSTRACT

Parkinson's disease (PD) is a severe, progressive neurodegenerative disorder characterized by aggregation of the protein α-synuclein into amyloid fibrils, leading to the formation of Lewy bodies and Lewy neurites and degeneration of dopaminergic neurons in the substantia nigra. Although α-synuclein aggregation is a defining feature of PD, fundamental questions remain regarding how fibrils form, how aggregation pathways encode distinct structural polymorphs, and how these polymorphs influence prion-like propagation and neurodegeneration. This knowledge gap continues to challenge the development of effective therapeutics.

This thesis addresses several of these knowledge gaps by investigating the aggregation and prion-like propagation of α-synuclein amyloid fibrils using wild-type and familial PD-associated variants. First, to understand how assembly conditions shape α-synuclein fibril formation and structure, I examined the effects of monovalent cations. I show that the physiologically abundant cations Na^+ and K^+, although often treated as interchangeable, produce distinct effects on aggregation kinetics and fibril morphology, demonstrating that changes in ionic conditions can reshape α-synuclein fibril assembly pathways. I next investigated consequences of fibril fragmentation, a mechanism that rarely occurs *in vitro* but can be significant *in vivo*, showing that early-onset PD variants underwent pronounced structural evolution following fragmentation, reflected in altered Thioflavin-T binding. This shows that α-synuclein fibrils are more structurally heterogenous than previously believed and that they may continue to remodel their architecture over the course of PD. To resolve such heterogeneity, I established a Thioflavin-T fluorescence-lifetime spectroscopy-based methodology for phenotyping of α-synuclein polymorphs. Cross-seeding experiments revealed variant-specific structural trajectories, including faithful templating, monomer-driven restructuring, and emergence of *de novo* polymorphs, highlighting the vast structural landscape accessible to α-synuclein fibrils. Finally, I investigated whether these *in vitro* traits influenced prion-like propagation in cells, showing that α-synuclein variants differed markedly in uptake efficiency, induction of endosomal enlargement, and ability to seed endogenous α-synuclein aggregation. These cellular outcomes aligned with the structural and kinetic behaviors observed *in vitro*, demonstrating that propagation efficiency is strongly shaped by intrinsic fibril properties.

Altogether, this work advances the mechanistic understanding of α-synuclein aggregation and propagation in PD and highlights fibril assembly pathways and resulting fibril structure as critical targets for future therapeutic strategies.

Keywords: Parkinson's disease, α-synuclein, protein aggregation, amyloid fibrils, amyloid kinetics, fragmentation, prion-like propagation, cross-seeding, fibril morphology, polymorphism

List of publications

The thesis is based on the work contained in the following papers

I. **Monovalent cations have different effects on the assembly kinetics and morphology of α-synuclein amyloid fibrils**
Fritjof Havemeister, Marziyeh Ghaeidamini and Elin K. Esbjörner
Biochemical and Biophysical Research Communications, (2023) 679, 31-36 doi:10.1016/j.bbrc.2023.08.061

II. **Fragmentation-induced disassembly and reaggregation of α-synuclein amyloid fibrils**
Fritjof Havemeister, Vesa Halipi, Marziyeh Ghaeidamini and Elin K. Esbjörner
ACS Chemical Neuroscience 17.11 (2026): 2057-2070
doi:10.1021/acschemneuro.5c00895

III. **Thioflavin-T fluorescence lifetime spectroscopy enables phenotyping of α-synuclein fibril polymorphs during cross-seeding**
Marziyeh Ghaeidamini, Fritjof Havemeister, Fredrik Edborgh, Mikaela Sjögren and Elin K. Esbjörner
Manuscript

IV. **Distinct uptake and seeding behaviors of wild-type and mutant α-synuclein variants in human and murine neuronal models**
Fritjof Havemeister, Andrea Ramnath, Andrea Lovincic Babic, Jeremias Brunbauer, Mikaela Sjögren, Olivia Borg, Elin Allgén, Maitrayee Sinha, Marziyeh Ghaeidamini, Johan Pihl, Linnea Strid Orrhult, Lotta Agholme and Elin K. Esbjörner
Manuscript

Contribution report

Details of my personal scientific contribution to each of the papers in the thesis:

Paper I. I conceived the idea and conceptualized the study together with my supervisor. I established the methodology and planned the investigation. I did all experiments, data curation, formal analysis, validation, and visualization. I interpreted the data and wrote the paper together with my supervisor.

Paper II. I conceived the idea and conceptualized the study together with my supervisor. I established the methodology to assess aggregation kinetics and fragmentation. I led the investigation and performed most of the experiments. Cytotoxicity studies were performed in collaboration with V.H. I did the data curation, formal analysis, validation, and visualization of the data. I interpreted the data and wrote the paper together with my supervisor.

Paper III. I contributed to establishing the methodology for the project and to the investigation, especially to the production and characterization of pre-formed fibrils. I did not do the time-resolved fluorescence measurements, but curated, analyzed, and visualized the data together with M.G. and my supervisor. M.G. wrote the first draft, whereas I finalized the paper together with my supervisor.

Paper IV. I contributed to conceptualizing the project and the method development. I led the investigation and took lead in data curation, formal analysis, validation, visualization. I produced and characterized all fibril samples and performed flow cytometry-based uptake experiments. I did not do the confocal imaging and the primary cell cultures (including fibril treatments, staining and imaging). I interpreted the data and wrote the manuscript together with A.R and my supervisor with input from other co-authors.

PREFACE

This dissertation was submitted for the partial fulfillment of the degree of Doctor of Philosophy. The original work presented in this thesis was carried out between September 2021 and August 2026 at Chalmers University of Technology, Department of Life Sciences, under the supervision of Associate Professor Elin. K Esbjörner. The research was funded by the Swedish Research Council and the Knut and Alice Wallenberg Foundation.

Fritjof Havemeister

August 2026

Table of Contents

Introduction

Parkinson's disease (PD) is the second most prevalent neurodegenerative disorder after Alzheimer's disease (AD), affecting an estimated 12 million people worldwide, a number that has nearly tripled since 1990 [1]. Demographic projections indicate that this number will rise to approximately 25 million by 2050, driven primarily by global population ageing, highlighting its growing impact on global health [2]. Although PD is not itself a direct cause of death, patients exhibit elevated mortality rates [3], largely due to complications such as aspiration pneumonia resulting from dysphagia, which represents the leading cause of death among individuals with PD [4]. A central pathological hallmark of PD is the presence of Lewy bodies, which are large intracellular inclusions that are predominantly composed of highly ordered, β-sheet rich amyloid fibrils formed by the misfolding and self-assembly of the protein α-synuclein (α-syn) [5].

Over 200 years after James Parkinson's original description of PD [6], continued research has substantially expanded our knowledge of the disease. Lewy bodies were first discovered by Friedrich Heinrich Lewy more than a century ago [7] but their association with PD was established a few years later by Constantin Tretiakoff [8]. It was first many decades later, in 1997, that Spillantini and colleagues discovered that the protein α-syn is main constituent of Lewy bodies [9]. Within the following year, the same group identified α-syn as the major component of the filamentous inclusions in Lewy bodies, which were later recognized as amyloid fibrils implicated in driving PD pathology [10]. Thereafter, Braak and colleagues proposed that PD pathology progresses through a predictable series of anatomical stages [11], a concept that gained mechanistic support with the discovery that α-syn fibrils can propagate in a prion-like manner, evidenced by the appearance of α-syn inclusions in grafted neurons years after transplantation into a patient [12]. Around the same time, the first reports emerged showing that wild-type and mutant α-syn can assemble into fibrils with distinct morphologies, establishing the concept of α-syn fibril polymorphism [13,14]. These discoveries have shaped the field for decades, driving extensive investigation into the molecular mechanisms underlying fibril assembly, cell-to-cell propagation, and the structural heterogeneity of amyloid conformations.

Today, our understanding of these processes is far more advanced, as new methodologies and technologies have made it possible to study the mechanisms underlying α-syn aggregation, propagation and fibril architecture in more detail. Biophysical advances have made it possible to follow amyloid aggregation kinetics and revealed that α-syn self-assembly proceeds through a series of microscopic steps in which small nuclei form, elongate, and amplify in number, predominantly through surface-catalyzed secondary nucleation, with additional contributions from fibrils fragmentation, processes that depend highly on solution conditions [15,16] and thus on the biological environment in which α-syn resides. Advances in cell-based microscopy have enabled visualization of cell-to-cell transfer of α-syn aggregates, revealing endocytosis as a major pathway involved in propagation of PD pathology [17,18]. In recent years, the emergence of near atomic-resolution cryo-electron microscopy (cryo-EM) has fundamentally reshaped the ability to resolve amyloid fibril architectures [19], and provided deeper structural evidence of that amyloid fibrils are highly polymorphic [20]. Even more recently, cryo-EM based studies revealed that *in vitro* generated fibrils are structurally different from those found in human post-mortem brain tissue and that distinct fibril

structures are associated with specific diseases [21]. In addition, compelling cryo-EM evidence shows that amyloid fibrils are not structurally static but can evolve with time [22,23], prompting the question if fibril species that initiate and drive disease are different from those found post-mortem. Just as protein function emerges from the structures that proteins adopt, the pronounced heterogeneity of amyloid fibril structures may likewise influence their biological activity, a hypothesis that has gained increased attention in recent years.

Although these advances have substantially advanced our understanding of amyloid fibrils and Parkinson's disease, PD remains a disorder for which no disease-modifying therapy or cure currently exists. Following Arvid Carlsson's discovery of dopamine as a critical neurotransmitter in 1957 [24], levodopa (L-dopa) was introduced in 1970 as a symptomatic treatment for PD to compensate for the loss of dopaminergic neurons. Despite its limited long-term efficacy and the development of motor fluctuations, dyskinesias and other adverse effects [25], it remains the most widely used therapy for PD to this day, underscoring the lack of therapeutic progress. The key challenge is that we still do not understand with sufficient detail what triggers α-syn misfolding and aggregation, which species drive disease, or how they damage neurons and propagate. This limits our ability to target these processes therapeutically. Nevertheless, a recently approved antibody therapy targeting amyloid-β (Aβ) has shown to slow early AD progression [26]. Although it is not a cure, it provides strong proof-of-concept that amyloid fibrils are therapeutically relevant targets and that it is possible to design drugs that ameliorate their toxic effects, showing that the field is moving in the right direction toward disease-modifying treatments or possibly even cure. However, antibody therapeutics face additional challenges in PD. Since α-syn pathology is predominantly intracellular, antibodies are required to not only cross the blood-brain barrier, a process hindered by their large molecular size [27], but also to enter cells. With increasing knowledge, emerging strategies are now working on overcoming this challenge [28].

PD is a complex neurodegenerative disorder in which multiple pathogenic processes converge to drive neurodegeneration. Compelling evidence implicates misfolded and aggregated α-syn as the central pathological driver. A major contributing factor is thought to be increased local α-syn concentration caused by disrupted proteostasis, involving impaired trafficking and clearance which raises the probability of nucleation and aggregation. Defining how different molecules and ions interact with α-syn, how distinct aggregation mechanisms and propagation pathways function, and how these assemblies perturb cellular function is therefore essential for advancing our understanding of PD pathogenesis and for future development of therapeutics.

The goal of my thesis was to expand our current knowledge of the mechanisms involved in α-syn aggregation and propagation, and how these processes contribute to PD disease pathology. In **paper I**, I show that different monovalent cations, although often overlooked, have distinct, and in some cases opposing effects on WT α-syn aggregation and morphology. These findings have biological relevance as monovalent cations are highly enriched in both the intracellular and extracellular environments of neurons. **Paper II** demonstrates that fragmentation, a comparatively understudied process due to its limited natural occurrence *in vitro*, can alter α-syn aggregation kinetics and drive structural evolution of WT and mutant variant fibrils. Fragmentation is likely to be more prevalent *in vivo* because of the influence of cellular machinery on protein aggregate integrity and structural changes to amyloid fibrils

are pathologically meaningful, given that growing evidence links fibril conformation to pathological function. **Paper III** shows that cross-seeding, a pathologically relevant mechanism in familial cases of PD, can alter the aggregation and morphological outcome of WT and mutant α-syn fibrils, and that these structural changes can be sensitively mapped using ThT fluorescence lifetime analysis. **Paper IV** integrates several earlier findings by demonstrating that fragmented and structurally diverse WT and mutant α-syn fibrils differ markedly in their cell uptake efficiency and their propensity to induce enlarged endosomes in SH-SY5Y cells. Furthermore, these fibrils demonstrate distinct cross-seeding efficiencies of endogenous α-syn and generate inclusions of diverse morphologies in both mouse and rat primary neurons.

Thesis outline

In the first part of this thesis, I introduce the research field, outlining its historical foundations, current understanding, and future outlook, setting the stage for investigating α-syn aggregation, propagation and its pathological implications. In chapters 1-4 I cover the background for this thesis, including proteins, protein misfolding and aggregation, polymorphism, Parkinson's disease, α-syn and the prion hypothesis. Chapter 5 provides a description of the methods and techniques used in the experimental work. Finally, chapter 6 concludes the thesis by summarizing and discussing the main findings from **Papers I-IV**.

1. Proteins

Today, roughly 20,000 protein-coding genes have been identified in humans. Through alternative splicing, post-translational modifications, and single amino acid polymorphisms, these genes can express over 100,000 distinct proteoforms, each with distinct functions [29,30]. The blueprint for proteins is encoded in the human genome in the form of Deoxyribonucleic Acid (DNA) and contains instructions for protein synthesis. Although only about 1-2% of the human genome consists of protein-coding DNA, the vast non-coding portion plays essential regulatory roles, controlling when protein-coding genes are transcribed and translated into functional proteins [31].

Proteins, in addition to nucleic acids, lipids and carbohydrates, are fundamental biomacromolecules which make up the human body. Proteins have a key standing as they govern practically every biological process within living organisms, from catalyzing reactions [32] and DNA replication [33] to providing structural support to cells and tissues [34], and transporting molecules, both within and between cells [35]. Given the vast diversity of proteins in the human body, and their wide range of functions, as well as the complex processes involved in their synthesis, folding and maintenance, it is unsurprising that disruptions in these mechanisms underlie many diseases. In this thesis, I will focus on one such disease, Parkinson's disease, which is associated with the dysfunction of the protein α-synuclein (α-syn).

1.1. Protein chemistry

To understand how a protein becomes dysfunctional, it is essential to first understand the fundamentals of protein structure. Proteins consist of linear chains of amino acids which are covalently linked together by peptide bonds, forming an array referred to as a polypeptide. Each amino acid consists of a central α-carbon (C) bonded to a hydrogen atom (-H), an amino group ($-NH_2$), and a carboxyl group (-COOH) [36], together constituting the backbone. Each amino acid is, additionally, distinguished by its unique functional group (-R) which is also conjugated to the central α-carbon (Fig. 1).

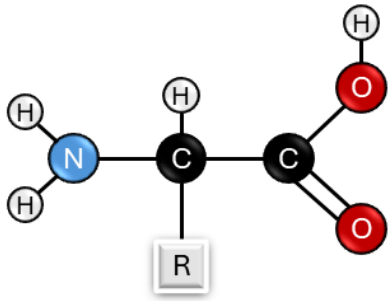

Figure 1. *Chemical structure of the amino acid backbone including the functional group (R).*

Generally, the backbone of an amino acid is considered to have a net neutral charge at physiological pH (pH 7.2-7.4) where the amino group usually carries a positive charge whereas the carboxyl group carries a negative charge, effectively turning each amino acid or polypeptide zwitterionic, but with an overall neutral charge. The distinct chemical identity of each amino acid is instead determined by its functional group [37]. There are 20 standard amino acids required for protein synthesis in the human body. These can be classified into several different categories based on the chemistry of their functional groups, such as polar or

nonpolar, hydrophobic or hydrophilic and charged or uncharged [38]. The chemistry of amino acids, along with in what order they are joined together in the formation of a protein, plays a crucial role in the resulting protein structure and function.

1.2. Protein structure and folding

As previously mentioned, in a polypeptide, the amino acids are covalently linked by peptide bonds, forming a chemically repetitive backbone. To form these peptide bonds, the amino group of one amino acid is joined with the carboxyl group of the neighboring amino acid in a hydrolysis reaction. The resulting linear amino acid sequence is referred to as the primary structure of the protein [39].

During protein folding, peptide bonds not only connect amino acids, but also contribute to important structural features. The amide hydrogen of one amino acid's backbone can form a hydrogen bond with the carbonyl oxygen of a nearby amino acid residue. When these interactions occur in a regular, repeating pattern, they can give rise to α-helices and β-sheets, which are stable local folding patterns that constitute the secondary structure of a protein [40]. An α-helix is formed by a single polypeptide strand that adopts a right-handed helical conformation, with 3.6 amino acid residues per turn. The structure is stabilized by intramolecular hydrogen bonding with an amino acid four residues earlier in the amino acid sequence [41] (Fig. 2A). In contrast, β-sheets are stabilized by hydrogen bonding between neighboring β-strands, either within a single polypeptide or between adjacent polypeptide chains [42] (Fig. 2B). β-sheets can be arranged either in parallel, where the strands are oriented in the same direction, or in antiparallel, where the strands are oriented in opposite directions. My work focuses mainly on the formation of intermolecular β-sheets, which are the main building blocks of amyloid fibrils.

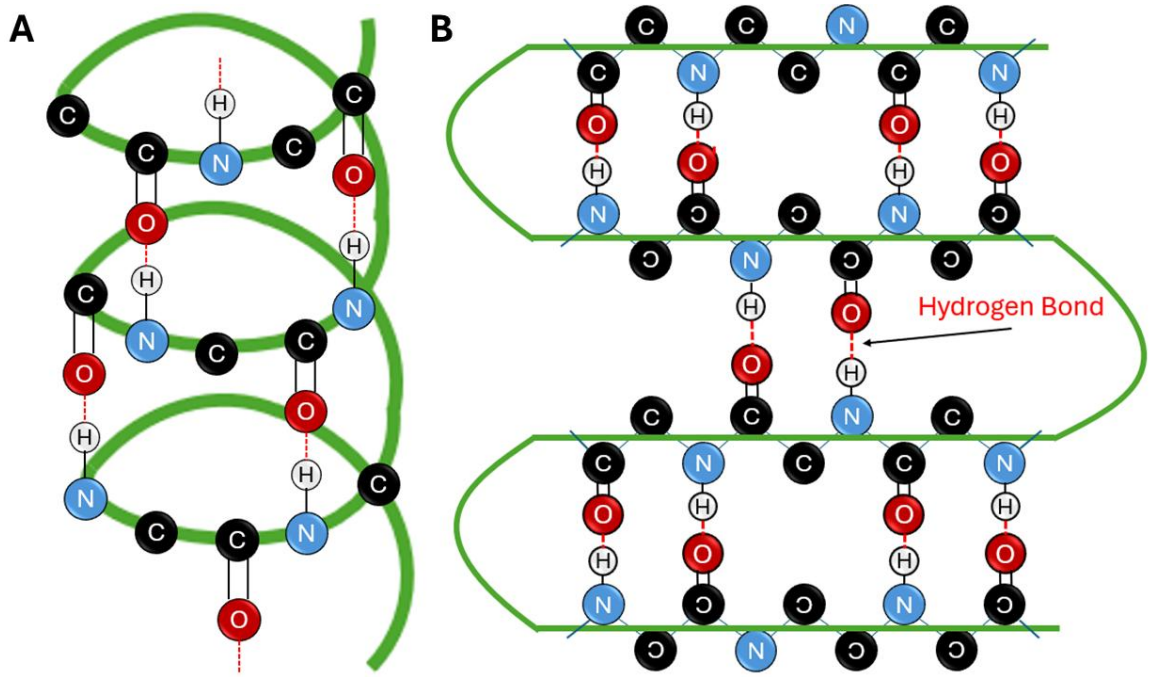

Figure 2. *Chemical structure of a-helix and an antiparallel β-sheet.*

In contrast to the covalent bonds that link amino acids in the primary structure, the bonds formed between the majority of amino acid functional groups and between peptide bonds, are noncovalent, with cysteines being the exception since they are capable of forming covalent disulfide bonds. Typical intramolecular interactions involved in protein folding include ionic bonds between charged amino acids, hydrogen bonds between polar amino acids, and van der Waals forces involving hydrophobic side chains [43]. The chemical properties of each amino acids functional group, alongside the specific sequence in which they are assembled, govern these intramolecular interactions that drive the folding into the three-dimensional, or tertiary, structure, which is typically required for the protein to become functional [44]. If multiple polypeptide chains are assembled to form a functional protein, the resulting multimer arrangement is referred to as the quaternary structure (e.g. Hemoglobin) [45]. These structural features, governed by the chemical properties of each amino acid, are fundamental to the protein's stability and biological function

Theoretically, proteins could fold into a countless number of structures. How then is it possible for proteins to fold into their native, functional conformation within a timeframe ranging from seconds [46] to microseconds [47]? To answer this question, one needs to consider both the kinetic and thermodynamic aspects of protein folding. The current most refined model of protein folding considering both aspects, is the protein folding funnel [48] (Fig. 3).

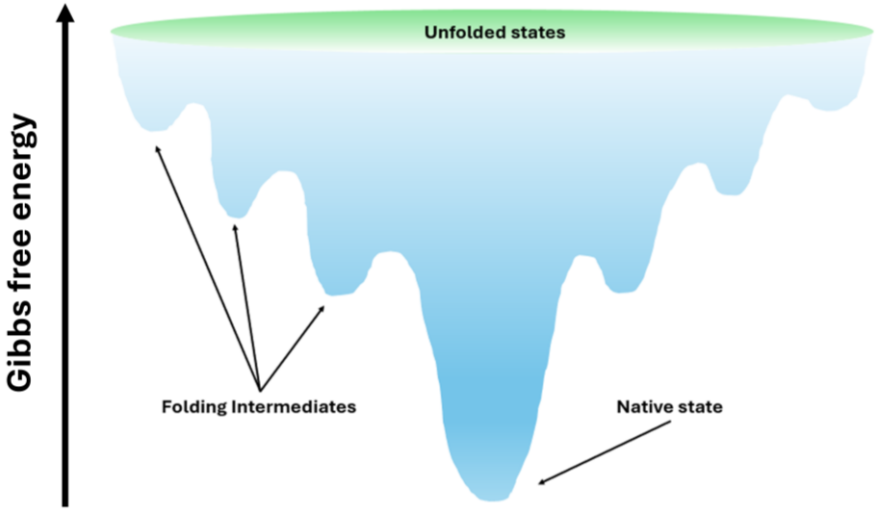

Figure 3. *Protein folding funnel illustrating the free energy landscape of protein folding. The protein passes through a number of intermediate conformations going from unfolded (top) to its native state (bottom), progressively decreasing its free energy while being guided toward its lowest energy, functional structure.*

The folding funnel is a visualization of the free energy landscape of protein folding. A protein in its unfolded, high-energy state sits at the top of the funnel with a vast number of possible confirmations available (represented by the width of the funnel). As folding begins, the unfolded random coil rapidly collapses, reducing its free energy and conformational flexibility, as it starts its descent toward lower free energy states further down in the funnel. Along this descent, the protein may pass through one or more folding intermediates, which are represented by local minima on the energy landscape [49]. The number of intermediates

which the protein must pass through to achieve its native state can vary between proteins, with some proteins folding through multiple intermediates, while others can fold without detectable intermediates, so called two-state folders [50]. One intermediate that is commonly detected experimentally is the molten globule [51], represented by a partially folded structure with much of the native secondary structure in place but where the tightly packed tertiary structure of fully folded proteins is still missing [52]. Ultimately, the protein reaches its lowest free-energy native and functional state at the bottom of the funnel. Kinetic factors, such as the rate of folding, and energy barriers between intermediates, determine the time required for a protein to reach its native state [53].

2. Amyloid fibrils

2.1. Protein misfolding

Given that during our lifetime an unimaginable number of proteins are going through folding and unfolding processes, it is not surprising that sometimes proteins are not folded correctly or fail to remain correctly folded. A protein that cannot achieve or maintain its correctly folded native state is considered as misfolded. If the misfolding persists, this can lead to either loss of function or toxic gain of function. Cells have therefore developed exquisite proteostasis networks to ensure protein homeostasis and avoid the accumulation of misfolded proteins [54]. These networks include proteins which assist and facilitate folding, such as chaperones [55] and folding enzymes [56], along with systems for degrading misfolded or damaged proteins, such as the Ubiquitin-proteasome system [57].

Although cells possess a highly refined proteostasis network, extensive misfolding can sometimes overwhelm the system, allowing misfolded protein to accumulate, in some cases leading to the formation of aggregates which are resistant to degradation [58]. Proteostasis network dysfunction increases significantly with age, which is also why many of the protein misfolding diseases are age related. Apart from age, additional risk factors include genetic mutations [59] and cellular [60] or environmental stress [61]. Protein misfolding diseases are usually associated with specific proteins and can be classified into categories, such as neurodegenerative proteinopathies. Examples are Alzheimer's disease (Aβ42) [62], Parkinson's disease (α-syn) [63], and ALS (TDP-43, SOD1) [64], which manifest in the brain and are characterized by the aggregation of proteins into insoluble amyloid fibrils [65]. Other categories include systemic amyloidosis diseases, in which misfolded proteins circulate and deposit across multiple organs, such as transthyretin amyloidosis (TTR protein) [66] and lysozyme amyloidosis [67], and loss-of-function diseases, for example cystic fibrosis (CFTR protein) [68] and alpha-1 antitrypsin deficiency (alpha-1 antitrypsin) [69], which result from loss of function, i.e. misfolded proteins failing to perform their normal biological function. In the context of this thesis, the focus will be on neurodegenerative proteinopathies, specifically Parkinson's disease, which involves the formation of amyloid fibrils derived from misfolded α-syn protein.

2.2. Amyloid fibrils, aggregation and disassembly

Amyloid fibrils are a specific form of protein aggregate composed of a single protein species. They are characterized by a linear, fibrillar morphology and a dense cross β-sheet core structure. A mature amyloid fibril is usually made up of two or more protofibrils which are twisted around each other, resulting in fibrils with typical diameters of about 7-13 nm whereas they can extend to several micrometers in length [70,71]. Amyloid fibrils are commonly associated with neurodegenerative or other protein deposition diseases [65,72], however, under the right conditions, most, if not all, proteins can form amyloid fibrils. In some cases, amyloid structures have even been shown to have functional biological roles, for example in biofilm formation of bacteria [73] and in transcriptional regulation in yeast [74].

As explained in chapter 1.2, a protein's native state is typically considered its most stable conformation, corresponding to a global free energy minimum. However, amyloid fibrils represent an even more thermodynamically stable state, with a lower free energy than the native fold [75], accessible due to the intermolecular interactions that stabilize the fibril. This

can be schematically visualized by expanding the free energy protein folding landscape from chapter 1.2 to include an adjacent funnel for misfolding and aggregation (Fig. 4).

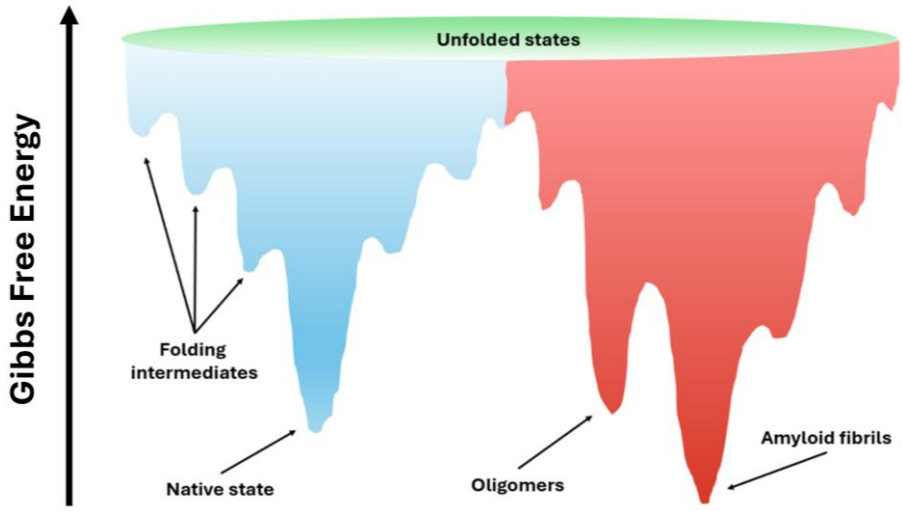

Figure 4. *Expanded protein folding landscape, including both the native state and amyloid folding funnel.*

Formation of the characteristic amyloid cross-β structure of amyloid fibrils requires the polypeptide chain to be partially or fully unfolded, exposing aggregation-prone regions [76], and making the fibrillar state kinetically accessible. This exposure can occur when the native fold of a protein is destabilized by factors such as mutations [77], changes in pH [78] or temperature [79], or through interactions with other components naturally present in the cellular environment, like lipids [80] or metal-ions [81], that help overcome the kinetic barrier of unfolding. In contrast, intrinsically disordered proteins (IDPs), which are the focus of this thesis, naturally lack a stable folded structure, making them inherently prone to aggregation and facilitating the initial step of fibril formation [82]. However, IDPs are still influenced by the same external factors as described above, which can modulate their aggregation kinetics and propensity, as well as alter the mechanisms by which they assemble. A common feature of amyloid formation is that aggregation occurs under supersaturated conditions, in which the monomer concentration surpasses the protein's solubility threshold, enabling nucleation and subsequent fibril growth [83].

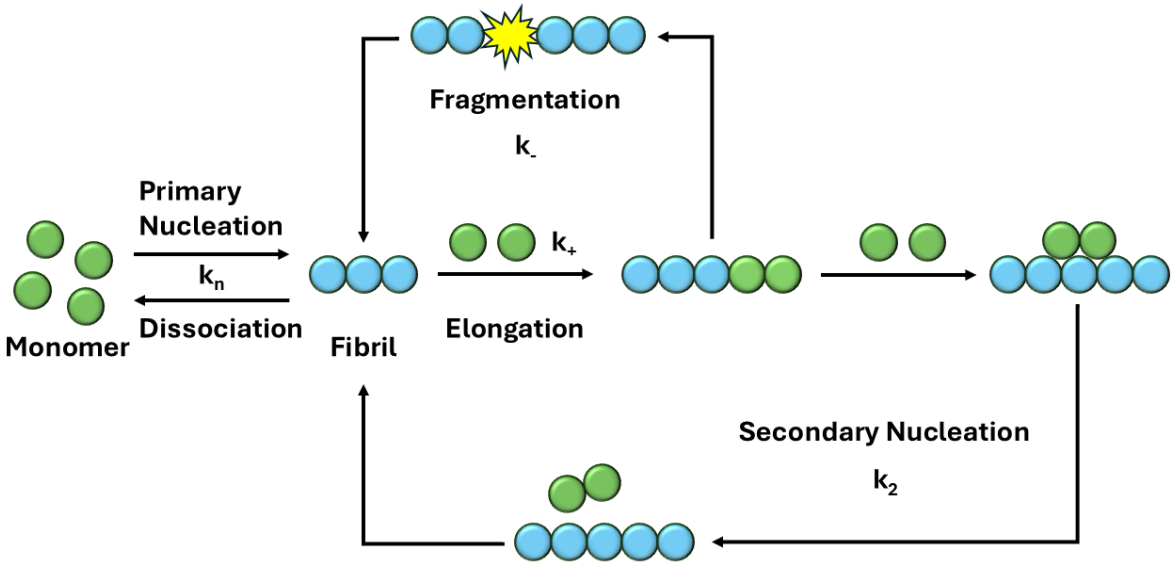

Figure 5. *Schematic overview of the microscopic steps that drive amyloid fibril formation. The schematic encompasses primary nucleation and dissociation, elongation, fragmentation, secondary nucleation and their respective rate constants* k_n, k_+, k_-, *and* k_2.

Once a protein is unfolded, be it naturally or via misfolding reactions, the aggregation process can proceed according to the reaction scheme depicted in Fig. 5. Partially or fully unfolded proteins can associate to form small assemblies known as nuclei in a process called primary nucleation. This step can occur in bulk solution or at a surface, such as the air-water interface [84,85]. These nuclei consist of either oligomeric species or very short fibrillar fragments, and their formation represents the slowest step in the aggregation pathway, corresponding to the highest free energy barrier and the lowest rate [86]. The initially formed nuclei can then grow through monomer addition at their ends in a process known as elongation, which proceeds with a lower energy barrier compared to primary nucleation, and therefore occurs with a correspondingly higher rate [83]. Fibrils can also form on the surfaces of existing aggregates, where the fibril surface catalyzes the formation of new nuclei in a process known as secondary nucleation [84]. This pathway has a low free energy barrier and therefore proceeds with a high rate. Once a nucleus forms on the fibril surface, it can detach and elongate independently, rapidly amplifying the total number of aggregates [84]. Although amyloid fibrils are generally considered highly stable, they can also undergo disassembly, either by fragmentation or through monomer depolymerization from fibril ends. Fragmentation occurs when a fibril breaks into smaller segments, each of which can act as an independent fibril, thereby increasing the number of available ends for elongation [87]. Monomer depolymerization can occur when a solution is undersaturated, meaning that the monomer concentration is below the solubility limit and fibrils dissolve to restore equilibrium [83], or it can be triggered by external factors that help shift the equilibrium, such as temperature changes [88,89], chemical denaturants [90], or the action of chaperones [91].

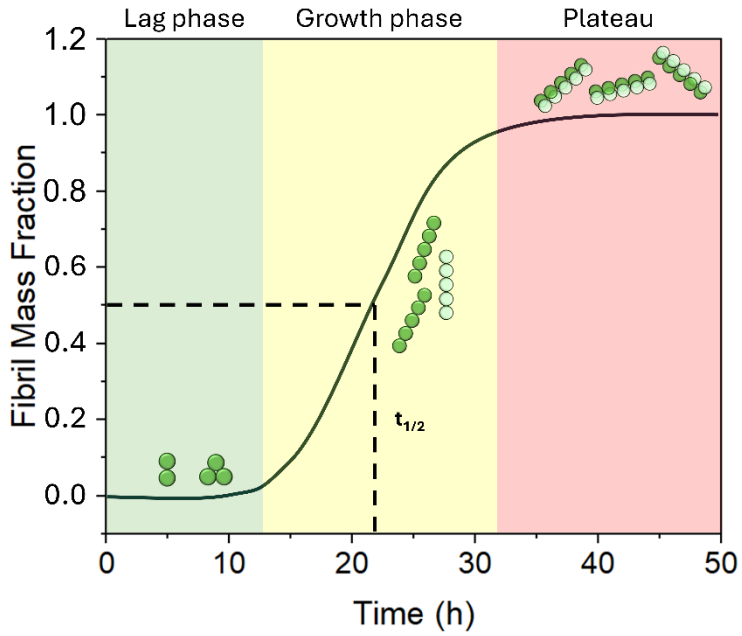

Figure 6. *Illustration of a sigmoidal aggregation curve showing the lag, growth, and plateau phase. The half-time, corresponding to the time it takes for 50% of the total fibril mass to form*

The kinetics of amyloid formation can be monitored using biophysical aggregation assays. The reactions typically follow a sigmoidal trajectory, which can be described as consisting of three distinct phases (Fig. 6). The kinetics start with a lag phase, during which primary nucleation and the formation of nuclei is dominant and the formation of fibrils remain undetectable [92]. This is followed by the growth phase, which is mainly driven by elongation and secondary nucleation, and results in a rapid increase in fibril mass [93]. Finally, under conditions where the available pool of monomers is constant, a plateau phase is reached, where fibrils and monomers are at equilibrium [94]. Fragmentation and monomer depolymerization can occur in any of these phases, but are more prominent in the growth and plateau phase, where the fibril mass is higher [95].

2.3. Fibril structure and polymorphism

Despite distinct differences in the amino acid sequence and biological function of amyloid forming proteins, most fibrils share common structural features that contribute to their high stability [96]. Whether fibrils originate from hen egg white lysozyme (Fig. 7A), which requires destabilization of its native fold, or α-syn fibrils (Fig. 7B), where the protein is intrinsically disordered, the characteristic cross β-sheet structure and key morphological characteristics are largely conserved. To achieve a more detailed distinction between fibrils, scientists have over the years attempted to acquire deeper structural information to reveal their molecular architecture.

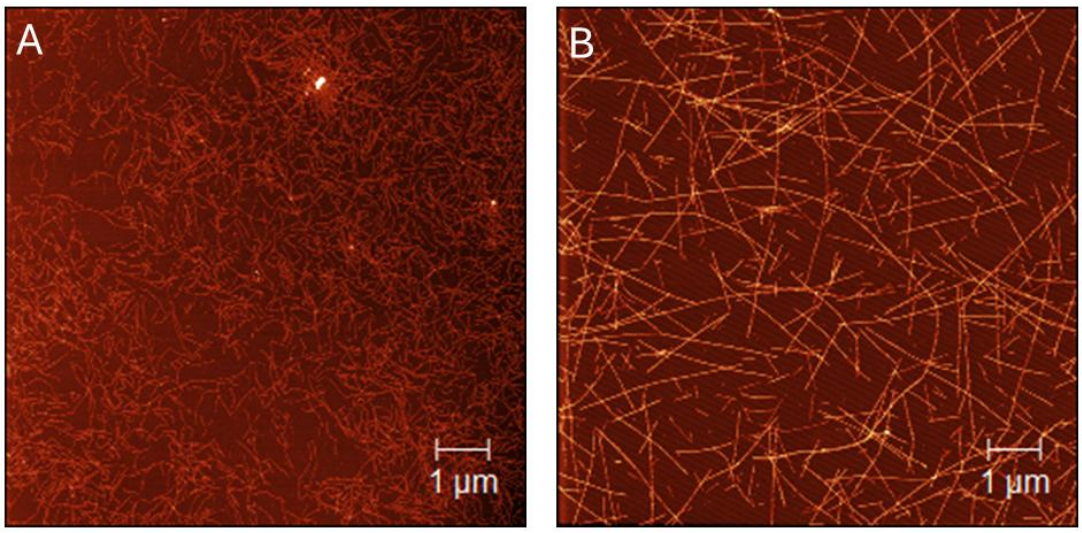

Figure 7. *Atomic Force Microscopy (AFM) micrograph of (A) hen egg white lysozyme amyloid fibrils, which in its native state degrades bacterial cell walls and (B) α-synuclein amyloid fibrils, the central pathological hallmark of Parkinson's disease.*

Already over a century ago abnormal inclusions were found in the brains of Alzheimer's [97] and Parkinson's [7] patients. These inclusions were later found to contain amyloids using Congo red staining [98]. Years later, the filamentous structure of amyloid fibrils was first observed using electron microscopy [99] and the paired helical structure of amyloid fibrils was identified using negative-stain electron microscopy [100]. Subsequently, X-ray fiber diffraction revealed the hallmark cross-β architecture, characterized by a 4.7 Å reflection pattern corresponding to the hydrogen bonding distance between β-strands and a 10-11 Å reflection arising from the spacing between β-sheets (Figure 8) [101]. It was, however, not until decades later that the specific proteins responsible for amyloid fibril formation in diseases such as Alzheimer's (Aβ42) [102] and Parkinson's (α-syn) [9] were identified.

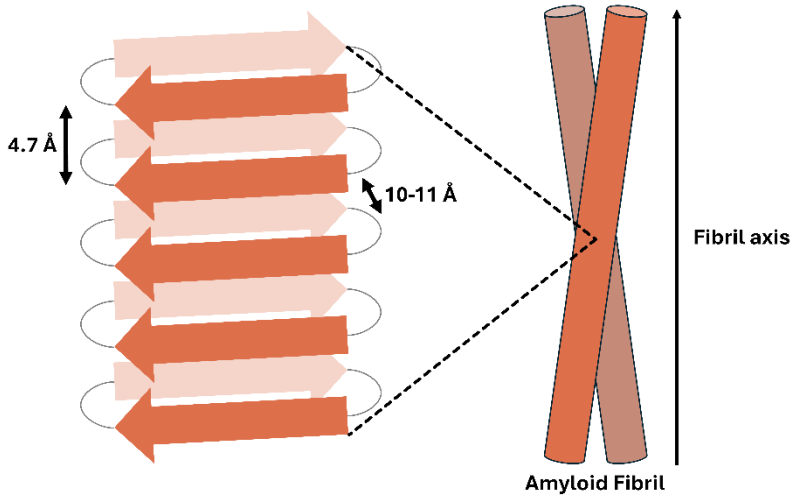

Figure 8. *Schematic illustration of an amyloid fibril highlighting the characteristic cross-β architecture, including the 4.7 Å reflection corresponding to the spacing between β-strands and the 10-11 Å reflection arising from the distance between β-sheets (left). Two or more protofibrils associate laterally to form a mature amyloid fibril (right).*

To achieve deeper structural understanding of amyloid fibrils, approaching atomic resolution, even more powerful techniques were, however, required. Using X-ray crystallography it was possible to study fibrils formed by shorter peptides [103], but this has not been suitable for more complex amyloid fibrils due to their inability to crystallize. The first molecular level resolution structures of amyloid fibrils from full-length proteins were instead solved using solid-state nuclear magnetic resonance (ssNMR) [104], but the technique is restricted to recombinant amyloid fibrils due to the need for isotope labelling. Cryo-electron microscopy (cryo-EM), although developed in the 1980s, eventually made it possible to overcome these limitations. With major advancements in detector technology and image processing in the 2010s, cryo-EM nowadays achieves atomic-level resolution, enabling characterization of both brain-derived and *in vitro* formed fibrils [105,106].

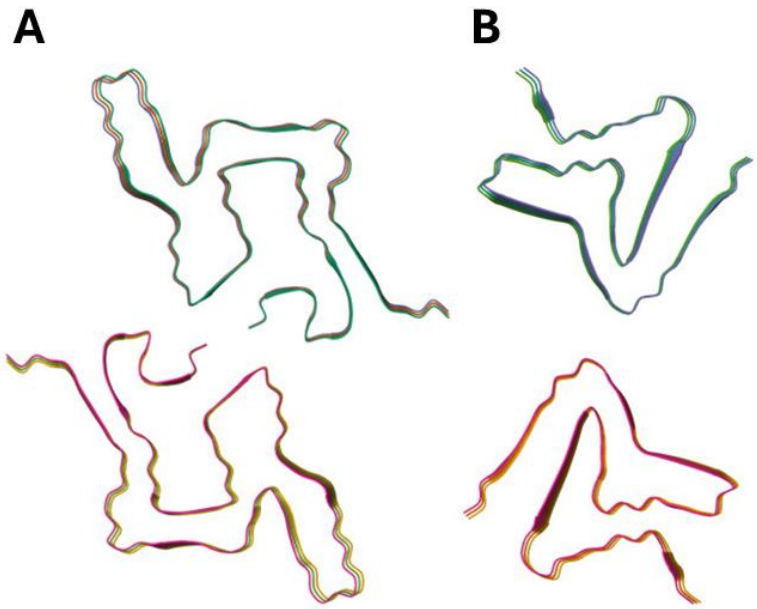

Figure 9. *Cryo-EM structures of two protofilaments making up the mature fibril. (A) WT α-synuclein 5a fibril, PDB: 8ZLP [107]. (B) WT α-synuclein P8 fibril, PDB: 9LON [108].*

The recent advancements in high-resolution imaging techniques have also brought renewed attention to the topic of structural polymorphism in amyloid fibrils, which refers to the existence of different folds and interaction surfaces between the monomer units in amyloid fibrils formed by the same protein, as highlighted by two of the, by now many, available high-resolution structures of WT α-syn fibril assemblies shown in Fig. 9A and 9B [107,109]. The concept of amyloid polymorphism was first noted in the late 1990s, when transmission electron microscopy (TEM) and early cryo-EM studies revealed polymorphic forms of amylin fibrils [110], and a few years later, structural polymorphism at the molecular level was reported for Aβ40 fibrils using ssNMR [111]. However, interest in the topic expanded substantially in 2017, when advancements in cryo-EM technology enabled the first atomic-resolution structures of tau fibrils, revealing fibril polymorphism at atomic scale [105]. The advancements have since led to many new discoveries, several of which have had a large impact on the field. Cryo-EM experiments of post-mortem brain samples revealed that individual neurodegenerative diseases are associated with one or several distinct fibril polymorphs [21]. For example, α-syn fibrils from Parkinson's (PD) patients displayed a

single distinct structure [112], whereas samples from patients with the related α-synucleinopathy multiple system atrophy (MSA) contained two structurally distinct polymorphs [113], both different from the PD fold. Similar disease-specific structural signatures have been observed in other disorders, including Alzheimer's disease [114,115] and ALS [116,117], where fibril folds appear to differ between different subtypes of disease, suggesting a possibility of structure-based classification. Importantly, the polymorphs identified in post-mortem brain tissue are structurally distinct from the polymorphs generated *in vitro* [21]. Amyloid formation was long assumed to occur predominantly through templated aggregation, whereby structural features of an existing fibril are maintained during elongation and secondary nucleation [118]. However, recent work has demonstrated that even though templating occurs to some extent, the resulting fibril structures are highly sensitive to solution conditions, often more so than to the structure of the parent seed, particularly during secondary nucleation [119,120], and even elongation can result in fibrils that are structurally different from the parent seed [121]. Furthermore, time-based aggregation studies of recombinant IAPP [22] and tau [23] combined with cryo-EM have now intriguingly revealed that fibril structures, even within a sample kept under constant physiochemical conditions, can evolve over time, such that some fibril structures present at earlier timepoints of aggregation can disappear while new ones are formed as aggregation progresses. These findings highlight that fibril polymorphism is dynamic, even under controlled *in vitro* conditions. The relationship between fibril polymorphs identified *in vitro* and those observed *in vivo* remains unclear, and a central open question is how distinct polymorphs contribute to toxicity and neurodegeneration. This uncertainty underscores the need to determine whether fibril structures isolated from post-mortem brain tissue, which unavoidably represents the end-stage of a long disease process, accurately reflect the conformations present earlier in disease and which may thus be the primary cause of neurodegeneration. In other words, it is possible that early-stage fibrils adopt distinct, transient conformations that later mature into the late-stage folds observed in patient brains, raising important questions about which conformations that are most relevant for disease initiation and progression

In **paper II**, I expand on the concept of structural evolution in α-syn amyloid fibrils. In **paper IV**, I examine how distinct α-syn polymorphs generated from different familial mutants influence fibril uptake and the in-cell seeding of endogenous α-syn, demonstrating how structural variation can influence disease progression.

3. Parkinson's disease

Parkinson's disease (PD), originally known as 'Shaking Palsy', was first discovered in 1817 by the surgeon James Parkinson, who characterized it as a neurological syndrome based on six clinical cases [6]. Today, PD is known as the second most common neurodegenerative disease after Alzheimer's, affecting 12 million of people worldwide [122]. PD is commonly recognized as an age-related disorder, with the typical onset occurring around 60-65 years of age [123]. However, this pattern mainly reflects sporadic cases. Familial forms of disease, caused by inherited genetic mutations and accounting for roughly 5-15% of all cases, can onset much earlier in life [124], with first symptoms developing as early as the age of 20, and in rare instances even earlier, which is classified as juvenile PD [125]. The genes currently known to cause familial PD when mutated include SNCA (the α-syn encoding gene), LRRK2, VPS35, and GBA, which are associated with autosomal-dominant PD and PRKN, PINK1, and PARK7/DJ-1, which lead to autosomal-recessive forms of the disease [63]. Other than mutations, risk factors also include lifestyle, health factors, traumatic brain injuries and environmental factors [126]. The focus of this thesis will specifically be on mutations in the SNCA gene, causing single amino acid substituted variants of α-syn examined in **papers II-IV**.

PD is characterized by the loss of dopaminergic neurons, which are most abundantly found in the substantia nigra region of the brain [127]. Dopamine as a crucial neurotransmitter was first discovered by Arvid Carlsson in 1957 [24] and has important functions in brain processes coupled to, for example, reward, motor control and motivation [128]. Dopamine deficiency is related to symptoms commonly associated with PD, such as tremors, bradykinesia, muscle rigidity, and postural instability, which typically appear only after a substantial loss of dopaminergic neurons in the substantia nigra [129]. Despite extensive efforts and decades of research aimed at developing new treatments for PD, L-dopa, a precursor to dopamine, remains the primary and most widely used therapy since its introduction in 1970. As a precursor to dopamine, it partially restores dopamine levels and compensates for the loss of dopaminergic neurons [130]. However, L-dopa is only effective as a symptomatic treatment and is limited by declining long-term efficacy as well as the development of side effects such as motor fluctuations, dyskinesias and other adverse effects [25], and a much-needed cure remains to be found. The underlying causes behind the loss of dopaminergic neurons have not yet been fully identified, however growing evidence point towards synaptic, mitochondrial and endolysosomal dysfunction as important mechanisms involved in disease development [131]. Preceding this dysfunction is the aggregation of α-syn, a protein thought to be involved in synaptic vesicle trafficking and neurotransmitter release, which can aggregate into toxic amyloid fibrils and deposit into larger inclusions known as Lewy bodies, a pathological hallmark for PD [132].

The subsequent sub-chapters will address α-syn, the core protein of this thesis, and its aggregation, accumulation into Lewy bodies as well as promising future treatments.

3.1. α-synuclein

In 1997, α-syn was identified as the main constituent of Lewy bodies, establishing its critical role in PD [9]. The protein is a 140 amino acid long, 14.4-kDa protein encoded by the SNCA gene which, together with β-synuclein and γ-synuclein, makes up the synuclein family [133]. α-syn is highly abundant in the brain and is predominantly localized to presynaptic nerve

terminals in neurons. In the cytosol, α-syn is an intrinsically disordered protein which adopts a random coil structure [134]. However, it can bind to membranes and adopt a partially α-helical conformation [135] and if misfolded, α-syn can aggregate into amyloid fibrils with a cross-β-sheet structure and subsequently deposit into larger inclusions called Lewy bodies, which are a pathological hallmark for PD [77]. Although not yet fully understood, the normal function of α-syn has been assigned to regulating neurotransmitter release, such as dopamine, by binding to and modulating synaptic vesicles in the presynaptic nerve terminals [136]. Particularly, α-syn has been found to be involved in synaptic vesicle clustering [137], vesicle recycling [138], and vesicle docking [139].

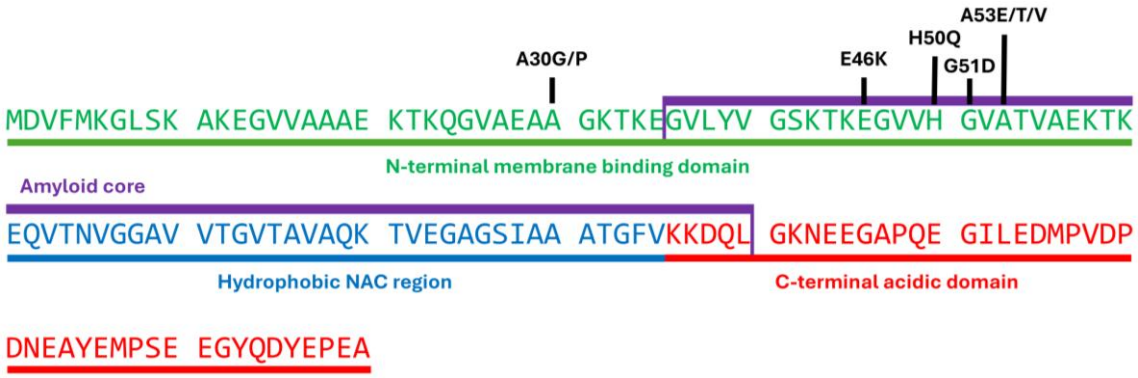

Figure 10. *Primary sequence of α-synuclein showing the N-terminal membrane binding domain (green), the hydrophobic NAC region (blue), the C-terminal metal-binding domain (red), and the amyloid core (purple). The positions of the hereditary point mutations are indicated with black pins.*

The primary sequence of α-syn (Fig. 10) has classically been divided into three domains; the positively charged N-terminal membrane binding domain spanning residues 1-60, the hydrophobic NAC region, spanning residues 61-95, and the negatively charged metal binding C-terminal domain, spanning residues 96-140. The N-terminal part is important for binding to lipid membranes, such as synaptic vesicles, where it adopts a primarily α-helical conformation [140]. The NAC region was originally thought to be the primary driver of β-sheet formation, but recent Cryo-EM studies have shown that the core region of α-syn fibrils is larger than that represented by the NAC, and this annotation can therefore be considered as somewhat obsolete. Most reported high-resolution structures identify approximately residues 36-100 as forming the core of α-syn amyloid fibrils [141], thus suggesting overlap between the N-terminal membrane interaction part and the fibril core forming region. The C-terminal region plays a crucial role in aggregation, despite not being part of the fibrillar core structure, as screening of its negative charges, for example through the interaction with metal ions [81] [142] or changes in pH [143], can increase the aggregation propensity of α-syn.

To date, eight point-mutations in the SNCA gene (A30G, A30P, E46K, H50Q, G51D, A53E, A53T, A53V) have been identified as associated with hereditary PD [144]. All are located within the N-terminal domain of α-syn, and all except A30P and A30G, are positioned within the amyloid core (Fig. 10). Although these variants are quite rare, accounting for about 0.5% of all PD cases [145,146], they represent important research models as they alter α-syn folding and aggregation behavior [147]. Furthermore, all these point mutations are associated with early-onset PD, with the exception of H50Q, which causes late-onset PD [147]. In this

thesis, **paper I** focuses on wild-type (WT) α-syn, while **paper II-IV** extends the analysis to include the A30P, E46K, H50Q, and A53T variants.

3.2. α-synuclein aggregation

Beyond its physiological roles, α-syn can misfold and assemble into amyloid fibrils. As outlined in the previous chapter, the focus of this thesis is on WT α-syn and the hereditary mutant variants A30P, E46K, H50Q, and A53T. The aggregation kinetics and underlying mechanisms of these variants will be covered in detail in this chapter.

The aggregation mechanism of α-syn follows the same fundamental steps described in chapter 2.2, involving primary nucleation, elongation and secondary nucleation, and to a lesser extent fragmentation and depolymerization. Primary nucleation of α-syn in bulk solution is generally considered to be very slow, resulting in extended lag times [84]. Because of this, primary nucleation is often triggered in *in vitro* studies to allow aggregation to be observed within a reasonable timeframe. Common strategies to accelerate α-syn aggregation include addition of salts to reduce electrostatic repulsion [81,148], increasing monomer concentrations to promote primary nucleation [149], applying mechanical stress through agitation [150], introducing catalytic surfaces such as lipid membranes [151], taking advantage of the walls of non-binding reaction plates and tubes [84], or altering the chemical environment through metal ions [152] or pH changes [153]. An increasingly common alternative to these methods is the addition of low concentrations of pre-formed fibril (PFF) seeds to bypass primary nucleation [15]. In practice, several of these conditions are often combined to drive reproducible fibril formation.

Following primary nucleation, α-syn fibril mass is first amplified through elongation, in which monomers add to the ends of existing fibrils [154]. *In vitro*, elongation of α-syn proceeds at approximately ~10^3 $M^{-1}s^{-1}$ [15], a rate that is relatively slow compared with for example Aβ42, for which elongation is reported to be about three orders of magnitude faster [155]. As fibril mass increases, the growing fibril surfaces act as catalysts for the formation of new nuclei via secondary nucleation, which becomes the main source of new aggregates and the dominant driver of the growth phase for α-syn [16]. These newly generated nuclei elongate and, in turn, provide additional surfaces for further secondary nucleation, resulting in a self-amplifying cycle that accelerates the overall aggregation process [16]. Secondary nucleation of α-syn, unlike elongation, has been reported to become much more efficient at acidic pH, which is important in a biological context given that, in cells, α-syn is internalized through the endolysosomal pathway, where pH progressively decreases [15], a topic discussed in a later chapter.

It is generally possible to shorten the lag phase of α-syn by bypassing the slow primary nucleation step of protein aggregation via the addition of pre-formed fibrils (PFFs) as seeds [15]. Under these conditions, α-syn aggregation is dominated by secondary nucleation at low seed concentrations, whereas at high seed concentrations elongation becomes the main contributor to the overall kinetics [156]. α-syn fibrils can also undergo fragmentation, which increases the number of available ends for elongation. *In vitro*, spontaneous fragmentation of α-syn fibrils occurs at a much lower rate than secondary nucleation or elongation and therefore contributes only modestly to the overall aggregation kinetics [157]. However, *in vivo* the fragmentation rate may be substantially higher due to cellular processes, such as the activity of chaperones like Hsp40, Hsp70 and Hsp104 which have been shown to fragment

fibrils [158,159]. Thus, to obtain fragmentation *in vitro*, mechanical methods such as agitation [160] or sonication [161] are typically used. Notably, familial α-syn mutations are known to modulate the relative contributions of the microscopic steps involved in α-syn aggregation, altering the time course of self-assembly, which is further discussed below.

Apart from forming fibrils, α-syn also adopts oligomeric states as part of the aggregation process. Oligomers are difficult to characterize due to their heterogeneity, transient nature, and low abundance. Despite this, numerous studies have shown that α-syn oligomers are highly toxic, implicating them as possible major pathological contributors in Parkinson's disease [162,163]. Secondary nucleation has been shown to generate not only new fibril nuclei, but is also the main source of oligomeric α-syn species [157]. *In vitro*, oligomeric species were found to mainly form in the lag and growth phase, reaching their highest mass concentration around the aggregation half-time. By the plateau phase, however, oligomeric species were no longer detectable [157]. Mature α-syn fibrils also contribute substantially to cytotoxicity [164] and they play a central role in the cell-to-cell propagation of PD pathology [165].

As outlined in chapter 2.2, mutations can modulate the aggregation kinetics of amyloid formation and this thesis focuses on the hereditary PD variants A30P, E46K, H50Q, and A53T. These variants demonstrate altered aggregation rates compared to WT α-syn *in vitro,* but nevertheless follow the same aggregation mechanisms [166]. The A30P mutation, which is located outside of the amyloid core [113,167], has been reported to aggregate at a similar rate [168], slower [169] or faster [170] compared to WT α-syn. Notably, A30P shows an increased propensity to form oligomeric species compared to WT α-syn [171]. The E46K, H50Q, and A53T mutations are all located within the fibril core and these variants exhibit an increased rate of aggregation compared to WT α-syn [170,172,173] and also typically greater cytotoxicity [173-175]. A shared feature among the E46K, H50Q, and A53T mutants is their ability to form distinct fibril polymorphs which differ from those of WT α-syn [20,90,109,176]. A30P, on the other hand, appears to adopt the same fibril structure as WT α-syn [169,177]. While these macroscopic differences in aggregation behavior highlight the diverse effects of familial mutations, their underlying origins become clearer when examining how each variant perturbs the microscopic steps of the aggregation process compared with the WT protein.

Although reaction conditions used to trigger α-syn aggregation play an important role in modulating the relative contributions of each microscopic step, studies have shown important differences between the α-syn variants. All four variants, A30P, E46K, H50Q and A53T have been reported to facilitate primary nucleation. The effect is modest for A30P [178] but markedly stronger for E46K [179], H50Q [180] and A53T [178]. E46K has been shown to slightly accelerate elongation [166], and A53T increases the elongation rate more substantially [166]. A30P has shown mixed effects on elongation, with reports of both slightly faster [166] and slightly slower elongation [181] relative to WT. Secondary nucleation is also affected in a variant-dependent fashion. A53T has been suggested to promote secondary nucleation [182], whereas E46K reduces secondary nucleation [166], and H50Q exhibits negligible secondary nucleation under acidic conditions [166,180]. Several variants also alter the propensity of α-syn fibrils to fragment. E46K has been reported to increase fragmentation propensity [183], while A30P confers a slight increase in resistance to sonication-induced fragmentation and A53T exhibits an even stronger resistance to such

fragmentation [161]. H50Q appears to be more thermodynamically stable than WT [184], suggesting it may also influence fragmentation propensity, although dedicated fragmentation studies for this variant are still lacking.

The fact that mutant variants of α-syn show divergent aggregation behavior and structures makes them important model systems for investigating polymorphism, and to explore how chemical modifications to the α-syn sequence may influence pathogenic processes of relevance for the onset and progression of PD, as highlighted in chapter 2.3.

3.3. Parkinson's neurotoxicity: from monomer to Lewy bodies

The aggregation mechanisms described in the previous chapter gain biological relevance in the neuronal environment, where α-syn transitions from its physiological role as a presynaptic protein to a central driver of PD. The exact underlying causes and mechanisms driving this aspect of PD pathology remain, however, unclear, making it important to continue to explore how normally functional, physiological α-syn is converted to β-sheet rich, pathogenic oligomers and fibrils.

Based on current knowledge, and consistent with the *in vitro* aggregation behavior described in chapter 3.2, higher intracellular concentrations of α-syn in neurons increases the likelihood for aggregate formation [185]. This can result from duplication or triplication of the SNCA gene [186,187], or through mutations in the LRRK2 [188] and GBA [189] genes, which increase α-syn synthesis or impair its degradation. Other factors correlating with elevated α-syn levels in the synapse include interaction partners like synapsin [190], VAMP2 [191] and CSPα [192], all of which are involved in synaptic vesicle regulation and neurotransmitter release. The enrichment of α-syn in synapses suggests that this is a primary site for initial aggregate formation, aligning also with observations that early stage synaptic dysfunction precedes neuronal death [193].

Mitochondrial dysfunction is another well-known contributor to α-syn aggregation. Neurons contain an extensive mitochondrial network to meet their high energy demands, and if damaged, this can reduce ATP production, thereby impairing ATP dependent processes such as synaptic transmission, axonal transport and protein-degradation pathways which can result in α-syn buildup, increasing the risk for aggregation [194,195]. Furthermore, dysfunctional mitochondria produce reactive oxygen species (ROS) and increases oxidative stress which can damage DNA, lipids and proteins [196], thereby promoting misfolding and aggregation of α-syn [197]. Moreover, α-syn aggregates, but not physiological α-syn, have been found to bind mitochondria, impairing their function and creating a vicious, pathological cycle [198].

Membrane association, in a more general sense, is also known to play a role in α-syn aggregation. Under physiological conditions, α-syn binds to membranes through its N-terminal domain, where it assembles into multimers and facilitates neurotransmitter release [199]. Membrane binding has also been shown to promote aggregation in some cases [151,199]. However this effect appears to depend strongly on membrane composition [200], with anionic lipids being most effective [201]. In contrast, N-terminal mutations preventing α-syn membrane binding have been shown to increase aggregate formation by increasing cytosolic levels of α-syn [202], a feature which has been demonstrated for the hereditary A30P mutant whose proline substitution acts as an α-helical breaker diminishing membrane binding [203].

In addition, post-translational modifications (PTMs), have also been implicated in the aggregation of α-syn [5]. For example, physiologically relevant C-terminal truncations were shown to promote fibrillization [204]. Ubiquitination which, among other functions, normally marks misfolded or excess protein for degradation, can be impaired in PD, leading to elevated intracellular α-syn concentration [205]. Phosphorylation, which typically regulates protein function, has also been shown to increase the aggregation propensity of α-syn [206]. Notably, these PTMs of α-syn are consistently enriched within Lewy bodies and Lewy neurites, highlighting their relevance in PD pathology [5].

Ultimately, these processes converge and drive the formation of Lewy bodies and Lewy neurites, which mainly consist of α-syn and are key pathological hallmarks of PD. Lewy neurites, which are smaller, more abundant inclusions that precede the formation of Lewy bodies [207], generally manifest in the axons of neurons, where they have been shown to disrupt axonal transport of cell constituents [208] such as endosomes [209], mitochondria and lysosomes [210]. Larger Lewy body inclusions usually manifest in the cell soma of neurons [211] and disrupt the normal cellular function, for example by causing mitochondrial damage and synaptic dysfunction [212]. The formation of Lewy bodies and Lewy neurites are generally considered a later event in PD pathology [213]. Some researchers even propose that Lewy body formation serves as a protective mechanism, isolating highly toxic α-syn aggregates that can otherwise spread pathology to neighboring cells through prion-like propagation, a topic discussed in a later chapter [214].

3.4. Future treatments of Parkinson's disease

For Alzheimer's disease, there has been recent clinical breakthrough following the approval of the first disease-modifying treatment, Lecanemab, which is a monoclonal antibody that binds to Aβ aggregates and mediates their degradation [26,215,216]. Although the effect is modest, it has provided important validation of the amyloid hypothesis. In contrast, as discussed in chapter 3, L-dopa remains the most effective and widely used treatment for PD and corresponding anti-aggregation antibody-based treatments are not yet as advanced. In 2023 there were 139 registered clinical trials for PD treatment, including both symptomatic and disease-modifying treatments [217].

Symptomatic treatments in clinical trials focus largely on improving L-dopa delivery, reducing the duration of symptom return (off time) and dyskinesia. These strategies aim to extend release or to continuously infuse levodopa-carbidopa to provide more consistent exposure (IPX203, foslevodopa-foscarbidopa, ND0612, DopaFuse) [218-221]. New dopaminergic drugs are also being tested, including Tavapadon [222] and Mesdopetam [223], which target specific dopamine receptors to reduce dyskinesia. Additional approaches aim to restore dopaminergic function through gene therapy (AB-1005, AADC gene therapy) [224,225], designed to support neuronal survival or enhance dopamine synthesis, and cell-based therapies (bemdaneprocel, ANPD001) [226,227], which aim to restore dopamine function by either increasing neuronal survival or by replacing damaged neurons. These medicines are essential for patients; however, they do not halt the progression of the underlying disease.

Similar to how lecanemab targets Aβ in Alzheimer's disease, there are currently a few disease-modifying treatments in clinical trials which aim to reduce the aggregate burden of α-syn. Antibodies and small molecules are being tested for their ability to reduce α-syn

aggregation, either by targeting aggregated α-syn (prasinezumab) [228], by binding the C-terminal of α-syn (minzasolmin) [229], by suppressing α-syn translation (buntanetap) [230], by more generally blocking α-syn aggregation (anle138b) [231], or by reducing inflammation (tomaralimab) as an aggregation driver [232]. For PD, however, targeting α-syn is challenging because the protein is predominantly intracellular, requiring antibodies to both cross the blood-brain-barrier and enter neurons, processes which are hindered by the large molecular size of antibodies [27]. In contrast, Aβ aggregates are mainly targeted extracellularly and therefore more accessible to antibody-based therapies [233]. Additional disease-modifying approaches focus on genetic risk factors, including therapies that specifically target mutations in LRRK2 [234] and GBA[235].

3.5. Diseases beyond Parkinson's disease

Misfolding and aggregation of α-syn is, apart from PD, also implicated in other rarer neurodegenerative diseases such as dementia with Lewy bodies (DLB) and multiple system atrophy (MSA), which vary in their site of onset inside the brain, symptoms and disease progression [236].

DLB is, after Alzheimer's disease, the second most common form of dementia, accounting for roughly 15-20% of all cases of dementia [237]. PD and DLB cases often share many symptoms, such as visual hallucinations, REM sleep behavior disorder and parkinsonism, and some researchers advocate that they may in fact be one and the same disease [238]. However, there are subtle differences in diagnosis, which is that if dementia precedes or manifests within one year of onset of parkinsonism, the disease is classified as DLB [239]. Nevertheless, both diseases share the aggregation of α-syn and the subsequent formation of Lewy bodies and Lewy neurites, but differ in the onset of cognitive impairment, which usually manifests earlier in the limbic and cortical regions in DLB cases [213].

Although demonstrating overlapping symptoms with PD while also being classified as a synucleinopathy, MSA differs significantly in onset and disease progression [240]. Unlike PD, where α-syn aggregates primarily accumulate in dopaminergic neurons, MSA is characterized by α-syn inclusions within oligodendrocytes, forming glial cytoplasmic inclusions (GCIs) [113]. While α-syn inclusions are also found in neurons of MSA patients, they appear at a much lower frequency compared to GCIs [241]. The α-syn aggregates from GCIs have been found to be many times more potent at seeding aggregation than Lewy body derived aggregates [242], which could partly explain the rapid symptomatic progression of MSA patients, leaving patients bedridden after 6-8 years with common symptoms of parkinsonism, poor muscle coordination (cerebellar ataxia) and autonomic failure [243]. In all synucleinopathies, the spreading of α-syn aggregates and subsequent seeding of endogenous α-syn in neighboring cells, through a process called prion-like propagation [244], has become a central concept in recent years. The next chapter will cover prion-like propagation in detail, and it is also a key focus of **paper IV**.

4. Prion hypothesis in Parkinson's disease

In its mature form, the prion protein (PrP^C) is a 209 amino acid long cell-surface glycoprotein most abundantly found in a variety of cells in the central nervous system (CNS) [245]. PrP^C has been ascribed to functions like myelin maintenance [246] and cell differentiation [247]. However, it can misfold into its aggregation prone isoform PrP^{Sc}, which is associated with diseases such as Creutzfeldt-Jakob disease. In this state, it has been shown to spread from cell to cell, converting endogenous PrP^C into the misfolded isoform and resulting in rapid spread of neurodegeneration [248]. In a similar fashion, α-syn aggregates have been shown to spread between cells, enabling a prion-like mechanism of propagation [249], albeit without being transmissible between species or humans.

4.1. Evidence for prion-like propagation of α-synuclein

The first evidence of systematic pathological propagation in PD was proposed by Braak et al. in the early 2000s. They classified disease onset into six distinct stages, in which α-syn inclusions (Lewy bodies) spread in a predictable pattern from the peripheral and lower brainstem regions, advancing to the midbrain and finally to cortical areas [11,250]. A few years earlier, in an effort to restore dopamine production, dopaminergic neurons were transplanted into PD patients by different research groups. Although the grafted neurons survived for several years, post-mortem analysis revealed extensive α-syn aggregate formation within these new neurons, providing further evidence that pathological α-syn aggregates can propagate from diseased to healthy neurons over the course of the disease. Although the grafting strategy was considered clinically unsuccessful at the time, it has contributed significantly to solidify the prion-like propagation hypothesis [12,251].

These findings led to extensive research into animal models such as mice and monkeys [252,253]. Some research groups used α-syn aggregates isolated from post-mortem PD brains [253] or homogenates from mice with α-syn pathology [164,254], while others tested whether *in vitro* generated α-syn PFFs could similarly induce neurodegeneration [244,255]. Additionally, prion-like propagation has been demonstrated in cell lines such as SH-SY5Y cells [256,257]. In every case, the exogenously applied α-syn PFFs were capable of seeding the endogenous α-syn of the animal and cell model, demonstrating the prion-like propagation capacity of α-syn aggregates. Consistently, prion-like propagation has also been demonstrated in MSA, where transgenic mice injected with brain homogenates from MSA patients experienced neurodegeneration [258]. However, no direct evidence of cell-to-cell propagation of MSA pathology in humans has yet been reported, largely due to that the rareness of the disease has resulted in a shortage of clinical data [259]. These findings, together with the earlier observations from grafted neurons, established prion-like spread as a central concept in PD pathogenesis.

4.2. Mechanisms of α-synuclein prion-like propagation

The mechanisms by which α-syn aggregates propagate between neurons are not yet fully understood, but several cellular pathways have been implicated in the process.

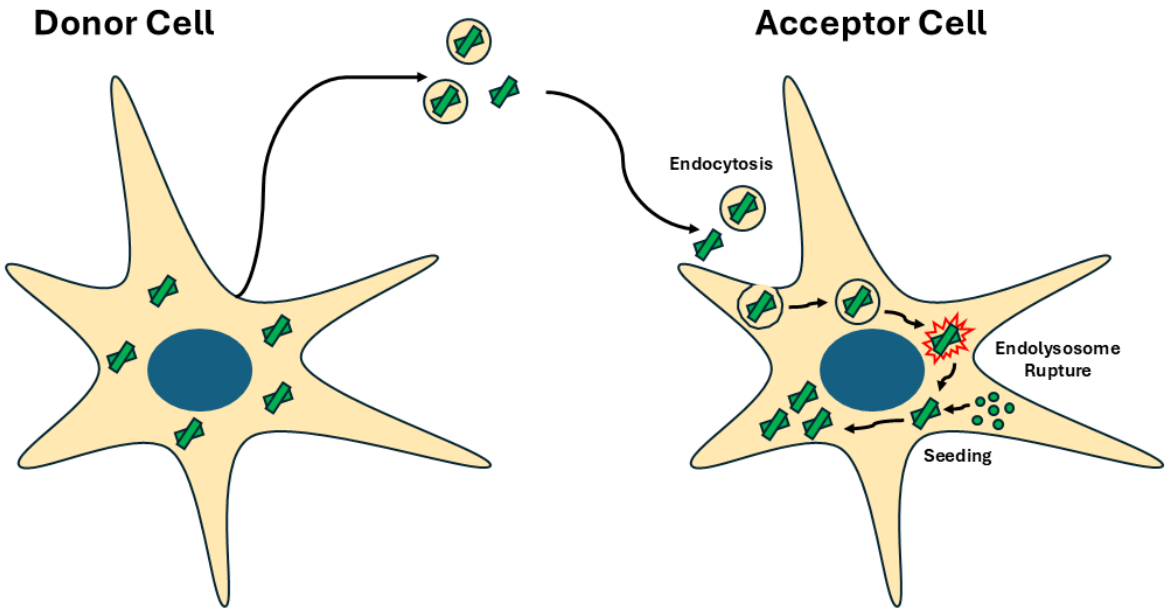

Figure 11. *Illustration of the prion-like propagation of α-synuclein aggregates between a donor cell and an acceptor cell via the endosomal pathway. Aggregates are released by the donor cell either packaged within vesicles or by direct secretion into the extracellular space and taken up by the acceptor cell mainly through endocytosis. Once in the endosomal pathway, the aggregates can induce rupture of endolysosomes and escape into the cytosol. In the cytosol, the aggregates can seed the formation of new α-synuclein aggregates by recruiting endogenous α-synuclein.*

The primary mechanisms by which α-syn aggregates spread between neurons in a prion-like fashion involve their release from donor cells followed by uptake into acceptor cells [249], as illustrated in Fig. 11. In this pathway, α-syn aggregates can be secreted directly from neurons into the extracellular space [260] or packaged within vesicles, such as exosomes [261,262]. In addition, microglia have also been implicated in secreting exosomes loaded with aggregated α-syn aggregates [263]. Following secretion, internalization by the acceptor neuron occurs predominantly through endocytic routes, including for example macropinocytosis mediated by the binding of α-syn aggregates to cell-surface heparan sulfate proteoglycans (HSPGs) [264], or processes dependent on clathrin, caveolae, and actin dynamics [265]. Receptor-mediated endocytosis via the lymphocyte activation gene 3 (LAG3) receptor has been suggested [265], and possibly also via neurexin 1β, and APLP1 [266]. Another receptor which has been recently implicated in the endocytic uptake of α-syn aggregates is FAM171A2, where its overexpression enhanced aggregate internalization, whereas the knockdown showed adverse effects [267]. Furthermore, aggregate size has been shown to be an important determinant of α-syn uptake, with larger aggregates exhibiting a reduced uptake efficiency and an overall lower cytotoxicity compared to smaller aggregates [160,257]. Once internalized, α-syn aggregates are typically routed through the endolysosomal pathway, first entering early endosomes (~pH 6), which then mature into late endosomes (~pH 5.5) and

ultimately fuse with lysosomes to form endolysosomes (~pH 5), where the aggregates should normally be degraded [268]. It has furthermore been shown that α-syn aggregates can escape from endolysosomal compartments by inducing vesicle membrane rupture [269,270], constituting an ill-defined, but important mechanism of entry to the cytosol. Once released, the exogenous α-syn aggregates can seed the formation of new aggregates by recruiting the endogenous cytosolic or presynaptic α-syn, thereby driving the prion-like propagation of pathology [271,272]. Although these key steps in the propagation pathway have been defined, important information on how different α-syn assemblies and polymorphs trigger each event is still missing, making the molecular and mechanistic understanding of the process incomplete. The uptake of exogenous α-syn variants and their distinct abilities to seed endogenous α-syn is a central focus of **paper IV**.

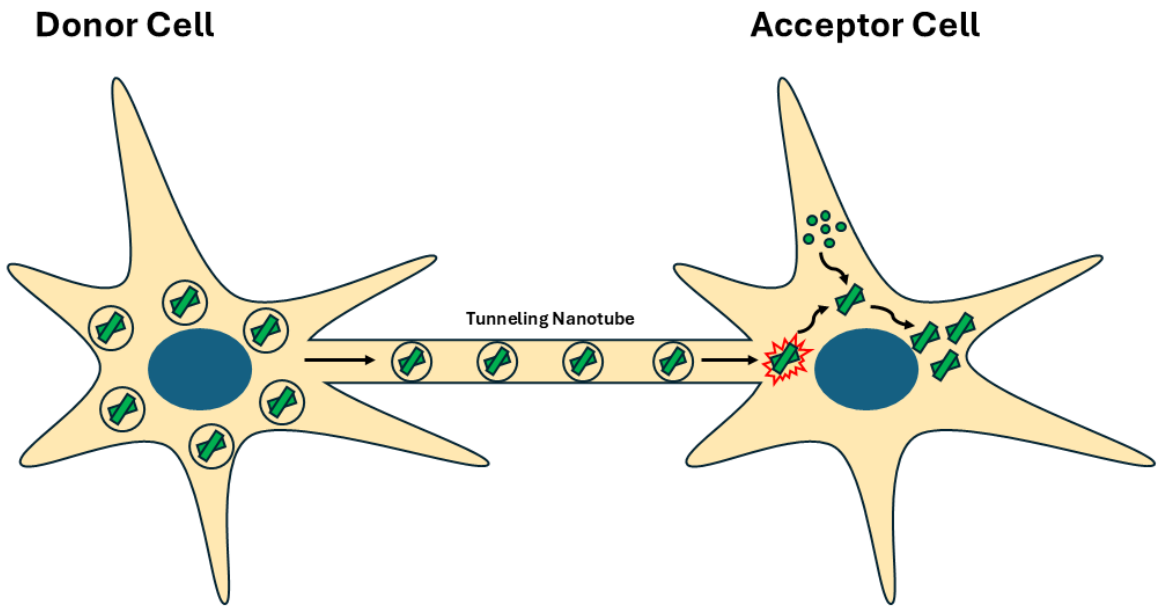

Figure 12. *Illustration of the prion-like propagation of α-synuclein aggregates between a donor cell and an acceptor cell via tunneling nanotubes (TNTs). When a neuron is overloaded with α-synuclein aggregates, it can offload part of this burden by transferring aggregates to a neighboring cell via TNTs. Once the transferred endolysosomes enter the recipient cell, they can rupture and seed the formation of aggregates by recruiting endogenous α-synuclein.*

Another way by which α-syn aggregates can spread to nearby cells is through direct transfer via tunnelling nanotubes (TNTs), as illustrated in Fig. 12. TNTs are filaments primarily composed of actin which act as bridges that connect donor and recipient cells, enabling direct intercellular communication and exchange of cellular components, including macromolecules and organelles [273]. Studies on both α-syn [274] and tau [275] have suggested that neurons can use TNTs to distribute the aggregate burden from an overwhelmed cell to a nearby healthier cell. Specifically, for α-syn, it has been suggested that α-syn fibrils can stimulate the formation of TNTs. Once these nanotubes form, lysosomes which were overburdened with α-syn aggregates were transferred through the TNTs to the healthier cell. The transferred aggregates could then escape the lysosomes and seed endogenous α-syn, thereby promoting the propagation of pathology [276].

5. Methodology

In this chapter, a brief description of the methodology and how each method was applied in the research underlying the papers will be given. A more detailed description can be found in each respective paper and manuscript.

5.1. Expression and purification of recombinant α-synuclein

Recombinantly produced WT α-syn was used in all experiments in this thesis (**papers I-IV)**. Additionally, recombinantly produced mutant α-syn (A30P, E46K, H50Q, A53T) was used in **papers II-IV**.

To obtain reliable aggregation kinetics, and because α-syn is prone to self-assembly, it is essential to start experiments with a high-purity, monomeric α-syn preparation. To achieve this, monomeric α-syn is typically produced recombinantly by expressing the protein in *Escherichia coli* (*E. coli*) bacteria, followed by a series of purification steps.

In this thesis, both WT and mutant (A30P, E46K, H50Q, A53T) α-syn were recombinantly expressed in *E. coli* BL21(DE3) carrying a pLysS plasmid, which helps control expression levels and prevents reduced protein yield that can result from host cell stress upon production of toxic proteins and protein aggregates. α-syn was further purified using an acid precipitation protocol [277], in which *E. coli* cells were lysed by sonication and contaminating proteins were precipitated by lowering the pH to 3.5, leaving α-syn in the supernatant. This separation is effective due to the intrinsically disordered structure and low isoelectric point (pI ~ 4.7) of α-syn, which keeps the protein soluble. In contrast, many globular proteins present in *E. coli* bacteria tend to unfold at low pH due to their high pIs, which exposes their hydrophobic cores, promotes aggregation and subsequent precipitation. Following precipitation, the pH of the α-syn containing supernatant is increased back to pH 7.5.

α-syn was further purified by two chromatography steps. In the first step, an anion exchange chromatography column was used to remove positively charged proteins. The bound protein was then eluted using a salt gradient, producing chromatographic peaks that reflect differences in binding affinity to the stationary phase. Proteins with weaker interactions elute earlier, while those with stronger interactions elute later, resulting in further separation. In the second step, size-exclusion chromatography (SEC) was performed, in which the sample passes over a porous stationary phase. Smaller proteins diffuse into the pores and are delayed while larger proteins cannot enter and elute earlier. Under these conditions, α-syn usually elutes as a single peak. After the chromatography steps, the fractions containing α-syn are aliquoted and thereafter stored in -80 ºC.

Prior to all experiments performed in **papers I-III**, an additional SEC was conducted to monomerize the protein and remove aggregates potentially formed in the freeze-thaw process which could influence the aggregation kinetics. In **paper IV,** this step was replaced by using 50 kDa centrifugal filters under a LAF bench to keep the monomeric solutions sterile and to minimize the loss of protein associated with column chromatography.

5.2. Aggregation kinetics of WT and mutant α-synuclein

Thioflavin-T (ThT) fluorescence was used to monitor the aggregation kinetics of α-syn fibril formation. ThT is the "gold standard" dye to monitor fibril aggregation kinetics *in vitro* due to its property of fluorescence enhancement upon binding to the cross-β-sheet of amyloid fibrils [278]. ThT is a benzothiazole dye which consists of a benzothiazole ring connected to a phenylamine ring by a carbon-carbon bond (Fig. 13). In its unbound state, the benzothiazole and phenylamine rings of ThT rotate freely around the central carbon-carbon bond. In this conformation, ThT has an excitation maximum of ~385 nm and an emission maximum of ~445 nm, but exhibits only weak (negligible) fluorescence. In contrast, when ThT binds to the cross-β-sheet structure of amyloid fibrils, the rotation is inhibited, and its excitation maximum shifts to ~450 nm and the emission maximum to ~482 nm, accompanied by an approximately 1000-fold increase in fluorescence intensity compared to the unbound dye, which makes it particularly well suited for monitoring fibril formation [279]. A ThT concentration of 20 μM was used in all aggregation kinetics experiments, which provides a strong fluorescence signal without influencing the aggregation process at the protein concentrations (50 μM α-syn) used [280].

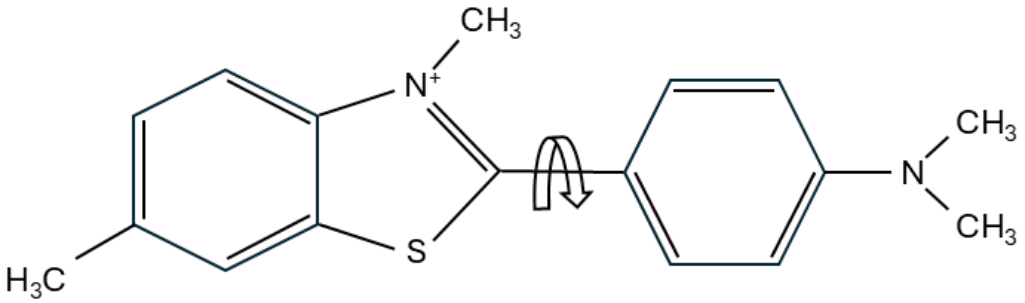

Figure 13. *The chemical structure of thioflavin-T. The rotation around the carbon-carbon bond is marked with an arrow.*

In **paper I**, the aggregation kinetics of WT α-syn were monitored in the presence of varying concentrations of different cations (Li^+, Na^+, K^+) using a plate reader. An orbital-shaking protocol with beads was used to accelerate fibrillation while still preserving a measurable lag phase [281]. In **papers II-III** a different strategy was adopted. Pre-formed fibrils (PFFs), prepared according to the standardized and highly reproducible Michael J Fox foundation protocol [282], were used as seeds to promote aggregation under quiescent conditions in a plate reader. This seed-based approach largely abolishes the lag phase of α-syn aggregation. At moderately high seed concentrations, the kinetics are dominated by secondary nucleation, whereas at high seed concentrations elongation dominates [156]. Additionally, in **paper II** the standard aggregation kinetic setup was modified by introducing a fragmentation step once the reaction reached the plateau phase. This cycle was repeated several times to monitor how the aggregation kinetics and morphology of the fibrils changed with each subsequent aggregation, establishing an entirely new means of studying aggregation.

From the aggregation kinetics curves, several key parameters can be extracted such as the lag time (the time required to reach 10% fibril mass), the half-time (the time required to reach 50% fibril mass), and the growth time (the interval between 10% and 90% fibril mass). To determine these parameters reliably, the raw fluorescence values must first be normalized. In

paper I lag-, half-, and growth-times calculated for all kinetic curves, whereas in **paper III** only the half-time was evaluated. Further, by fitting the raw ThT fluorescence to a model of exponential fibril growth, additional quantitative parameters such as the elongation rate constant (k_+) and elongation speed were estimated in **paper II**.

5.3. Absorption spectroscopy

Absorption spectroscopy is a method that measures the amount of light that is absorbed by a sample as it passes through it. Absorbance is measured using an absorbance spectrophotometer which in its simplest form consists of a light source, a monochromator and a detector (Fig. 14). Measurements are usually performed in the ultraviolet-visible range (~200-700 nm) using either a combination of a deuterium and a tungsten-halogen lamp or a single xenon flash lamp to cover the whole range.

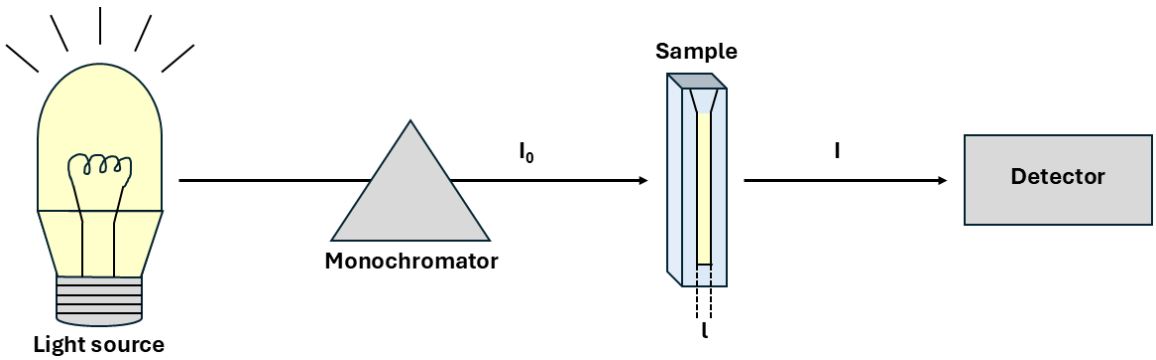

Figure 14. *Schematic illustration of an absorbance spectrophotometer. After passing through the monochromator and selecting the wavelength of interest, incoming light of intensity I_0 is passed through a sample with path length l, and the intensity of the transmitted light I is detected. Comparing the intensity of the incoming light and the transmitted light using Eq. 1 gives the absorbance of the sample.*

The monochromator positioned after the light source selects the wavelength of interest and directs it to the sample. The sample is usually kept in a cuvette made of quartz, due to its low inherent absorption and hence high transparency in the UV-Vis range. Some light will be absorbed by the sample, whereas the remaining light is transmitted to the detector. The logarithm of the ratio between the incoming light (I_0) and the transmitted light (I) defines the absorbance (A) (Eq. 1).

$$A = log \frac{I_0}{I} \quad (1)$$

Typically, absorbance measurements are performed over a range of selected wavelengths and represented as an absorbance spectrum. From the absorbance (A), the extinction coefficient (ε), which is defined by how strongly light is absorbed by a sample at a given wavelength and the optical path length (l), the concentration (c) of the sample can be calculated. This relationship is described by the Beer-Lambert law (Eq. 2).

$$A_\lambda = \varepsilon_\lambda lc \quad (2)$$

For proteins, absorbance is typically measured at 280 nm because the aromatic amino acids tryptophan and tyrosine strongly absorb at this wavelength. The extinction coefficient at 280

nm is the sum of the individual contributions from the aromatic amino acids in the protein, which for α-syn, with its four tyrosine's, is ε_{280} = 5,960 $M^{-1}cm^{-1}$. In **papers I-IV**, absorbance measurements are used to determine the concentration of α-syn prior to aggregation and the residual monomer content in supernatants of aggregated samples at the end-point of aggregation (as a means to estimate fibril yield).

5.4. Fluorescence spectroscopy

Fluorescence spectroscopy measures the light emitted by a sample after it has been excited by a light source. Excitation is closely linked to absorption, and for many molecules the excitation spectrum overlaps with the lowest energy absorption band. When a molecule is excited, it absorbs light and transitions from the ground sate to an excited state. Part of the energy it absorbs can be emitted as a photon when the molecule relaxes back to its ground state, which can be detected by a fluorescence spectrophotometer. A simple fluorescence spectrophotometer typically consists of a light source, usually a xenon arc lamp which provides a broad and continuous spectrum of light, two monochromators (or filters), which select for a wavelength of interest, and a detector (Fig. 15).

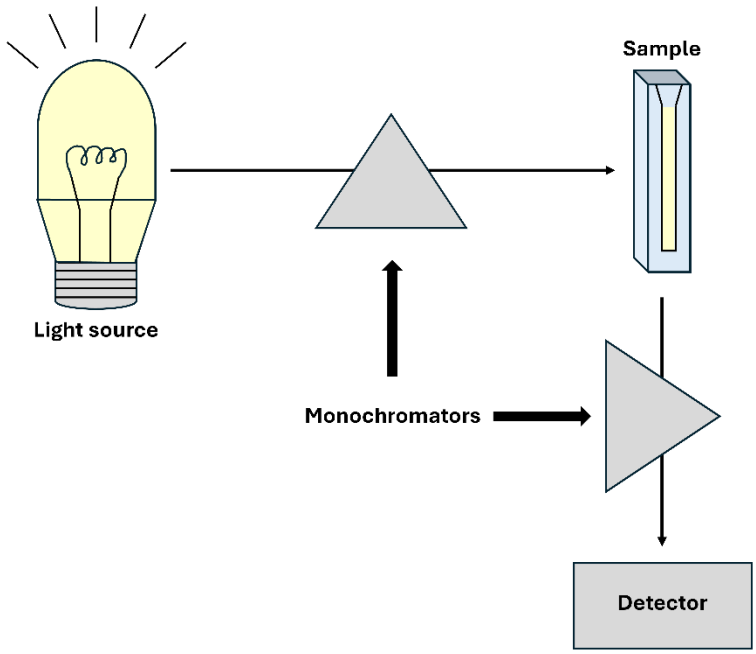

Figure 15. *Schematic illustration of a fluorescence spectrophotometer. Light from the light source passes through the first monochromator, selecting the excitation wavelength of interest. The incident light excites the sample, which emits light that is selected by the second monochromator and passed to the detector at a 90° angle to the incident light.*

The sample is placed in between the monochromators. The first monochromator isolates a narrow band of wavelengths from the light source and directs it onto the sample. The resulting fluorescence from the sample is passed through the second monochromator, which selects the emission wavelength that reaches the detector. To reduce interference from transmitted or reflected light, the detector is usually placed at a 90º angle from the incident light. By fixing the excitation wavelength through the first monochromator and varying the emission wavelength using the second monochromator, an emission spectrum can be

recorded. In contrast, varying the excitation wavelength of the incident light and fixing the emission wavelength produces an excitation spectrum. In **papers I-IV** fluorescence spectroscopy was used to verify the presence or absence of fibrils using ThT fluorescence. In **paper III** time-resolved fluorescence spectroscopy was used to measure fluorescence lifetime of different fibril variants in the presence of ThT. In **paper IV,** fluorescence spectroscopy was used to measure emission spectra of fibrils with ATTO488 and pHrodo fluorophores. Finally, in **papers I-III** high-throughput fluorescence spectroscopy using a plate-reader setup was used to monitor the aggregation kinetics of WT and mutant α-syn fibrils.

5.5. Fluorescence lifetime spectroscopy

When a fluorophore is excited, the subsequent emission of a photon typically occurs on timescales ranging from pico- to microseconds. The average time between the excitation of a fluorophore and the emission of a photon is known as the fluorescence lifetime. The most widely used method nowadays for measuring fluorescence lifetimes is time-correlated single photon counting (TCSPC), which is schematically shown in Fig. 16. In TCSPC, a pulsed light source, usually a laser, excites the sample at defined time intervals using a fixed wavelength. In tandem, each excitation pulse triggers a start signal in the time-to-amplitude converter (TAC). When an emitted photon is detected, it generates a stop signal. The TAC converter measures the time difference between the start and stop signal, after which the signal is digitalized by the analogue-to-digital converter (ADC) and the data is stored in digital memory (MEM). By repeatedly recording many thousands of such photon arrival times, either until a target of counts is reached in the top channel or during a predefined acquisition time, a histogram of photon counts versus time is constructed, representing the fluorescence decay. Once all photon counts are collected, the data can be fitted to an appropriate exponential decay model to obtain one or several fluorescence lifetimes (τ), which reflect the fluorophore's photophysical properties and the local environment in which it resides. Differences in fluorescence lifetimes can provide sensitive information about the fluorophore's microenvironment and hence sample properties. In **paper III**, ThT fluorescence lifetimes are used to probe structural differences in α-syn amyloid fibrils formed by self-seeding and cross-seeding of WT, A30P, E46K, H50Q, A53T fibrils, providing detailed insights into the conservation and evolution of fibril polymorphs.

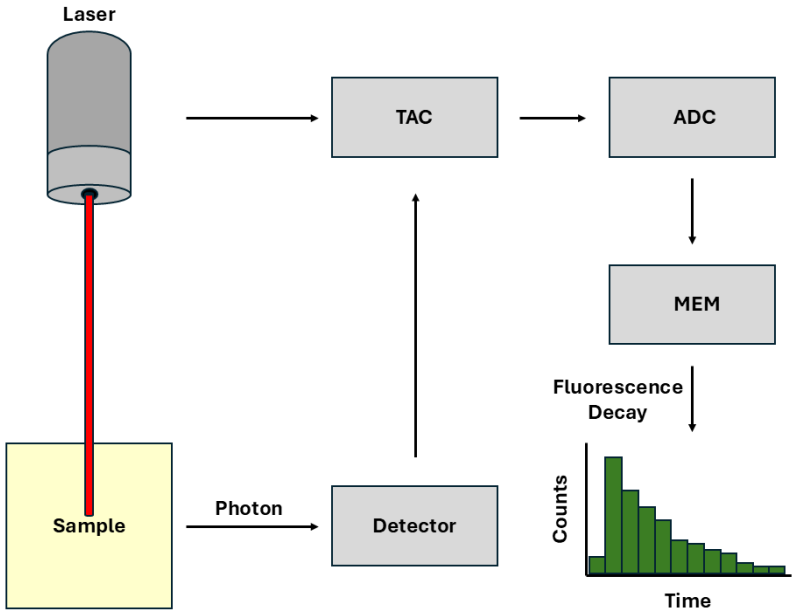

Figure 16. *Schematic illustration of a time-correlated single photon counter (TCSPC). A sample is excited by a pulsed laser at a fixed wavelength and time interval. Simultaneously, the laser initiates a start signal in the time-to-amplitude converter (TAC). When a photon is emitted by the sample a stop signal is triggered in the TAC. The time between start and stop is measured, converted to a digital signal by the analogue-to-digital converter (ADC) and stored in digital memory (MEM). Thousands of photons are recorded and used to construct a histogram of counts versus time, from which the fluorescence lifetime can be calculated.*

5.6. Circular dichroism spectroscopy

In contrast to conventional absorption spectroscopy, which uses unpolarized light, circular dichroism (CD) spectroscopy measures the difference in absorption between left- and right-handed circularly polarized light (Eq. 3).

$$\Delta A = A_L - A_R \tag{3}$$

Circularly polarized light is chiral and cannot be superimposed on its mirror image. Therefore, the sample must contain chiral molecules to generate a CD signal. Many biological molecules, such as DNA, carbohydrates and proteins are inherently chiral and are thus well suited for CD measurements. A CD spectrophotometer consists of a light source, typically a xenon arc lamp, a monochromator which isolates a narrow band of wavelengths, a linear polarizer which converts unpolarized to polarized light and a photo elastic modulator (PEM) which alternates the polarized light between left-handed (A_L) and right-handed (A_R) circular polarized light. The resulting differential absorption of A_L and A_R by the sample is then detected by a photomultiplier tube (PMT) detector. Commonly, CD spectroscopy is used for measuring the secondary structure content of protein samples, as it can distinguish between α-helices, β-sheets and random coil conformations due to the chirality of peptide bonds and the specific geometric configuration of secondary structure motifs which appear with highly characteristic spectral signatures. α-helices produce CD spectra defined by double negative peaks at ~222 nm and ~208 nm, and a positive peak at 190-195 nm. β-sheets produce a single negative peak at ~218 nm and a positive peak at 195 nm, whereas random coil conformations produce a single negative peak at ~195 nm (Fig. 17).

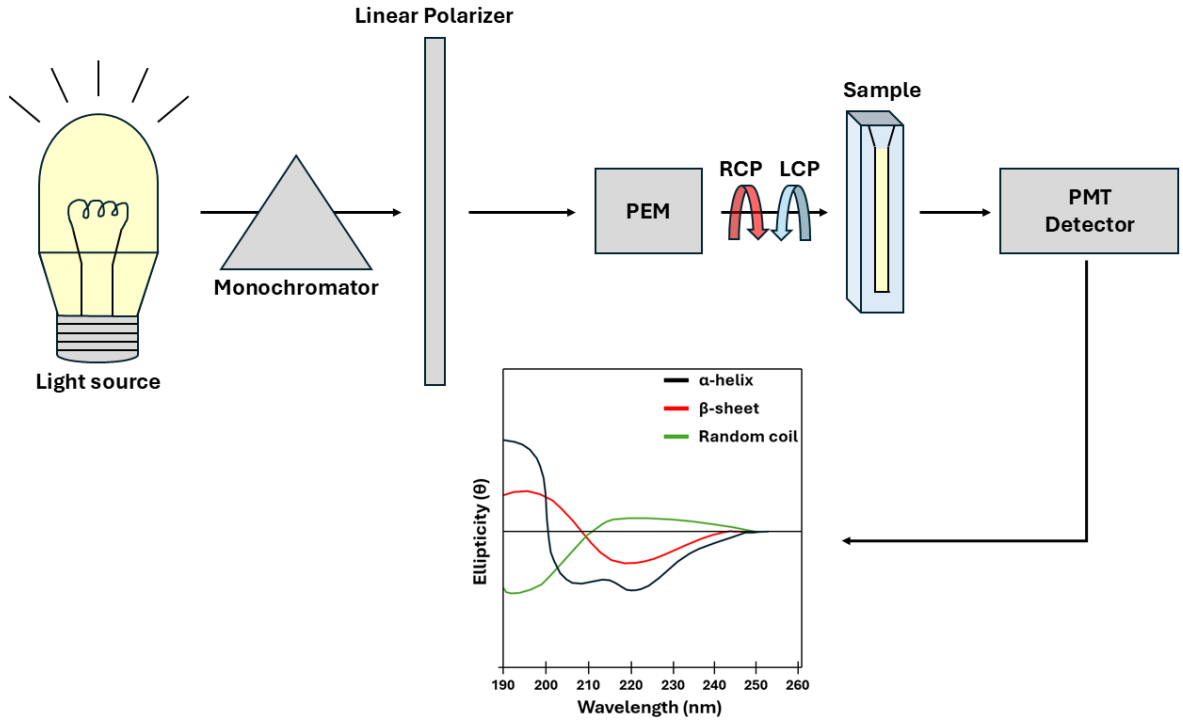

Figure 17. *Schematic illustration of a circular dichroism (CD) spectrophotometer. Light from the light source passes through a monochromator which selects a narrow band of wavelengths, the linear polarizer converts the unpolarized light to polarized light, the photo elastic modulator (PEM) alternates the polarized light between left-handed (LCP) and right-handed (RCP) circular polarized light. The difference in absorption of LCP and RCP by the sample is then detected by the photomultiplier tube (PMT) detector which results in characteristic negative peaks for α-helix (222 nm, 208 nm, black line), β-sheet (218 nm, red line), and random coil (195 nm, green line).*

Since many amyloid forming proteins, including α-syn, are intrinsically disordered, they adopt a random-coil conformation in their monomeric state. As these proteins aggregate into amyloid fibrils, they adopt the characteristic cross-β-sheet structure, and the transition from random coil to β-sheet can be monitored by CD spectroscopy. Conversely, the reverse transition from β-sheet back to random coil can also be detected, allowing the thermodynamic stability of fibrils to be determined [283]. This can be achieved by, for example, increasing the temperature, or by lowering the temperature of certain proteins, such as α-syn [88]. Typically, a CD spectrophotometer reports data as ellipticity (θ), which is reported in millidegrees (mdeg). For protein samples, however, the raw ellipticity is usually converted to mean residue molar molar ellipticity [θ] (deg*cm^2/dmol) which normalizes the signal for concentration and the average molecular weight of the amino acids the protein contains, allowing for comparison of the structural content between different samples.

CD spectroscopy is used in **papers I, III, IV** to determine secondary structure content of fibril samples following α-syn aggregation reactions and in the supporting information of **paper II** to monitor the loss of β-sheet structure during cold denaturation.

5.7. Atomic force microscopy

Atomic force microscopy (AFM) is a high-resolution microscopy technique that utilizes a sharp probe, often made of silicon, to scan the surface of a sample and measures the interaction forces, both attractive and repulsive, including van der Waals forces, electrostatic forces, and dipole-dipole interactions, between the tip and the sample. AFM can, for example, be used to probe the topography of a sample, including quantitative measurements such as the height and length of individual sample constituents, as well as to obtain information about mechanical properties. Due to not being limited by light diffraction, unlike light-based microscopes, AFM can achieve resolutions down to 1-10 nm, or even lower depending on sampling conditions.

The main components of an AFM include the probe, which consists of a reflective cantilever with a sharp tip on the non-reflective side and a laser, which is focused on the cantilever, and reflected onto a photodiode. The photodiode converts changes in the reflected laser position into an electric current and allows the detector to measure the cantilevers deflection. A feedback control system processes the signal received by the detector and the piezoelectric scanner adjusts the stage which moves the sample vertically to maintain a constant interaction between the tip and the sample, while the scanner simultaneously moves the sample laterally in a predefined raster pattern (Fig. 18).

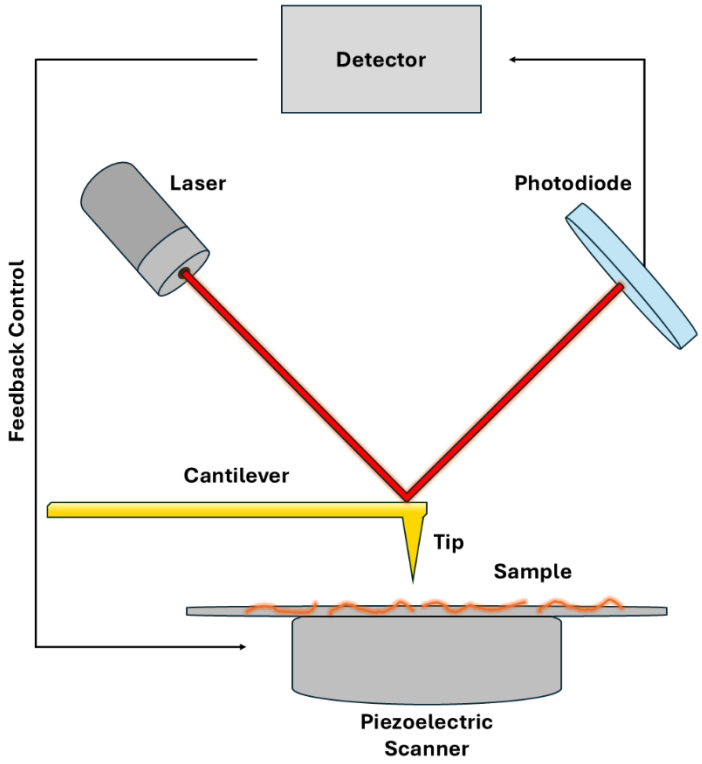

Figure 18. *Schematic illustration of an atomic force microscope. A laser directed at the cantilever is reflected onto a photodiode and the signal is received by the detector which measures the cantilevers deflection. A feedback control system processes the signal, and the piezoelectric scanner adjusts the stage vertically, maintaining a constant interaction between tip and sample. Simultaneously, the scanner moves the sample laterally in a predefined raster pattern.*

The most commonly used AFM operating mode is semi-contact, also known as tapping mode. It utilizes vibration of the cantilever near its resonance frequency to maintain intermittent contact between the tip and the sample. Semi-contact mode significantly reduces lateral forces, and damage to the sample which makes it the preferred mode of imaging for biomacromolecules and polymers, such as amyloid fibrils. Another essential component in AFM is the substrate used to mount the sample. To achieve a good contrast between the sample and the background, the substrate must have an atomically smooth surface. For imaging amyloid fibrils, a mica sheet, typically composed of muscovite is used as the substrate. Mica sheets are hydrophilic and negatively charged, making it suitable for fibril adsorption to the surface. Finally, specialized software is required to visualize and analyze the data produced with an AFM. In this thesis, AFM images were processed using Gwyddion [284], WSxM [285] and Easyworm [286] to visualize fibril morphology, and to measure the lengths, heights, and persistence lengths of α-syn fibrils.

AFM was used in **papers I-IV** to visualize fibril morphology following aggregation. Furthermore, in **paper I** AFM was used to measure the persistence lengths of fibrils formed in the presence of different monovalent cations and concentrations. In **paper II** length and height distributions of WT and mutant fibrils were determined following multiple rounds of aggregation and fragmentation. Finally, in **paper IV**, AFM was used to verify uniform size distribution of WT and mutant fibrils prior to their addition to cells.

5.8. Flow cytometry

Flow cytometry is a high-throughput, fluorescence-based technique that analyzes individual cells or particles to measure their physical and biochemical characteristics. The advantage of flow cytometry is the ability to rapidly measure multiple characteristics of interest, such as estimating the size and granularity of cells, identifying different cell types in a sample, distinguishing between live and dead cells, and quantifying the abundance of fluorescently labelled proteins or other fluorescently labelled molecules of interest.

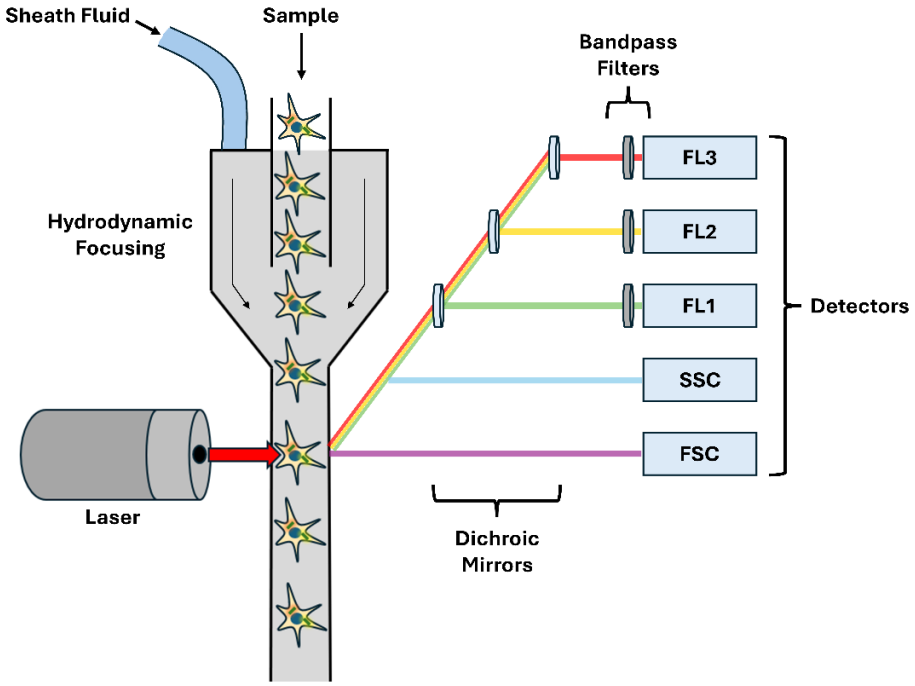

Figure 19. *Schematic illustration of a flow cytometer. Cells are injected into the fluidic system and aligned by hydrodynamic focusing of the cells by using sheath fluid with a laminar flow. Cells are passed through the laser one at a time and the forward scatter (FSC), side scatter (SSC), and fluorescent light (FL1-FL3) is detected, allowing measurement of multiple characteristics of interest simultaneously.*

The main components of a flow cytometer include the fluidics system, the optical system and the detectors (Fig. 19). The cell suspension is injected into the flow cytometer's fluidic system, where hydrodynamic focusing aligns cells into a single line by using sheath fluid with a laminar flow, ensuring that the cells pass through the laser one at a time. The cells pass through one or more laser beams in the optical system, causing them to scatter light. If they contain fluorescent markers that correspond to the laser's excitation wavelength, those markers are excited and emit fluorescent light. Light scattered in the direction of the laser beam is detected by the forward scatter (FSC) detector, which is used for estimating cell size. Light scattered at a 90º angle is routed to the side scatter (SSC) detector, where the detected light reports on granularity (complexity) of a cell. By plotting FSC against SSC, it is possible to distinguish different cell populations from each other, and identify dead cells, debris, and clumped cells. This plot provides the first essential separation of events in flow cytometry, and gating is then used to separate specific cell populations for downstream analysis. Fluorescent light emitted by markers added to the cells is separated by wavelength using dichroic mirrors and directed to specific fluorescence detectors (FL1, FL2, FL3). Before reaching each detector, the light passes through a bandpass filter that selects a narrow wavelength range appropriate for that channel. Depending on the marker used, the fluorescence signal can be applied for downstream analysis, such as assessing cell viability, identifying cell populations by cell specific markers, or quantifying specific proteins within the cells.

Flow cytometry was used in **paper IV** to monitor the uptake of WT, A30P, E46K, H50Q, and A53T α-syn fibrils in SH-SY5Y cells. Monomeric α-syn was labeled with ATTO488, which provides stable fluorescence independent of its environment or with pHrodo, whose

fluorescence intensity increases as pH decreases, which is relevant for the acidic environment in the endolysosomal system. The labeled monomers were then mixed with unlabeled protein to produce sparsely double-labeled amyloid fibrils. This enabled their cell uptake to be monitored and distinguished from cell surface associated fibrils in studies using SH-SY5Y cells.

6. Original Work

In this chapter, I present an overview of the key findings of this thesis and discuss their contribution to the field. In the first part, I compare how different monovalent cations affect the aggregation kinetics and morphology of the resulting WT α-syn amyloid fibrils (**paper I**). I then extended the scope of the subsequent projects to include the familial α-syn mutants A30P, E46K, H50Q, and A53T (**papers II-IV**). In **paper II**, I investigated how fragmentation influences the aggregation kinetics and morphology of WT and mutant α-syn amyloid fibrils. I then extended this work in **paper III** by examining how self-seeding and cross-seeding among the different α-syn variants affect their aggregation behavior and structural properties. Finally, in **paper IV**, uptake efficiencies of the WT and mutant α-syn fibrils and cellular responses were monitored in SH-SY5Y cells. Furthermore, the seeding efficiencies and resulting inclusion morphologies of the different fibril variants were assessed in primary neuronal cultures from rats and mice.

6.1. Monovalent cations have distinct effects on the aggregation kinetics and morphology of α-synuclein fibrils

Salts play a well-established role in protein aggregation by shielding charges, reducing electrostatic repulsion, and modulating intermolecular interactions, thereby facilitating aggregation and influencing aggregation kinetics. While it has been shown that various anions [148] and multivalent cations [287] have distinct effects on the aggregation of α-syn, the role of monovalent cations has received considerably less attention, possibly because their relative effects have been regarded as minimal due to their identical charge. During my master's thesis I worked with α-syn aggregation in the presence of potassium chloride (KCl) to replicate aggregation conditions in a published structural report [20]. After starting my PhD, I replaced KCl with sodium chloride (NaCl), and this change revealed a noticeable difference in the morphology of the resulting fibrils observed using AFM. Under KCl conditions individual fibrils were easy to distinguish, whereas in NaCl they tended to much more frequently appear in clusters. I noticed that researchers often relied on their preferred chloride salts without paying much attention to the specific monovalent cation, and sometimes even used these salts intermixedly [20].

In **paper I**, this observation prompted me to examine how different monovalent cations (Li^+, Na^+, and K^+) influence WT α-syn fibril formation, including effects on aggregation kinetics and fibril morphology.

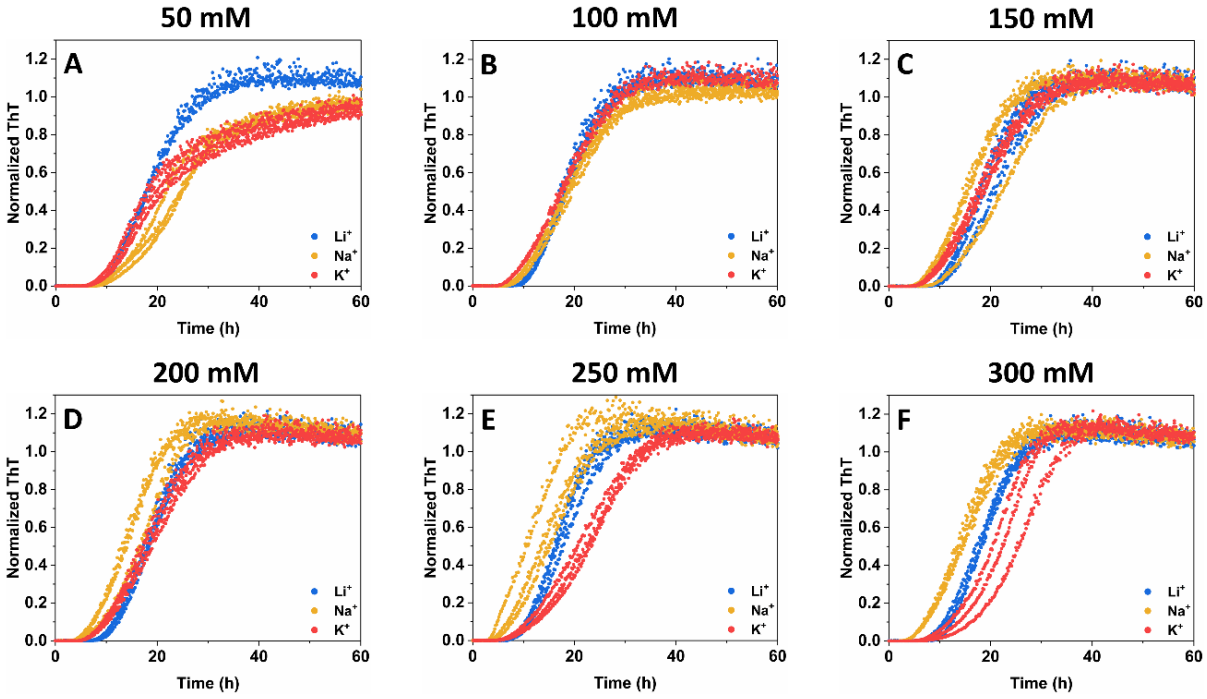

Figure 20. *Aggregation kinetics of α-syn in the presence of different chloride salt solutions. (A–F) Normalized ThT fluorescence measurements of 50 μM α-syn aggregated at 37 ºC (pH 7.4, 20 mM Tris-HCl, 200 rpm orbital shaking) in the presence of LiCl, NaCl, or KCl at different concentrations (n = 3). Reproduced from Havemeister et al., 2023, 'Monovalent cations have different effects on assembly kinetics and morphology of α-synuclein amyloid fibrils', Biochemical and Biophysical Research Communications, under the CC BY 4.0 license.*

By following α-syn aggregation with a ThT assay across a range of monovalent cation concentrations (50-300 mM, chloride salts), I observed distinct cation- and concentration dependent effects. At the lowest concentration (Fig. 20A), K^+ promoted the most rapid aggregation kinetics, while Na^+ resulted in the slowest aggregation kinetics. Increasing salt concentration progressively inverted this relationship (Fig. 20B-F), while Li^+ displayed intermediate kinetic behavior throughout the concentration range (Fig. 20A-F). The aggregation-promoting effects observed for α-syn in the presence of Na^+ and Li^+ are consistent with earlier findings showing that charge neutralization by various anions [148] promotes α-syn aggregation, and that various salts can accelerate fibril formation of several other amyloid-forming proteins [288-290]. In contrast, increasing the concentration of K^+ resulted in clear aggregation-retarding effects, resembling the slowed α-syn fibrillation reported under acidic conditions [291] and the inhibitory influence of multivalent metal ions on other amyloidogenic systems [292,293]. The divergent behaviors of Na^+/Li^+ versus K^+ can in part be explained by their different interactions with carboxylate groups, where Na^+ binds most strongly, followed by Li^+, whereas K^+ shows markedly weaker affinity [294]. This trend is consistent with the empirical matching water affinities principle, which attributes ion-specific effects to differences in hydration enthalpies and the tendency of ions to associate with counterions of similar hydration enthalpies [295]

These findings strongly suggest that monovalent cations, in addition to anions and multivalent cations, play a significant role in modulating the aggregation kinetics of α-syn amyloid fibril formation, and that this effect varies with concentration. The results are physiologically relevant because the high intracellular concentration of K^+ and the transient Na^+ influxes that occur along the axons during neuronal activity modulate α-syn behavior in its native cellular environment.

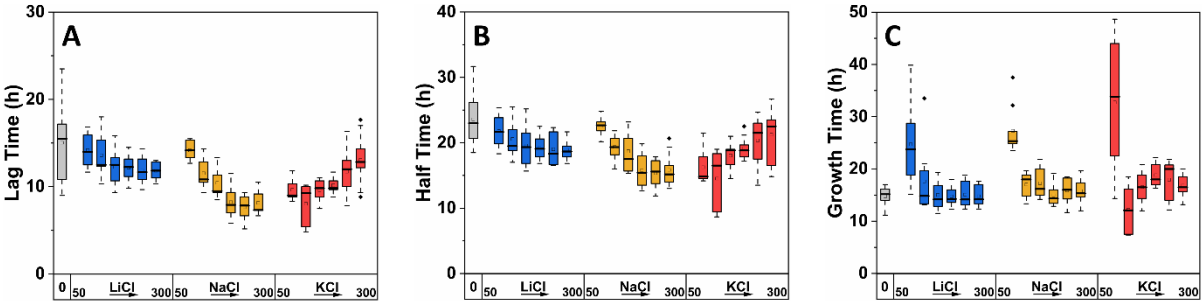

Figure 21. *Quantification of α-syn aggregation kinetics under the conditions assayed in Fig. 20. (A) lag times, (B) half times, and (C) growth times. The 0 mM salt condition is shown for reference. Error bars represent SD (N = 2; n = 3). Reproduced from Havemeister et al., 2023, 'Monovalent cations have different effects on assembly kinetics and morphology of α-synuclein amyloid fibrils', Biochemical and Biophysical Research Communications, under the CC BY 4.0 license.*

To identify which step of the aggregation process is most affected by the different monovalent cations, I extracted the lag, half, and growth times from the aggregation curves in Fig. 20. The largest cation effects were observed for the lag time. Both Li^+ and Na^+ shortened the lag phase in a concentration dependent manner, whereas K^+ produced the opposite trend (Fig. 21A). In contrast, the growth time was largely unaffected by either the type or

concentration of the monovalent cation (Fig. 21C). These observations strongly suggest that the aforementioned factors affecting the divergent behaviors of Na^+/Li^+ versus K^+ primarily influence primary nucleation.

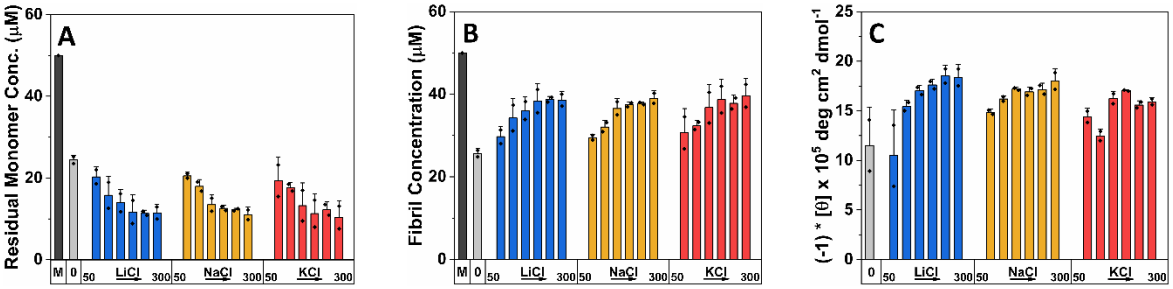

Figure 22. *Salt-dependent changes in fibril yield and secondary structure. (A, B) Quantification of residual monomer (A) and fibril yield (B) based on absorbance of the supernatant. The initial monomer concentration was 50 μM. (C) Circular dichroism (CD) signal at 218 nm reflecting β-sheet content in non-centrifuged end-point samples. (A-C) Measurements include 0 mM and 50-300 mM salt conditions (50 mM intervals). Error bars denote SD (N = 2, n = 3). Adapted from Havemeister et al., 2023, ´Monovalent cations have different effects on assembly kinetics and morphology of α-synuclein amyloid fibrils´, Biochemical and Biophysical Research Communications, under the CC BY 4.0 license.*

The influence of monovalent cations was also assessed with respect to residual monomer content, fibril yield and β-sheet content using absorption spectroscopy and circular dichroism spectroscopy (CD) (Fig. 22). Although the residual monomer content and fibril yield remained largely unaffected by the cation type (Fig. 22A-B), small differences in β-sheet content were observed (Fig. 22C). Li^+ and Na^+ produced slightly higher β-sheet content than K^+, which may reflect the intrinsic properties of the ions. Li^+ and Na^+ are kosmotropic ions and tend to stabilize protein structures [296], whereas K^+ is weakly chaotropic and can promote structural destabilization [297]. My data suggest that this also affects protein aggregate structure. Moreover, these ion-specific kosmotropic and chaotropic properties likely also contribute to the differences in aggregation behavior observed in Figure 20-21.

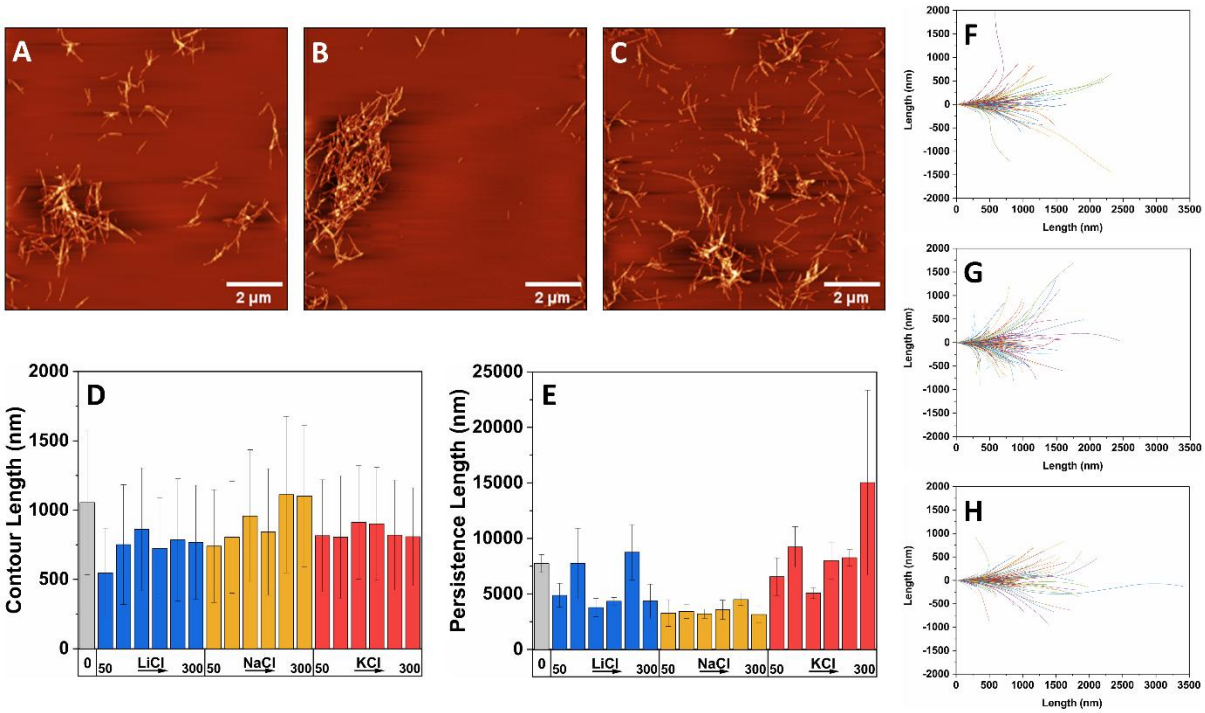

Figure 23. *Salt-dependent morphological changes in α-syn fibrils. (A-C) Representative AFM micrographs of fibrils assembled in 100 mM LiCl (A), NaCl (B), or KCl (C). (D-E) Distributions of contour length (D) and persistence length (E) for fibrils formed across 0-300 mM salt (50 mM intervals). Error bars denote SD (n = 200). (F-H) Fibrils aligned horizontally to their initial tangent for comparative visualization: LiCl (F), NaCl (G), KCl (H). Reproduced from Havemeister et al., 2023, 'Monovalent cations have different effects on assembly kinetics and morphology of α-synuclein amyloid fibrils', Biochemical and Biophysical Research Communications, under the CC BY 4.0 license.*

Finally, the α-syn fibrils formed at increasing concentrations of each monovalent cation were analyzed by atomic force microscopy (AFM). From these images, I quantified the contour length and persistence length to enable a comparative analysis of the physical properties of the fibrils (Fig. 23). The AFM images (Fig. 23A-C) showed that fibrils formed in the presence of Na^+ (Fig. 23B) displayed a greater tendency to cluster compared to fibrils formed in the presence of K^+ (Fig. 23C). Fibril length (Fig. 23D) remained largely independent of the monovalent cation used during aggregation. This can likely be attributed to the shaking conditions and glass bead used to enhance aggregation, which induces fragmentation and hence is a strong determinant of fibril length in the assayed system. In contrast, analysis of the persistence length (Fig. 23E), a measure of fibril rigidity which is defined by the distance over which the fibril maintains a straight trajectory, revealed that fibrils formed in the presence of K^+ were substantially more rigid than those formed in the presence of Li^+ and Na^+. This observation aligns with previous findings showing that fibrils with a higher net protein charge tend to be more rigid [298], consistent with the lower binding affinity of K^+ to carboxylate groups [294]. This increased rigidity, and putatively charge, is likely to reduce the propensity of fibrils to cluster. The observation that monovalent cations can affect clustering propensity of fibrils may have implications for how α-syn fibrils organize into larger inclusion bodies, including Lewy bodies and Lewy neurites.

In summary, I demonstrated in **paper I** that monovalent cations play a substantial role in modulating the aggregation kinetics of α-syn fibril formation, with clear implications in both physiological processes and experimental design. I show that the type and concentration of monovalent cation can markedly influence primary nucleation, underscoring the need for careful consideration when selecting buffer composition for *in vitro* studies. Mechanistically, these effects can be partly explained by the distinct affinities of different monovalent cations for carboxylate groups and the empirical matching water affinities principle [295], which gains physiological relevance in the cell where α-syn is exposed to high intracellular levels of K^+, and transient influxes of Na^+ during neuronal activity. Beyond kinetics, I also demonstrated that monovalent cations can subtly influence the structural properties of the resulting fibrils. Differences were observed in β-sheet content as well as in fibril morphology, including rigidity and clustering propensity, parameters that may be important depending on the experimental or biological context. These findings raise the question of whether monovalent cations might also influence deeper structural features, such as internal packing and polymorph selection, which has previously been demonstrated for anions [20]. Finally, the observed effects on clustering may have relevance for PD, where Lewy bodies and Lewy neurites, which are primarily composed of α-syn aggregates, are pathological hallmarks. Understanding how monovalent cations influence both the aggregation kinetics and fibril morphology could therefore provide insights into primary nucleation and inclusion formation *in vivo*.

The main findings of **paper I**, specifically that Na^+ shortens the lag time in a concentration dependent manner by promoting primary nucleation while also stabilizing fibril structure, motivated my decision to use NaCl as the salt throughout the remainder of this thesis. These results also prompted me to do deeper investigation into the mechanisms governing α-syn aggregation kinetics and fibril structure, which I pursued in **papers II-III**

6.2. Impact of fragmentation on α-synuclein fibril formation

Having established that monovalent cations influence the aggregation kinetics and morphology of WT α-syn (**paper I**), I next examined how fragmentation affects aggregation kinetics and fibril morphology. To broaden the scope, I extended the analysis to include the familial α-syn mutants A30P, E46K, H50Q, and A53T, several of which are already known to form distinct fibril polymorphs (chapter 3.2), suggesting that they may also be differently susceptible to fibril breakage. Thus, in **paper II**, I investigated whether these mutants show different mechanistic responses and morphological outcomes when exposed to fragmentation compared to WT α-syn fibrils.

Studies in recent years on IAPP [22] and tau [23] have shown that *in vitro* generated fibrils are composed of heterogenous mixtures of polymorphs and that these populations can evolve over time through structural conversion. In this process, less stable polymorphs disassemble while more stable polymorphs form and grow, consistent with a rugged energy landscape model [299] in which multiple kinetically trapped polymorphs of similar stabilities can coexist. As described in chapter 3.2, α-syn aggregation *in vitro* is governed primarily by primary nucleation, elongation and secondary nucleation, while fibril fragmentation occurs at a comparatively slow rate. Consequently, fragmentation has been studied less extensively, even though it can modulate fibril growth by increasing the number of ends for elongation [87] and, inversely, facilitate disassembly by increasing the number of depolymerization sites [158].

6.2.1. Fragmentation differentially alters the aggregation kinetics of WT and mutant α-synuclein

To determine whether fragmentation can alter kinetic trajectories and increase structural conversion efficiency of WT and mutant (A30P, E46K, H50Q, A53T) variants of α-syn, I modified the standard ThT aggregation kinetics assay used in **paper I** to include an ultrasonication step after the reactions had reached the plateau phase, whereafter the samples were returned to the plate reader and allowed to re-aggregate. I also extended the conventional kinetic analysis by collecting samples for absorbance, SDS-PAGE and AFM prior to each ultrasonication step. This cycle was repeated multiple times to mimic the prolonged disease course of PD, during which, in theory, fibrils may undergo repeated rounds of growth and fragmentation (Fig. 24A).

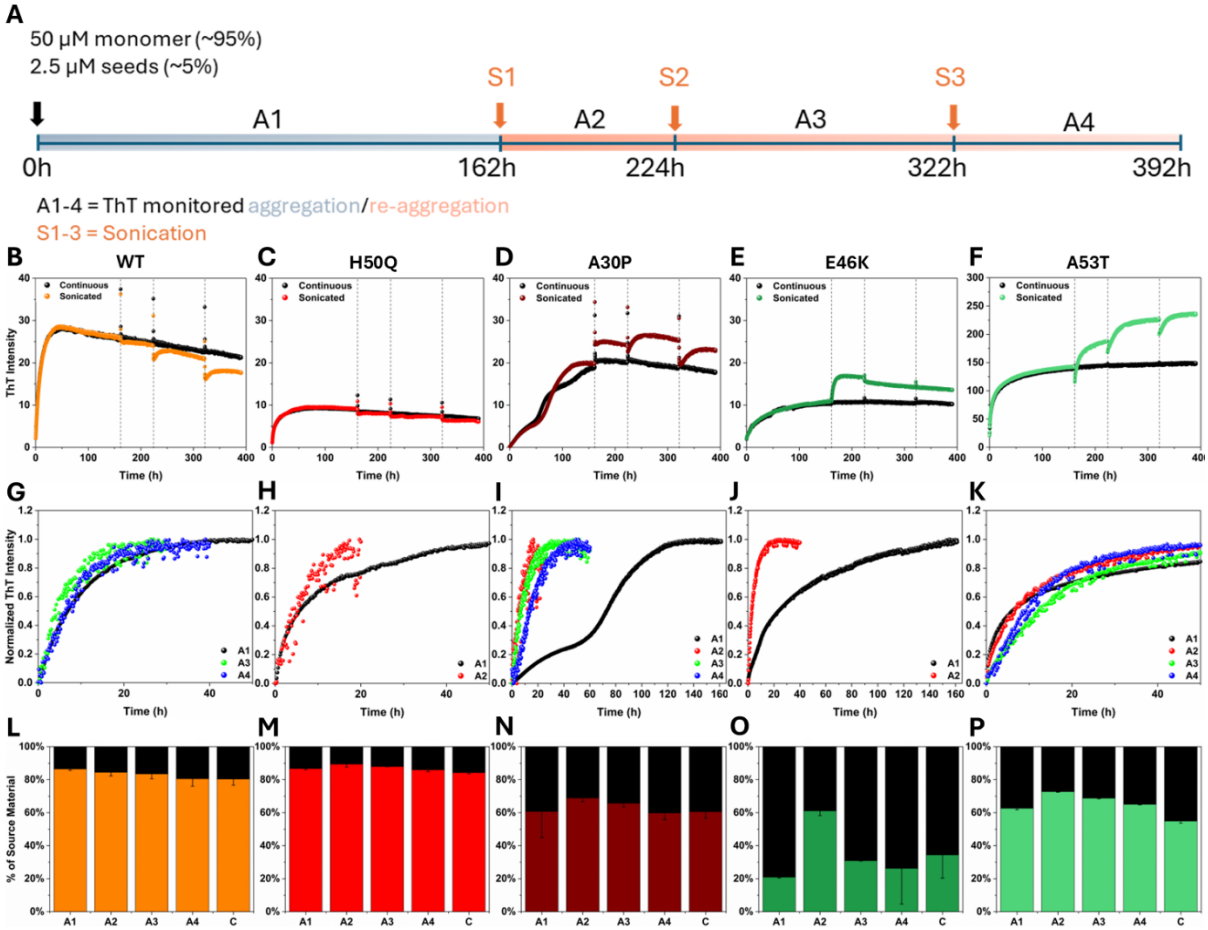

Figure 24. *Fibril fragmentation and re-aggregation in WT and mutant α-syn samples. (A) Schematic illustration of the experimental design. WT and mutant α-syn were subjected to multiple rounds of aggregation (A1-A4) and sonication (S1-S3) to generate shorter fibrils with increased number of ends while maintaining constant total α-syn concentration. Samples for absorbance spectroscopy, SDS-PAGE, and AFM were collected prior to each sonication, with additional AFM samples taken immediately afterward. Three independent experiments were conducted, and one representative dataset is shown (B-F) ThT-monitored aggregation kinetics for WT and mutant α-syn. Colored traces correspond to samples subjected to sonication at the indicated time-points whereas black traces represent continuously incubated controls. (G-K) Comparison of aggregation rates across A1-A4 for WT and mutant α-syn, displayed as normalized ThT fluorescence. (L-P) Distribution of WT or mutant α-syn (source material) between pellet and supernatant fractions at the end of A1-A4. C denotes end-point values for continuously incubated controls. Error bars represent SD (n = 2). All reactions contained 50 µM monomer, 2.5 µM PFFs, and 20 µM ThT in 20 mM Tris-HCl (pH 7.4) incubated at 37 ºC without further monomer addition. Reproduced from Havemeister et al., 2026, ´Fragmentation-Induced Disassembly and Reaggregation of α-Synuclein Amyloid Fibrils´, ACS Chemical Neuroscience, under the CC BY 4.0 license.*

Using this modified ThT assay (**paper II**), I found that ultrasonication-induced fragmentation produced clear changes in the ThT trajectories of the α-syn variants compared with the samples left unfragmented (denoted the 'continuous' samples in **paper II** and Fig. 24). After each sonication step, most variants showed a drop in ThT intensity relative to the pre-sonication level, strongly suggesting that fibrils rapidly disassemble upon fragmentation, resulting in a transient increase in the monomer pool available for renewed fibril growth.

During the subsequent re-growth phase, the variants separated into two distinct groups. WT and H50Q showed reduced ThT signal immediately after fragmentation but returned to approximately the same level as their respective 'continuous' samples (Fig. 24B-C). In contrast, A30P, E46K, and A53T showed reduced ThT fluorescence immediately after fragmentation but then exhibited progressively increasing ThT fluorescence (Fig. 24D-F). Strikingly, this division coincides with the timing of disease onset associated with the different variants, where WT and H50Q result in late-onset PD, whereas A30P, E46K, and A53T are associated with early-onset forms of disease. Among the early-onset variants, A30P and E46K re-aggregated considerably faster, whereas A53T re-aggregated more slowly (Fig. 24I-K). In contrast, the late-onset variants WT and H50Q showed only modestly accelerated kinetics during re-aggregation (Fig. 24G-H). These kinetic effects occurred despite overall fibril yield remaining stable for all variants except E46K, which showed an increase in both fibril yield and ThT fluorescence. Notably, the fibril yields also reflected the division between late- and early-onset, with late-onset variants producing considerably higher fibril yields than the early-onset variants (Fig. 24L-M)

The finding of increased ThT intensity for A30P, E46K, and A53T following re-growth after fragmentation, despite largely unchanged monomer and fibril concentration, strongly suggests that these changes arise from structural alterations within the fibril populations, consistent with previous reports on structural evolution for IAPP [22] and tau [23] fibrils. This is likely reflected in the enrichment or maturation of fibril polymorphs which either bind ThT more effectively or result in binding sites with higher quantum yield, or both. This pattern might reflect behavior consistent with fibril assembly progressing over a rugged energy landscape [299], where multiple polymorphic states become kinetically trapped and subsequently evolve. Sonication may accelerate this process by increasing the number of fibril ends available for depolymerization and elongation, thereby promoting the recycling of less stable fibril species and favoring the growth of more stable polymorphs, a mechanism previously implicated in fibril dynamics [300].

6.2.2. Fragmentation and re-aggregation drive changes in α-synuclein morphology

Having established that fragmentation can influence ThT binding and aggregation kinetics in a variant specific manner, I next wanted to investigate how repeated fragmentation and re-aggregation affected fibril morphology (length and height) using AFM, and whether these changes could provide insight into the observed variant specific ThT fluorescence alterations.

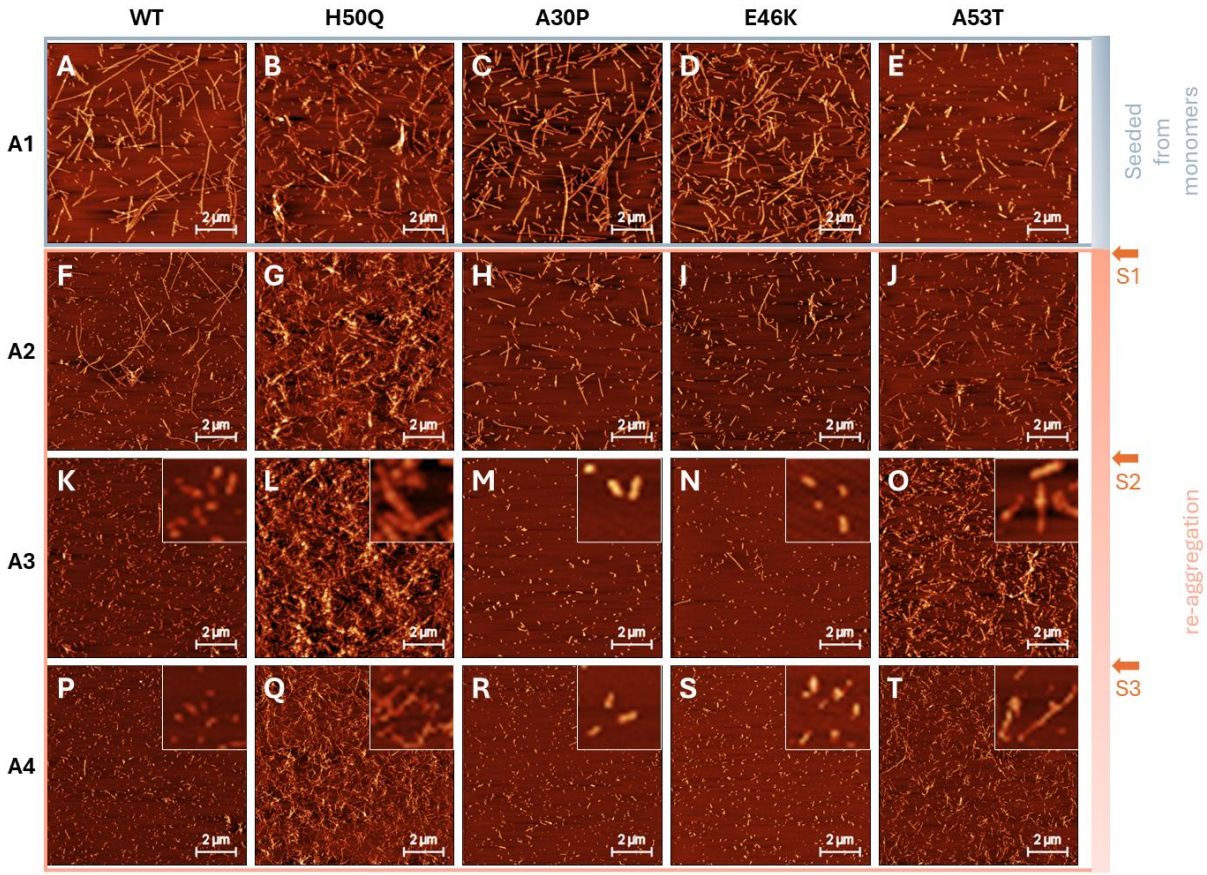

Figure 25. *AFM characterization of WT and mutant α-syn fibril morphology. AFM micrographs acquired at the end of aggregation A1-A4 (as defined in Fig. 24). (A-E) illustrate fibrils generated from monomer-seeded reactions, while (F-T) show the fibril morphologies observed following re-aggregation. Inserts in (K-T) show zoomed-in views to facilitate the visual interpretation of fibril structures. All images correspond to 10x10 µm regions, with 2 µm scale bars provided. Reproduced from Havemeister et al., 2026, 'Fragmentation-Induced Disassembly and Reaggregation of α-Synuclein Amyloid Fibrils', ACS Chemical Neuroscience, under the CC BY 4.0 license.*

Following the first aggregation which was seeded from monomers, WT and A30P α-syn fibrils predominantly appeared as long and straight (Fig. 25A, C), whereas H50Q fibrils were shorter and demonstrated a higher propensity to cluster (Fig. 25B). These features were also observed in **paper I**, where fibrils with higher net charge formed straighter, more rigid structures, while those with lower net charge were more flexible and prone to clustering. E46K fibrils had a curvilinear appearance (Fig. 25D), a morphology typically associated with protofibrils [301]. A53T fibrils were notably shorter and difficult to enrich on the mica (Fig. 25E), although the analysis of fibril yields showed that they formed with similar propensity as the other variants (Fig. 25P). This suggests that the A53T fibrils may have distinct surface properties. Structural differences between fibrils can strongly influence both ThT-binding affinity and quantum yield [302]. For Aβ, this principle has been demonstrated by markedly higher ThT fluorescence of Aβ40 fibrils compared with Aβ42 [303], which correspond to straighter versus more curvilinear fibril morphologies [304]. A similar structure-fluorescence relationship might explain the lower ThT emission observed for E46K and H50Q relative to WT, A30P, and A53T, suggesting that fibrils with greater structural order generally exhibit higher ThT fluorescence intensities (Fig. 24).

Following sonication, the fibrils became expectedly shorter (**Fig. 25F-T**). For H50Q fibrils, this prompted even more clustering (**Fig. 25G, L, Q**) whereas A53T fibrils appeared to adhere better to the mica with each successive fragmentation cycle (**Fig. 25J, O, T**), consistent with changes to their properties as suggested by the continuous increase in ThT fluorescence (**Fig. 24)**.

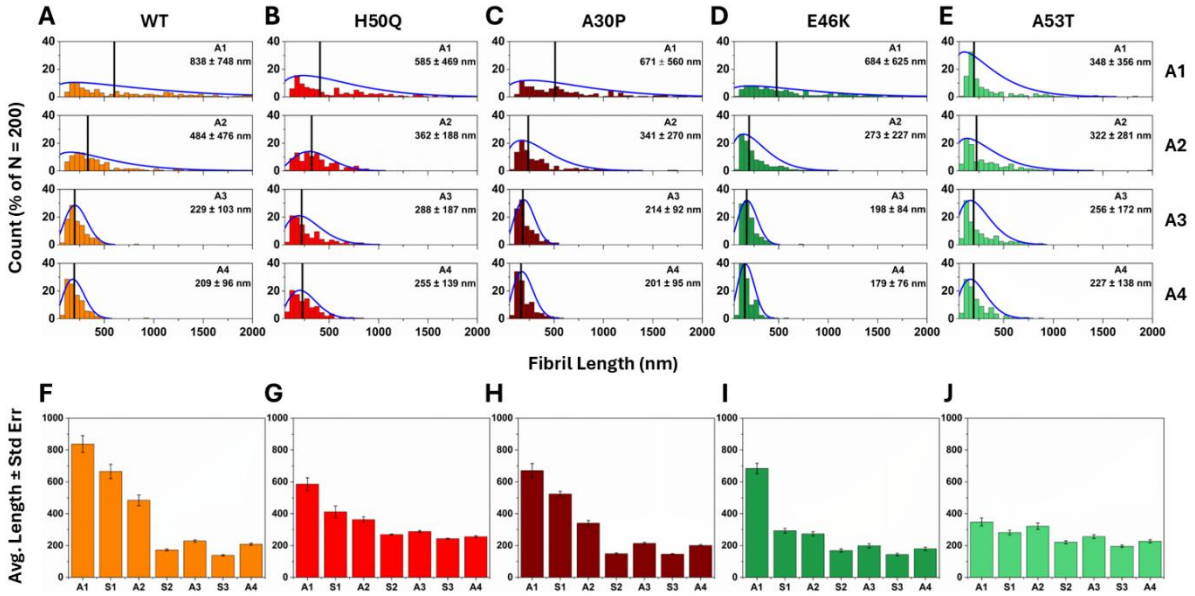

Figure 26. *Length characteristics of WT and mutant α-syn fibrils. (A-E) Fibril length distributions derived from AFM micrographs of the type shown in Fig. 25, acquired at the end of aggregation rounds A1-A4 (see Fig. 24). Mean lengths are indicated by black lines, while blue curves represent Weibull distribution fits to the data. The associated shape (κ)- and scale (λ) parameters are reported in the supporting information for this paper (Fig. S16). Data were obtained from 1-7 independent images per condition, comprising 200 fibrils in total (n = 200). (F-J) Mean fibril lengths ± standard error (n = 200) for each aggregation round, including S1-S3 samples collected immediately after sonication. Reproduced from Havemeister et al., 2026, 'Fragmentation-Induced Disassembly and Reaggregation of α-Synuclein Amyloid Fibrils', ACS Chemical Neuroscience, under the CC BY 4.0 license.*

I determined fibril lengths from the AFM images (Fig. 25) to quantify the observed progressive shortening of the fibrils following fragmentation. This analysis revealed that A53T formed considerably shorter fibrils than all other variants, already after the initial aggregation phase (Fig. 26). Fitting Weibull distributions to the length distribution data revealed that fragmentation became increasingly biased toward breakage of the persisting longer fibrils, while shorter fibrils fragmented less frequently. Notably, I had expected that the average fibril lengths would increase during the re-aggregation steps. This happened in the later phases of the experiments, whereas for the length distributions in A2 (following the first sonication (S1)), the opposite surprisingly occurred for all variants except A53T. A possible explanation to this observation is that depolymerization of unstable polymorphs occurs during A2, as indicated by the initial drop in ThT (Fig. 24B-F), and that new polymorphs form preferentially through processes such as secondary nucleation rather than elongation existing fibrils, resulting in the formation of more but shorter fibrils. Across re-aggregation steps A3 and A4, fibril lengths converged toward a stable interval defined by the

minimum imposed by sonication and the upper limit set by the renewed monomer-fibril equilibrium (Fig. 26F-J). Interestingly, the minimum lengths varied between variants, and the average lengths of H50Q and A53T fibrils were greater than those of other variants, suggesting that the fibril polymorphs formed for these variants may be slightly more resistant to fragmentation.

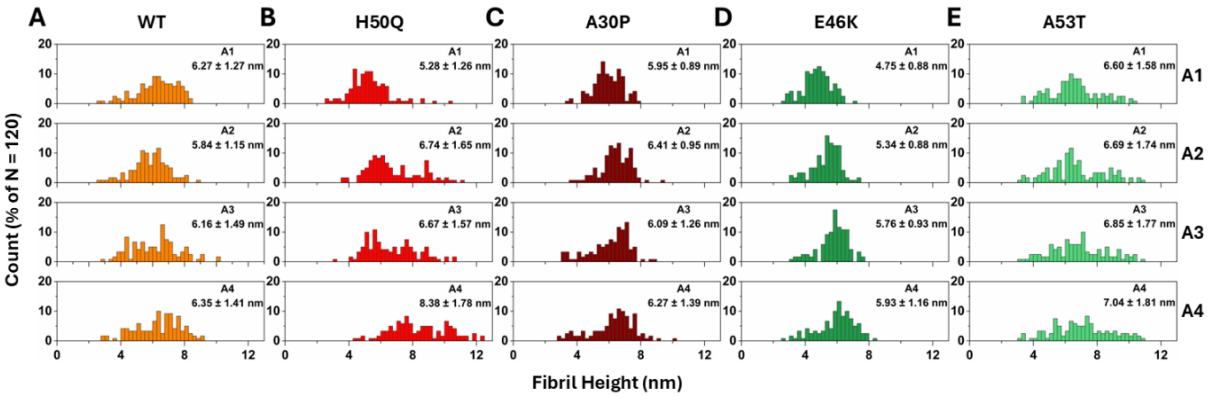

Figure 27. *Height characteristics of WT and mutant α-syn fibrils. Fibril height distributions for WT (A), H50Q (B), A30P (C), E46K (D), and A53T (E) fibrils were obtained from AFM micrographs similar to those in Fig. 25, collected at the end of aggregation rounds A1-A4 (see Fig. 24). Data were compiled from 1-7 independent images per condition, encompassing 120 fibrils in total. Reproduced from Havemeister et al., 2026, 'Fragmentation-Induced Disassembly and Reaggregation of α-Synuclein Amyloid Fibrils', ACS Chemical Neuroscience, under the CC BY 4.0 license.*

I also quantified fibril heights from the AFM images to determine whether repeated fragmentation and re-aggregation resulted in variant-specific differences in protofilament packing (Fig. 27). After the first aggregation, which was seeded from monomers (A1), all variants except E46K displayed average heights of ~5-6 nm, consistent with a two-protofilament arrangement [305]. The lower average heights of E46K fibrils aligns with their curvilinear appearance in the AFM images (Fig. 25D), further suggesting that E46K initially forms protofibrillar structures. A53T stood out by displaying a markedly broader height distribution than other variants, indicating a more heterogenous polymorph composition (Fig. 27A-E). Across the re-aggregation cycles, the most pronounced changes to fibril heights occurred for H50Q, which developed progressively broader height distributions, again consistent with polymorphic heterogeneity. Notably, H50Q and A53T, both showing broad height distributions, were also the only variants whose minimum fibril lengths remained larger than those of the other variants, suggesting that these thicker polymorphs may be more resistant to fragmentation. Meanwhile, E46K displayed a steady increase in average height across the re-aggregation cycles, consistent with maturation from protofibrils to thicker, more fully developed fibrils. This maturation of E46K fibrils is also reflected in the substantial enhancement of ThT intensity seen after the first sonication step (Fig. 24E). The results presented in Fig. 25-27 thus support the idea that fragmentation and re-aggregation can reshape fibril structure and favor certain polymorphs.

6.2.3. Re-aggregation after fragmentation shows distinct elongation rates in α-synuclein fibrils

Lastly, to further characterize the kinetics of seeded aggregation and re-aggregation, I combined the kinetic traces from Fig. 24 with the fibril length measurements from Fig. 26 to estimate elongation rates and the elongation speed per fibril.

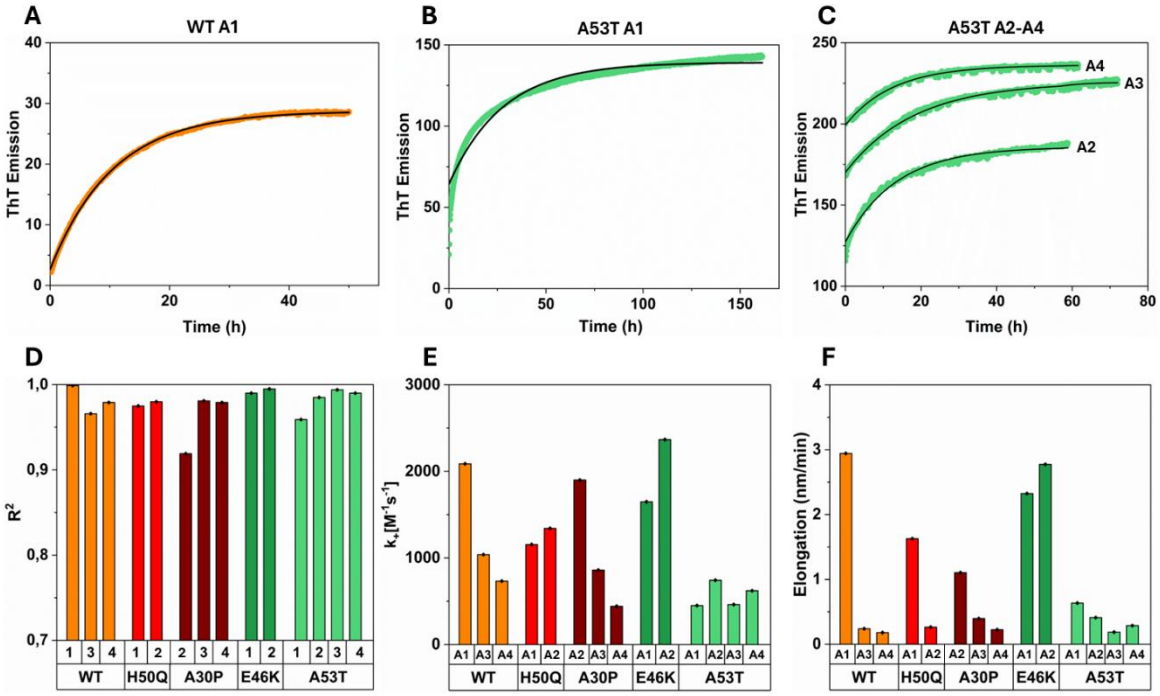

Figure 28. *Analysis of fibril elongation rates. (A-B) Representative kinetic profiles of WT and A53T from the first aggregation round (A1), fitted to a single-exponential model describing elongation-dominated growth behavior. (C) A53T re-aggregation curves from A2-A4, fitted using the same model. (D) R^2 values summarizing model fit quality for the datasets. (E) Estimated elongation rate constants ($M^{-1}s^{-1}$) and (F) corresponding fibril elongation speeds per fibril expressed in nm/min. Reproduced from Havemeister et al., 2026, ´Fragmentation-Induced Disassembly and Reaggregation of α-Synuclein Amyloid Fibrils´, ACS Chemical Neuroscience, under the CC BY 4.0 license.*

The kinetic traces were fit to single exponential functions (Fig. 28A-C) yielding consistently good fits in all cases ($R^2 > 0.9$, Fig. 28D), with most variants showing improved fits upon successive re-aggregation. This pattern suggests that elongation increasingly dominated the reaction kinetics, while secondary nucleation became less prominent. The variants differed with respect to elongation rates, and the rates during re-aggregation of each variant were generally different compared to its initially seeded reaction (Fig. 28E). WT α-syn showed an initial elongation rate of 2087 $M^{-1}s^{-1}$ consistent with previously reported values (2200 $M^{-1}s^{-1}$ [15], 3616 $M^{-1}s^{-1}$ [204]), and its elongation rate decreased with each re-aggregation. In contrast, E46K and H50Q elongated more rapidly after re-aggregation. A53T showed little difference in elongation rate, but a progressively better fit to the kinetic data was noted during the repeated re-aggregation (Fig. 28B-D). This, together with the findings that A53T formed much shorter fibrils in the first seeded reaction (Fig. 26J) could suggest that A53T aggregation was initially proceeding with higher contribution of secondary nucleation than

for the other variants. Elongation speed estimates (nm/min) were generally highest in the initially seeded reactions and decreased progressively with each re-aggregation, consistent with reduced monomer availability per fibril due to the progressively increasing number of fibril ends and due to that re-aggregation started with a lower available monomer pool. E46K was the exception, showing faster elongation per fibril during re-aggregation, in line with its altered monomer-fibril equilibrium and the curvilinear morphology which gradually transitioned into mature fibrils (Fig. 24-27).

In summary, in **paper II**, I demonstrate that α-syn fibrils are capable of structural conversion, yielding polymorphs with higher ThT fluorescence and that the propensity for such conversion is distinct for each variant. I show that fragmentation, despite receiving comparatively little attention in the field due to its lower *in vitro* frequency relative to primary nucleation, elongation, and secondary nucleation, can substantially reshape the polymorph composition of a fibril population. Fragmentation promotes the depolymerization of less stable polymorphs while simultaneously enabling the preferential growth of more stable ones, thereby driving structural conversion. I further show that the impact of fragmentation on aggregation kinetics and fibril morphology is highly variant specific. The early-onset familial mutants (A30P, E46K, A53T) appear to exhibit greater polymorphic flexibility, which may contribute to their earlier disease onset and more aggressive clinical progression. This is evident for E46K, which initially forms curvilinear, loosely ordered fibrils that, upon sonication, mature into thicker and possibly more stable and less cytotoxic structures, accompanied by increased ThT intensity. A53T shows an even more pronounced effect, with progressive ThT enhancement across all re-aggregation cycles and improved adherence to mica surfaces. Comparable morphology-dependent differences in fibril stability and toxicity have been observed across several amyloid system, including α-syn ribbons versus twisted fibrils [306], insulin fibrils [307], and prions [308]. Moreover, these findings reveal that, in addition to environmental factors such as monovalent cations and ionic strength (**paper I**), aggregation mechanisms like fragmentation can strongly influence the polymorphic landscape of α-syn fibrils.

In vivo, cellular factors such as chaperones [309] and proteolytic enzymes [310] are likely to increase the frequency of fragmentation beyond what is observed under controlled *in vitro* conditions, making fragmentation a potentially important driver of structural evolution and disease progression. These insights are relevant for understanding PD pathogenesis, where current structural knowledge is largely limited to fibrils isolated post-mortem and therefore reflects only the end stage of a long and dynamic disease process. They raise the possibility that less stable fibril polymorphs present early in disease may be more toxic than the more stable species that dominate later stages, an idea consistent with *in vitro* studies of Aβ42, in which less stable oligomers exhibit greater toxicity than their more stable counterparts [311].

6.3. Phenotyping cross-seeding polymorphs using fluorescence lifetime spectroscopy

In the first part of my thesis work, I showed that monovalent cations modulate both the aggregation kinetics and the fibril morphology of WT α-syn (**paper I**). I then demonstrated that fragmentation can further shape these processes, and that WT and the familial mutants A30P, E46K, H50Q, and A53T respond differently under such conditions, resulting in variant dependent polymorphism with fibril structures that can structurally evolve following sonication (**paper II**). Building on these findings, I next asked how these different α-syn variants influence one another through cross-seeding, and whether I could distinguish the resulting fibril polymorphs from that of the parent seeds using ThT fluorescence lifetimes (**paper III**).

Recent cryo-EM studies have revealed that several neurodegenerative disorders, including PD, are characterized by disease-specific fibril polymorphs [21]. For α-syn, this diversity is exceptional, with more than 130 distinct high-resolution structures having been resolved from both *in vitro* assemblies and *in vivo* derived fibrils [141]. In parallel, accumulating evidence indicates that multiple disease-associated proteins can undergo structural evolution over time [22,23,312]. However, the determinants that govern the emergence and persistence of specific fibril polymorphs remain poorly understood. Although cryo-EM provides high-resolution structural information, its time-intensive workflow, limited accessibility, and the need for substantial expertise make time-resolved studies challenging. As a result, cryo-EM alone is not sufficient to capture polymorph evolution across large sample sets, underscoring the need for complementary methods capable of probing fibril dynamics more efficiently. Dye-based assays, on the other hand, can provide a rapid and cost-effective means to distinguish fibril polymorphs, albeit with a lower level of structural detail. ThT, the most widely used probe for monitoring amyloid formation kinetics [302], acts as a molecular rotor [313], and binds to multiple sites located within the fibril structure [278,314] which are defined by local geometry and chemical microenvironment of the underlying fibril structure. Consequently, studies on Aβ fibrils have shown that different polymorphs generate distinct ThT fluorescence lifetime signatures [303], suggesting that this fluorescence methodology enables concentration-independent readouts of dye-binding microenvironments and sensitive discrimination of structural differences across fibril samples. In **paper III**, I expanded this concept to explore if fibrils formed from WT and mutant α-syn could be distinguished by their fluorescence lifetimes. I then used this approach to investigate cross-seeding outcomes, identifying effects arising from templated structural inheritance and distinguishing them from those dictated by monomer-specific conformational biases. Cross-seeding represents a disease-relevant scenario, given that autosomal inheritance ensures simultaneous expression of WT and mutant α-syn in patients carrying familial variants of the SNCA gene.

6.3.1. Self-seeding results in distinct aggregation kinetics and ThT fluorescence lifetime signatures

To lay the foundation for **paper III**, I started off by monitoring self-seeded aggregation kinetics of WT and mutant (A30P, E46K, H50Q, A53T) α-syn in the presence of 0-25% seeds (Fig. 29).

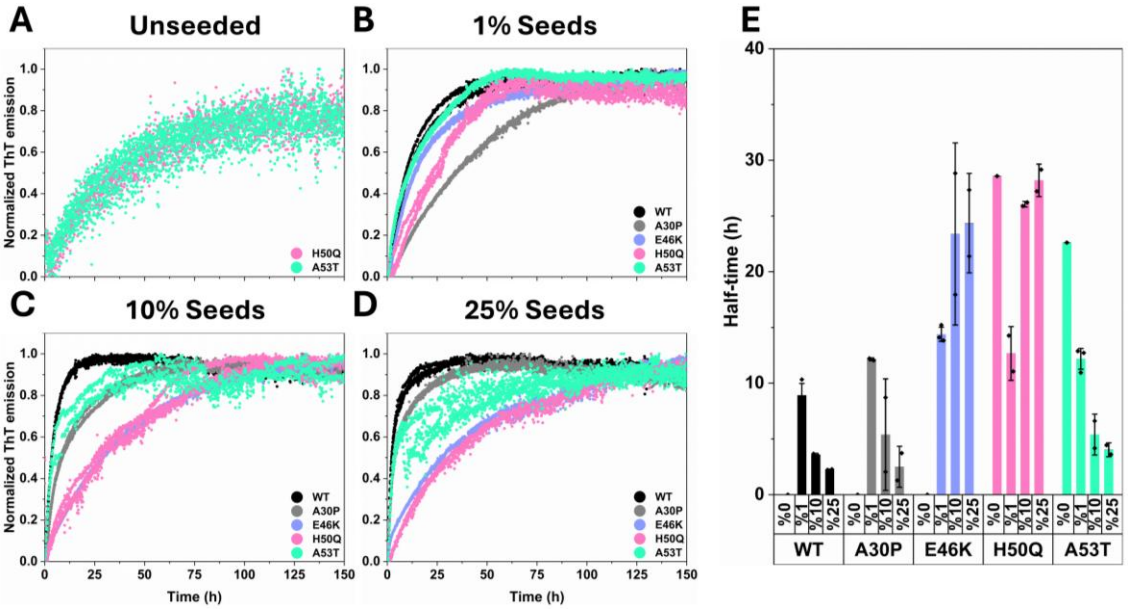

Figure 29. *Differences in spontaneous and self-seeded aggregation among α-syn variants. Aggregation kinetics were monitored by ThT fluorescence under quiescent conditions at 37°C in 20 mM Tris-HCl (pH 7.4) with 100 mM NaCl, using 50 μM total α-syn (monomer + seeds) and 20 μM ThT. All protein variants were monomerized by SEC prior to initiating the reactions. (A) Non-seeded aggregation of H50Q and A53T. WT and the remaining mutant variants did not aggregate in the absence of seeds. (B-D) Seeded aggregation with 1% (B), 10% (C), or 25% (D) PFFs, shown as normalized ThT fluorescence (technical triplicates, n = 3). Full experimental repeats are provided in the supporting information for this article. (E) Aggregation half-times calculated from the curves in A-D and the technical repeats from the supporting information, plotted as mean ± SD. N = 1, n = 3 for 0% seeds, N = 3, n = 3 for 1% seeds and N = 2, n = 3 for 10% and 25% seeds.*

First, I compared the aggregation kinetics of the α-syn variants and showed that all variants displayed distinct aggregation kinetics, similar to what was observed in **paper II**. Under the conditions tested, H50Q and A53T showed some limited spontaneous fibril formation in the absence of seeds (Fig. 29A), whereas all other variants strictly required seeds to initiate self-assembly (Fig. 29B-D). WT α-syn consistently aggregated more rapidly than the familial mutants. This observation contrasts with earlier reports showing that, under non-seeded conditions, the mutants are associated with accelerated aggregation [315,316], yet aligns with previous seeding-based studies [317]. This indicates that the familial α-syn variants strongly influence and enhance primary nucleation. Analysis of aggregation half-times revealed distinct seeding responses among the α-syn variants. WT, A30P, and A53T displayed progressively shorter half-times with increasing seed concentrations, which is the expected behavior in seeded aggregation. E46K and H50Q, on the other hand, aggregated more slowly

as the seed concentration increased (Fig. 29E). Such behavior has been recently described in systems where the number of added seeds approaches the number of aggregates formed *de novo* during the reaction [156]. In such a regime, nucleation is negligible and kinetics are governed almost exclusively by elongation.

After demonstrating that WT and familial α-syn variants follow variant-specific aggregation kinetics, I sought to determine whether these differences extend to their ThT fluorescence lifetimes (Fig. 30), which report on the dye-binding microenvironment.

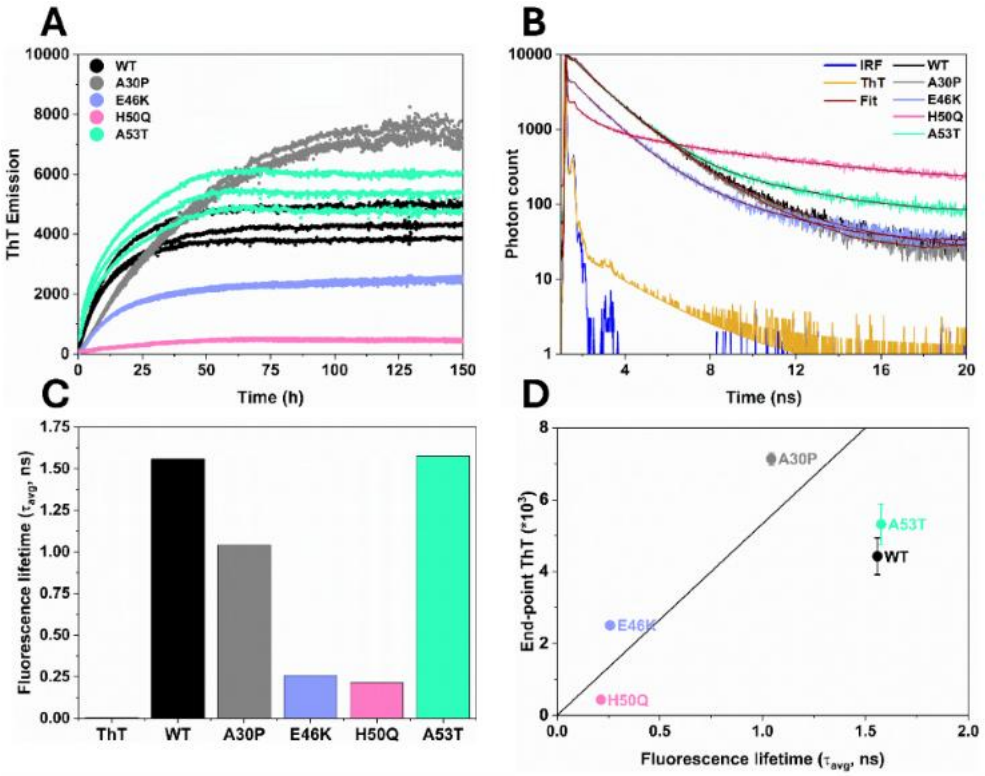

Figure 30. *ThT fluorescence lifetimes distinguish α-syn fibril variants. (A) Non-normalized ThT aggregation curves for α-syn seeded with 1% PFFs, corresponding to the normalized data in Fig. 29B. (B) Time-resolved ThT fluorescence decay profiles recorded for the different α-syn fibril variants at the end-points of the reactions shown in (A). Decays were acquired by time-correlated single-photon counting (TCSPC) with 10,000 detected photons in the top channel. ThT in buffer (orange) and the instrument response function (IRF, blue) are included for comparison. Triple-exponential decay functions (solid lines) were fitted to extract fluorescence lifetimes. (C) Amplitude-weighted average fluorescence lifetimes ($\tau_{avg} = \Sigma \alpha_i \tau_i$) derived from the fits in (B). (D) Correlation between end-point ThT fluorescence intensity and τ_{avg} with the linear regression fit ($R^2 = 0.72$). All measurements were performed using 5 μM fibrils and 20 μM ThT.*

All α-syn variants displayed clearly distinguishable end-point ThT emission (Fig. 30A), consistent with underlying differences in fibril structure, dye-binding microenvironments, and/or fibril mass. To probe these differences more directly, and to avoid concentration-dependent effects, time-resolved ThT fluorescence decay curves (Fig. 30B) were recorded for samples collected at the end-points of the aggregation reactions (Fig. 30A). All fibril samples exhibited substantially slower fluorescence decays than ThT in buffer, and the decay profiles differed markedly between variants. Triple-exponential fitting of the decay curves enabled estimation of amplitude-weighted average fluorescence lifetimes, revealing variant-specific lifetime signatures (Fig. 30C). Lifetimes ranged from fast-decaying (~0.25 ns, E46K, H50Q) to slower decaying species (~1.5 ns, WT, A53T), demonstrating that each variant produces distinct ThT-binding environments, consistent with previous reports showing that structural features of amyloid fibrils define the geometry and chemical properties of dye-binding sites [314,318,319]. Comparing end-point ThT intensity against the corresponding average lifetime revealed a moderately positive correlation (Fig. 30D), indicating that the intensity differences observed in Fig. 30A primarily reflect variations in ThT quantum yield, rather than differences in dye binding affinity or fibril mass. Despite this correlation, ThT intensity remains a one-dimensional readout and cannot discriminate between distinct polymorphs.

6.3.2. Monomer-seed pairing determines cross-seeding aggregation kinetics

Familial SNCA mutations follow an autosomal dominant inheritance pattern, whereby the WT allele remains expressed alongside the mutant allele. Consequently, multiple α-syn variants coexist within the same cellular environment, where they can interact and influence one another's aggregation behavior and possibly morphology. Such coexistence makes heterologous cross-seeding highly likely *in vivo*, yet its impact on aggregation kinetics and the emergence of distinct fibril polymorphs remains understudied.

Having established that fluorescence lifetime signatures can reliably distinguish the polymorphs formed by self-seeded WT and mutant α-syn variants, I next wanted to figure out whether I could use the same framework to categorize cross-seeded fibrils. Specifically, I wanted to examine whether fibrils generated through WT-mutant cross-seeding retain the lifetime signature of the parent seed, obtain the preferred lifetime signature of the seeding monomer, or possibly undergo structural evolution that produces an entirely new ThT lifetime signature. To address this, I first examined the aggregation kinetics for all pairwise seed-monomer combinations (Fig. 31). These measurements allowed me to assess how cross-seeding influences kinetic profiles and to determine whether kinetic behavior alone can provide clues about structural inheritance or divergence.

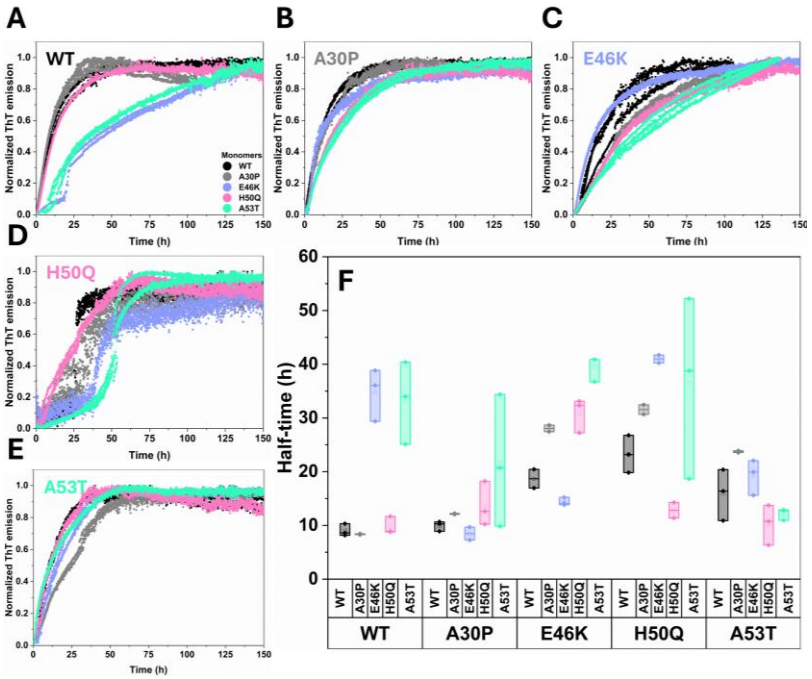

Figure 31. *α-synuclein fibril variants display distinct cross-seeding kinetic profiles. (A-E) Normalized ThT aggregation kinetics for 50 μM α-syn monomers cross-seeded with 1% PFFs of the indicated variants in 20 mM Tris-HCl, 100 mM NaCl, pH 7.4 and 20 μM ThT. All variants were monomerized by SEC immediately prior to initiating the kinetic experiments. All kinetic curves represent technical triplicates (n = 3). Independent experimental repeats are provided in the supporting information for this article. (F) Aggregation half-times extracted from the kinetic curves in panels A-E and from additional replicates in the supporting information, shown as mean ± SD (N = 3, n = 3).*

Analysis of the aggregation kinetics curves revealed that cross-seeding generally proceeded more slowly than self-seeding (Fig. 31A-F). The majority of reactions displayed concave, lag-free kinetics, consistent with elongation-dominated seeded growth. H50Q represented a notable exception. Whereas the self-seeded H50Q reaction displayed concave and lag-free kinetics, cross-seeding monomers of any other variant produced pronounced lag phases and sigmoidal behavior, indicating impaired elongation and limited sequence compatibility. Interestingly, A53T showed an asymmetric compatibility landscape. A53T monomers consistently exhibited slower fibril growth when seeded by other variants (Fig. 31A-D, Fig 31F), whereas A53T seeds efficiently recruited monomers from all other α-syn variants (Fig. 31E-F). This asymmetry suggests that A53T acts as a broadly permissive template, while A53T monomers impose stricter constraints.

6.3.3. Fluorescence lifetime signatures differentiate fibril polymorphs generated through cross-seeding

Having shown that cross-seeding produces seed-monomer dependent aggregation kinetics, I next wanted to perform a deeper analysis of these differences by examining the ThT fluorescence decay profiles and corresponding fluorescence lifetime signatures (Fig. 32).

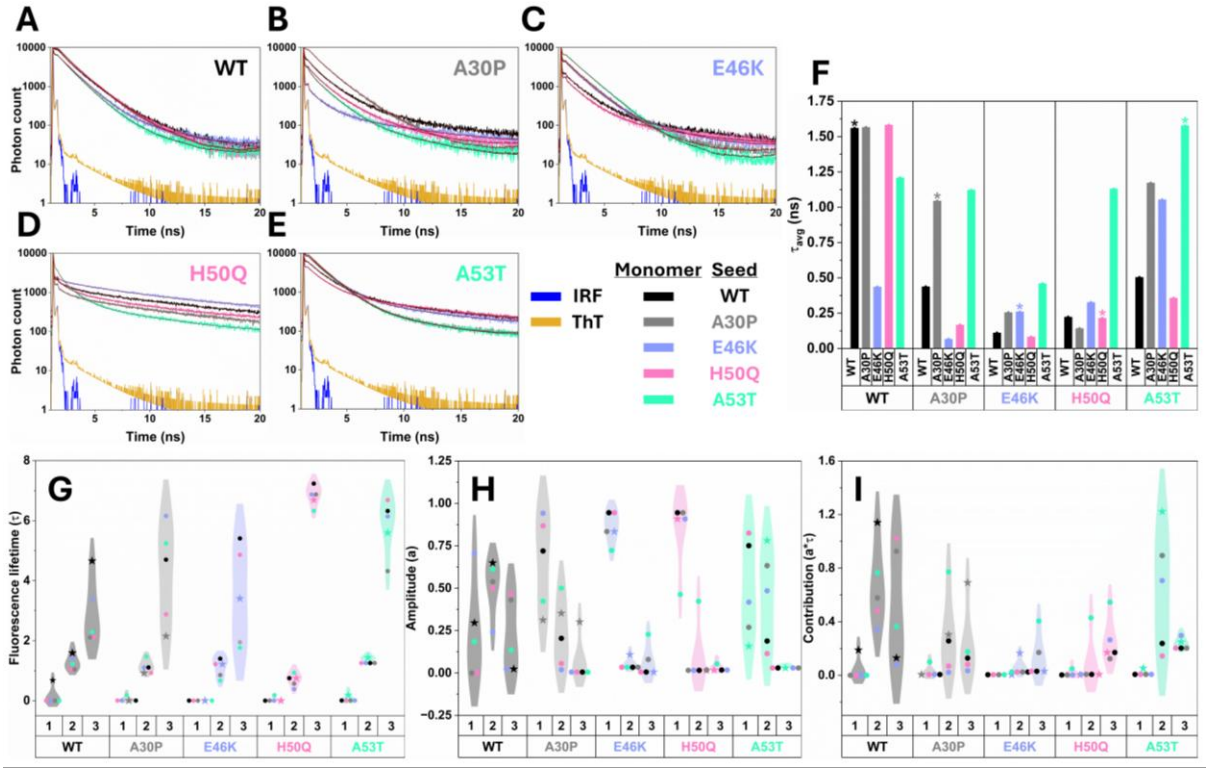

Figure 32. *Fluorescence lifetime component analysis reveals distinct signatures among cross-seeded α-synuclein fibril variants. (A-E) Time-resolved ThT fluorescence decay curves recorded for the different cross-seeded α-syn fibril samples. All measurements were performed on samples collected at the end-points of the kinetics reactions shown in Fig. 31A-E. The fibril concentration was 5 μM and ThT concentration 20 μM for all experiments. Decays were acquired by time-correlated single-photon counting (TCSPC) until 10,000 photons were collected in the top channel. For reference, decay curves for ThT in buffer (orange) and the instrument response function (IRF, blue) are included. Solid lines represent triple-exponential fits to the experimental data. (F) Amplitude-weighted average fluorescence lifetimes ($\tau_{avg} = \Sigma\alpha_i \tau_i$) derived from the fitted decay parameters in panels A-E. (G-I) Analysis of the three fitted lifetime components (τ_1, τ_2, τ_3), their associated amplitudes (a_1, a_2, a_3), and their absolute contributions to the overall decay ($a_1\tau_1$, $a_2\tau_2$, $a_3\tau_3$).*

Time-resolved ThT fluorescence decays (Fig. 32A-E) revealed pronounced seed-monomer dependent differences in the decay profiles. To quantify these differences, triple-exponential fitting, performed as in Fig. 29, yielded amplitude-weighted average fluorescence lifetimes, which differed substantially across the self- and cross-seeded samples (Fig. 32F). Across all conditions, τ_{avg} values fell within the 0.25-1.5 ns range of the self-seeding reactions, however, these lifetimes could not be accounted for by simple linear combinations of the seed and monomer lifetimes observed under self-seeding conditions. This deviation indicates that

cross-seeding does not merely propagate structural features of the seed through templating but instead generates more structurally complex fibril populations with distinct ThT-binding microenvironments.

To obtain a more detailed and discriminating analysis of these differences, I examined the three individual lifetime components separately (Fig. 32G-H). Across all seed-monomer combinations the analysis revealed a short-lived component (τ_1 = 80 ± 170 ps), an intermediate-lived component (τ_2 = 1.2 ± 0.34 ns), and a long-lived component (τ_3 = 4.7 ± 1.88 ns). These components can be interpreted as reflecting distinct types of ThT-binding modes, ranging from weakly associated dye populations to more tightly confined states with greater restricted rotational freedom, resulting in correspondingly longer lifetimes [302,319]. Notably, fibrils resulting from cross-seeding with H50Q seeds exhibited three tightly clustered and well-defined lifetime regimes, indicating a relatively homogenous ThT-binding environment. In contrast, the other variants showed greater variability, particularly in the long-lived component (τ_3), suggesting more structurally diverse fibril populations. Analysis of the amplitude distributions (a_1, a_2, a_3, Fig. 32H) showed that τ_1 amplitudes were highly variably across most variants and therefore provided limited discriminatory power. In contrast, τ_2 and τ_3 displayed more distinct and consistent patterns. WT, A30P, and A53T exhibited high a_2 and correspondingly elevated a_3, whereas E46K and H50Q showed markedly lower values.

To better capture the distinct fluorescent micro-environments of ThT bound to the fibrils, I analyzed the amplitude-lifetime products (Fig. 32I, $a_1\tau_1$, $a_2\tau_2$, $a_3\tau_3$, denoted as contributions in the figure), which provide a more representative measure of each lifetime component's contribution than amplitude or lifetime alone. This showed that variations in $a_2\tau_2$ and $a_3\tau_3$ dominate the differences observed between the cross-seeded samples, indicating that the intermediate- and long-lived states drive most of the fluorescence heterogeneity. A53T-seeded reactions varied mainly in $a_2\tau_2$, E46K and H50Q in $a_3\tau_3$, and WT and A30P in both, showing that cross-seeded fibrils can be effectively separated by their fluorescence lifetime signatures. The lifetime-derived structural variation (Fig. 30, 32) is in agreement with earlier observations that substitutions near or within residues 47-56 can remodel fibril structure [320]. E46K, H50Q, and A53T each perturb distinct stabilizing interactions, E46K the E46-K80 salt bridge [90], H50Q the H50-E57 protofilament interface [109], and A53T the protofilament alignment [176], while A30P, positioned outside the β-sheet core, maintains a WT-like fold [169].

Having established that the ThT fluorescence decay profiles of each seed-monomer combination contain highly discriminative structural information relevant to disentangle outcomes of self- and cross-seeded α-syn aggregation reactions, I next sought to differentiate α-syn polymorphs through multidimensional lifetime analysis (Fig. 33).

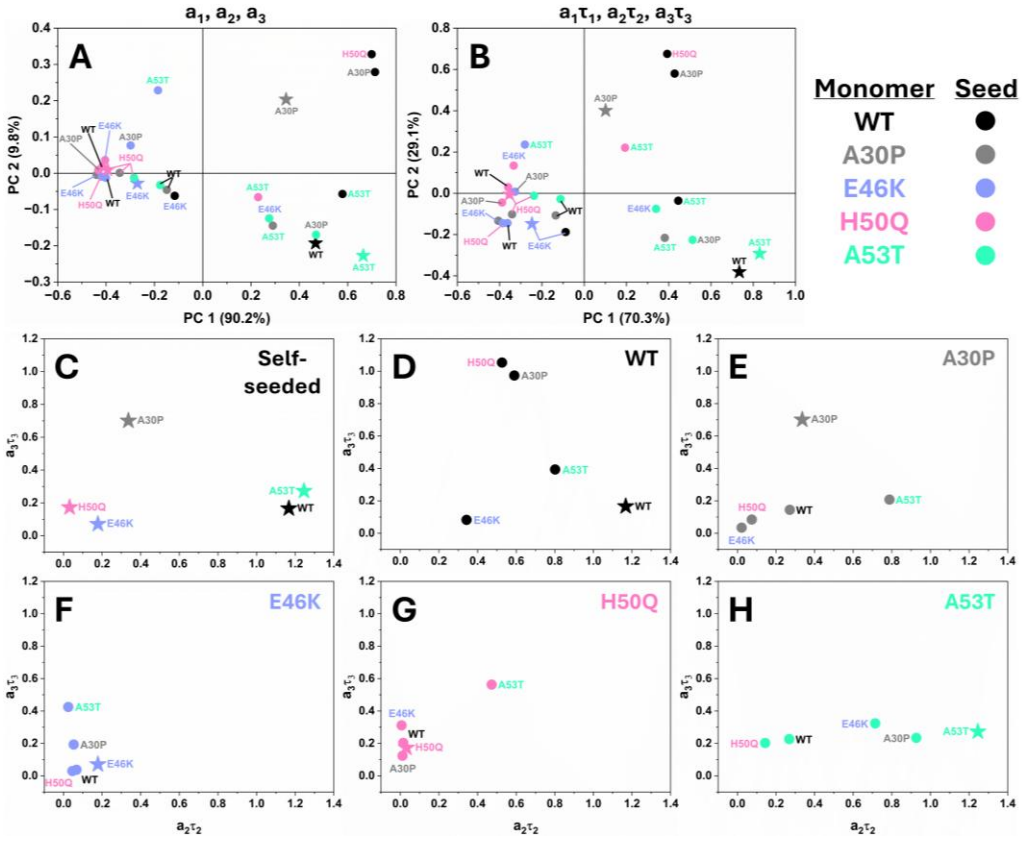

Figure 33. *PCA of ThT fluorescence lifetime parameters distinguishes α-synuclein fibril phenotypes arising from different seed-monomer combinations. (A-B) Two-dimensional PCA projections of the first two principal components (PC1, PC2) derived from (A) the lifetime amplitudes (a_1, a_2, a_3; PC1 = 90.2%, PC2 = 9.8%) and (B) the amplitude-lifetime contribution ($a_1\tau_1$, $a_2\tau_2$, $a_3\tau_3$; PC1 = 70.3%, PC2 = 29.1%) obtained from the fluorescence lifetime data in Fig. 32. (C-H) Distribution of self- and cross-seeded fibril variants in the $a_2\tau_2$ versus $a_3\tau_3$ contribution space. (C) shows the self-seeded samples as reference points, while (D-H) group the data according to the seed variant. Symbols are color-coded by fibril type, and labels denote the monomer identity as indicated in the top row legend. Star-shaped symbols in figures C-H denote the self-seeded controls.*

To contextualize the information obtained from the ThT decay profiles, I applied principal component analysis (PCA) and plotted the first two components (PC1, PC2) derived from the amplitudes a_1, a_2, a_3 (Fig. 33A) and from the corresponding contributions $a_1\tau_1$, $a_2\tau_2$, $a_3\tau_3$ (Fig. 33B). PCA analysis of the ThT lifetime amplitudes showed that most variance (~90%) was captured by PC1, reflecting shifts between the short- and intermediate-lived ThT states. This revealed clear clustering for fibrils seeded with E46K or H50Q at negative PC1, whereas WT-seeded samples were more dispersed at positive PC1 and A30P- and A53T-seeded samples were mostly unclustered. By also examining monomer-dependent patterns, I found that E46K and H50Q monomers consistently produced fibrils that preferentially clustered with their self-seeded states, irrespective of the nature of the seed. This indicates that these monomers strongly impose their preferred conformations on the aggregation product. A53T monomers showed similar clustering, although less pronounced, while WT and A30P monomers produced more heterogenous assemblies, indicating greater conformational flexibility.

The contribution PCA (Fig. 33B) largely recapitulated these relationships, with PC1 (~70% variance) dominated by $a_2\tau_2$ and PC2 (~29%) by $a_3\tau_3$. This confirms that the intermediate- and long-lived ThT states are the most discriminative factors of fibril structure as suggested by the data in Fig. 32. Because the PC1 and PC2 axes reflect largely independent photophysical features, the contribution PCA provided greater separation of fibril populations than the amplitude PCA. Motivated by this, I examined fibril distributions directly in the $a_2\tau_2$/ $a_3\tau_3$ feature space (Fig. 33C-H). This representation resolved self-seeded variants more clearly than average lifetimes alone and revealed that cross-seeding generally broadened the distribution, consistent with increased structural complexity. Notably, E46K- and H50Q-seeded fibrils remained tightly grouped with their self-seeded counterparts, supporting the conclusion of strong templating and a high degree of structural conservation as observed in the PCA. In contrast, WT-, A30P-, and A53T-seeded fibrils re-distributed more broadly, indicating greater conformational permissiveness and stronger monomer-dependent effects. Collectively, these patterns reveal a hierarchy of conformational influence, in which some monomers resist seed-imposed conformations and instead enforce their own preferred structures, while others are more susceptible to seed-driven propagation, producing a landscape of structurally diverse fibril polymorphs characterized by distinct ThT lifetime signatures. This is in line with previous observations showing that, although seeds can impose their structural features [174,321], fibril architecture can also be shaped by the identity of the monomer [120,322].

Having observed that ThT lifetime signatures can discriminate between fibril polymorphs, I next returned to the aggregation kinetics to assess whether a structure-kinetics derived landscape could further resolve templating strength. To this end, I plotted the aggregation half-time against $a_2\tau_2$, the dominant descriptor of variation in the fluorescence decay (Fig. 34).

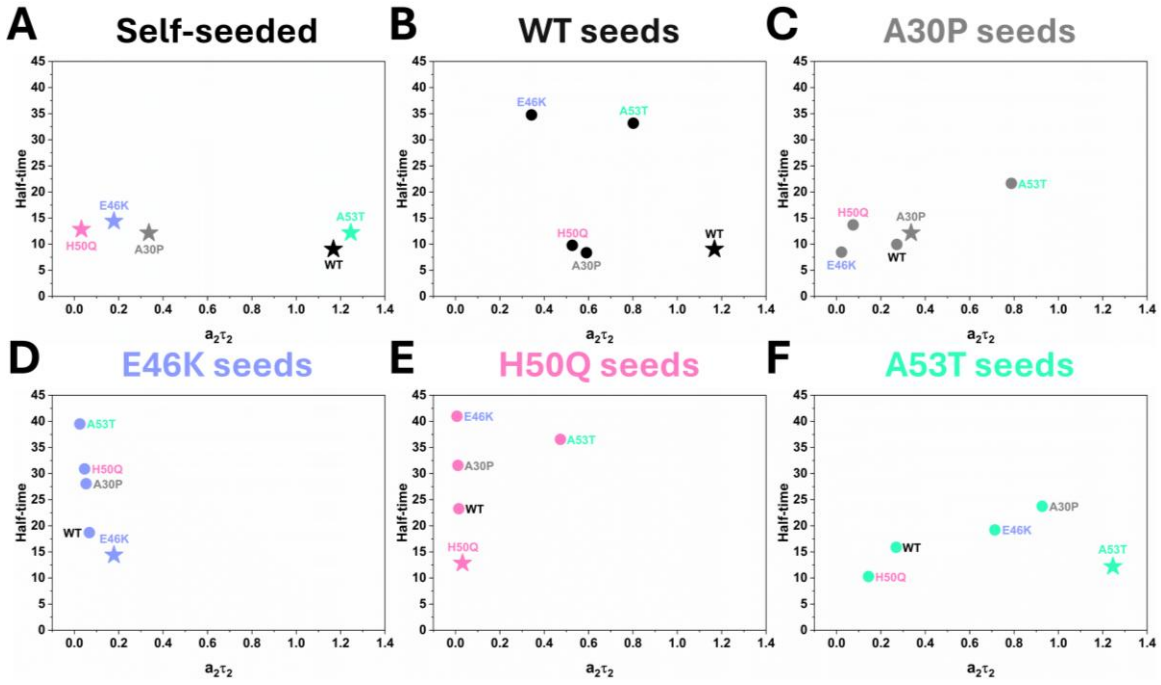

Figure 34. *Structure-kinetics landscapes for mapping α-synuclein fibril phenotypes. (A-F) Distribution of self- and cross-seeded α-syn variants within a structure-kinetics landscape defined by aggregation half-times and the $a_2\tau_2$ contribution parameter, using data from Fig.*

31F and Fig. 32. Symbols are color-coded by fibril type, and labels indicate monomer identity (WT = black, A30P = grey, E46K = purple, H50Q = pink, A53T = teal). Star-shaped symbols denote the self-seeded reference samples.

Generally, although the self-seeded samples spanned a range of $a_2\tau_2$ values (Fig. 34A), their aggregation half-times remained relatively similar (~10-15h), whereas many cross-seeding reactions exhibited substantially longer half-times (Fig. 34B-F). Notably, E46K- and H50Q seeded reactions consistently showed long half-times (Fig. 34D-E). When considered together with their distinct and clustered ThT lifetime signatures (Fig. 33F-G), these data suggest that highly selective structural templating is accompanied by a high kinetic cost. Cross-seeding with A30P seeds produced half-times comparable to self-seeding, even though their spread along the $a_2\tau_2$ axis indicates the formation of hybrid or monomer-biased polymorphs (Fig. 34C). This pattern points to good kinetic compatibility, but limited templating strength. A53T monomers, in contrast, consistently generated some of the slowest aggregation reactions (Fig. 34B-E), yet the resulting fibrils still tended to cluster near the A53T self-seeded state (Fig. 33A-B). Although this clustering was less tight than that observed for E46K and H50Q, it nonetheless suggests that A53T monomers exert strong structural control which can potentially override seed derived conformations.

In summary, in **paper III**, I demonstrate that ThT fluorescence lifetimes provide a highly sensitive readout of amyloid structural states, enabling reliable differentiation of α-syn fibril polymorphs without the need for atomic-resolution methods. Rather than aiming to reconstruct detailed structures, the approach offers a practical framework for phenotypic comparison and large-scale classification across diverse fibril preparations. Utilizing ThT's behavior as a molecular rotor [313], which enhances both quantum yield and fluorescence lifetime upon binding to cross-β architecture (Chapter 5.2) [278], allows us to probe structural environments within amyloid fibrils, thus complementing information on larger scale morphological variation that can be attained from AFM. Because fibrils present multiple, structurally distinct binding sites [314,318,319], lifetime measurements can resolve subtle concentration-independent differences that intensity-based assays fail to detect, making ThT fluorescence lifetime analysis a robust probe of structural variation across fibril populations [303]. Applying this approach revealed that WT and familial α-syn variants (A30P, E46K, H50Q, A53T) differ markedly in their behavior during cross-seeding. E46K and H50Q consistently preserved their self-seeded lifetime signatures in both seeding and being seeded contexts, indicating strong conformational enforcement, although at a kinetic cost. In contrast, WT and A30P displayed greater structural flexibility and permissiveness, while A53T exhibited intermediate behavior, supporting outcomes ranging from faithful templating to monomer-driven restructuring or the emergence of new polymorphs. Understanding these mechanisms is crucial in the context of familial Parkinson's disease, where disease progression may be shaped not only by mutation-specific fibril structures but also by the emergence of new assemblies generated through their interactions.

6.4. Linking biophysical characteristics of α-synuclein variants to cellular behavior

Having demonstrated in **papers I-III** that monovalent cations, fragmentation and cross-seeding can strongly modulate the aggregation kinetics and fibril morphology of WT and mutant (A30P, E46K, H50Q, A53T) α-syn *in vitro*, I sought to determine how these biophysically defined factors translate into uptake and seeding behavior within the cellular environments of SH-SY5Y neuroblastoma cells and primary mouse and rat neuronal cultures (**paper IV**).

Almost two decades ago, post-mortem analyses of PD patients who had received neuronal grafts revealed that α-syn pathology had propagated into the transplanted neurons, with Lewy body inclusions appearing in the grafted cells [12]. This phenomenon was subsequently reproduced in mouse models [244,323], primary cell models [276,324] and cell lines [256,257], establishing prion-like propagation as a central mechanism in the spread of α-syn pathology in PD. Prion-like propagation, defined by the recruitment of endogenous monomer into the amyloid state by propagated seeds has also been documented for several other amyloid forming proteins [325-330]. Although it is now clear that amyloid fibrils primarily internalize through the endosomal pathway [257,331] and that fibril size [87,257] and structure [332,333] critically influence uptake efficiency, major gaps remain in our understanding of the cellular routes and mechanisms governing fibril entry and release, the molecular determinants of seeded aggregation and subsequent assembly of larger Lewy body inclusions, and how specific fibril properties shape each of these steps.

6.4.1. α-synuclein variant-specific properties affect fibril internalization and cellular responses

To address some of these gaps, I began by examining uptake efficiencies of WT and mutant (A30P, E46K, H50Q, A53T) α-syn fibrils using a dual-labelling strategy in which fibrils were tagged with both the pH-insensitive fluorophore ATTO488 and the pH-sensitive fluorophore pHrodo (Fig. 35). This approach overcomes the challenge in distinguishing fibrils bound to the plasma membranes from those that enter the endolysosomal pathway [257], where progressive acidification selectively activates the pH-sensitive signal of pHrodo [334]. To ensure that differences in uptake reflected intrinsic properties of each fibril variant rather than size heterogeneity [87,257], all fibrils were ultrasonicated to a uniform length prior to cell treatment.

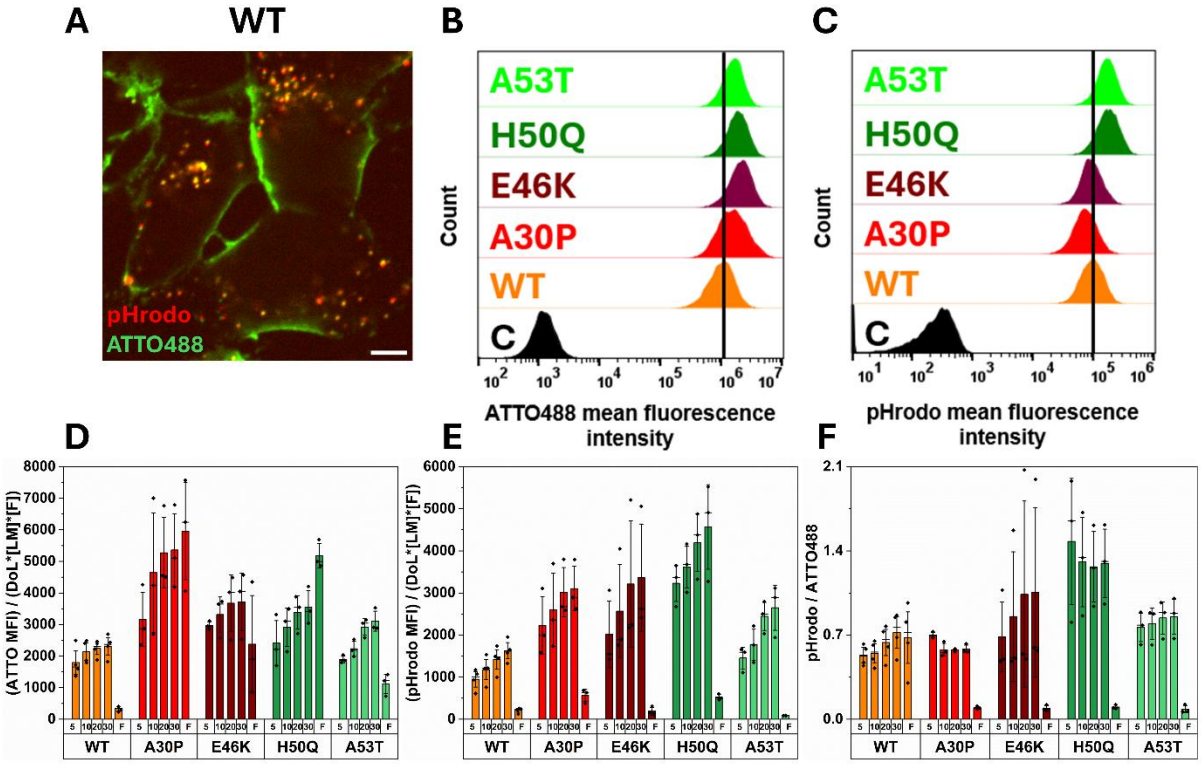

Figure 35. *Variant-specific uptake and endolysosomal trafficking of α-synuclein fibrils in SH-SY5Y cells. Flow-cytometric quantification of fibril internalization based on ATTO488 and pHrodo fluorescence for WT and familial α-syn variants (A30P, E46K, H50Q, A53T) in human neuroblastoma SH-SY5Y cells after 48 h of exposure in serum-free medium. (A) Confocal image of SH-SY5Y cells treated with 1 µM sonicated, dual-labeled WT fibrils for 2 h, showing ATTO488 signal (green) at both the plasma membrane and endolysosomes and pHrodo signal (red) restricted to acidic endolysosomal compartments. Scale bar: 5 µm. (B, C) Flow-cytometry histograms of mean fluorescence intensity (MFI) for ATTO488 and pHrodo in cells treated with 30 µM sonicated fibrils and untreated controls shown in black. Black vertical lines indicate the modal MFI for WT fibrils. (D, E) Corrected MFIs (mean ± SD; N=3, n=4) for cells treated with sonicated fibrils (5-30 µM) or full-length fibrils (30 µM). ATTO488 data in (D) pHrodo data in (E). Corrections account for minor differences in labeling efficiency, labeled monomer concentration, and fibril yield (Supporting Note 1). (F) Uptake index (pHrodo/ATTO488 MFI ratio) illustrating variant-dependent differences in membrane association versus endolysosomal accumulation.*

To validate that the dual-labeling strategy could reliably distinguish fibrils bound to the plasma membrane from internalized ones, I acquired live-cell confocal images of SH-SY5Y neuroblastoma cells treated with WT fibrils. These images showed that fibrils remaining at the plasma membrane displayed only the ATTO488 (green) signal, whereas fibrils that had entered the endolysosomal pathway appeared as puncta positive for both ATTO488 and the pH-activated pHrodo (red) (Fig. 35A). Flow-cytometric quantification of ATTO488 (Fig. 35B) and pHrodo (Fig. 35C) fluorescence further confirmed increases in both membrane association and endolysosomal uptake of fibrils relative to untreated controls. After applying minor corrections for differences in fibril yield across α-syn variants [312], which is important as it is primarily aggregated α-syn that is internalized [257,331], and for labeling efficiency, which determined the intensity of the fibrils, the analysis showed that uptake was

concentration dependent (Fig. 35D-E). Moreover, the mutant variants generally showed stronger association with SH-SY5Y cells (ATTO488, Fig. 35D) and higher internalization and accumulation within endolysosomal compartments (pHrodo, Fig. 35E) compared to WT fibrils. An uptake index (Fig. 35F), calculated as the ratio of pHrodo to ATTO488 mean fluorescence intensity, further showed that all fibril variants except A30P were internalized into endolysosomal compartments to a greater extent than WT, with H50Q showing the most superior uptake. These findings suggest that certain variants, like A30P, tend to remain associated with the cell surface with limited progression into the cell, whereas others, like H50Q, are more efficiently routed into endolysosomal compartments. One plausible explanation is that these mutations alter the structural architecture of the fibrils, such as the rearrangements reported for H50Q [109], thereby modifying interactions between neuronal receptor-binding sites [335] and ultimately influencing their efficiency of cellular uptake. This underscores that distinct intrinsic structural and physiochemical features of each fibril variant critically determine uptake efficiency.

Having observed clear differences in cellular uptake among the α-syn variants, I next asked whether these differences also translated into variant-specific uptake kinetics, intracellular localization and cellular responses. To address this, we monitored fibril internalization over a 20-hour period using time-lapse confocal imaging (Fig. 36).

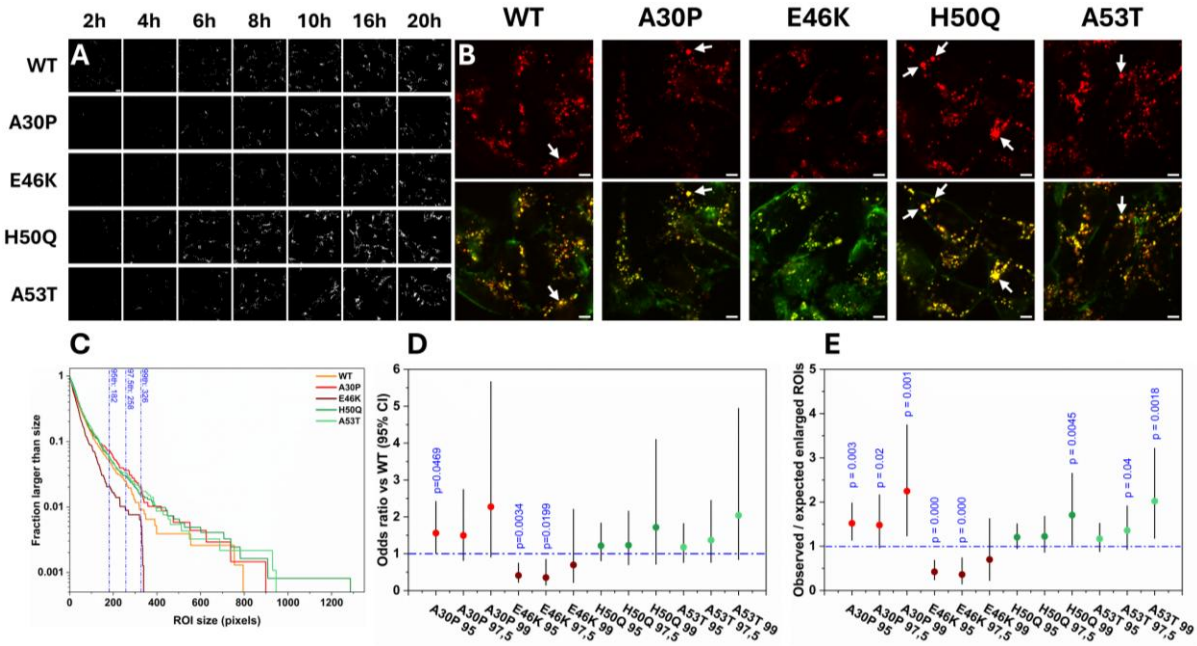

Figure 36. *Uptake kinetics and endosomal enlargement induced by α-synuclein fibril variants in SH-SY5Y cells. (A) Time-lapse confocal imaging of live SH-SY5Y cells treated with 1 µM WT or mutant α-syn fibrils, illustrating variant-dependent increases in cellular pHrodo fluorescence over 20 h. Scale bar (WT, 2 h): 10 µm. (B) Confocal images at the 20 h endpoint showing pHrodo fluorescence (top) and merged pHrodo/ATTO488 channels (bottom) for all variants. White arrows indicate enlarged endosomes. Scale bars: 5 µm. (C) Cumulative distributions of endosome sizes (pixel-based ROIs) in cells treated with WT or mutant fibrils; blue dotted lines mark the 95th, 97.5th, and 99th percentiles for WT. (D) Odds ratios quantifying the likelihood of endosomal enlargement in mutant-treated cells relative to WT (blue dotted line = 1). Statistical significance at each percentile threshold was assessed using*

Fisher's exact test; black lines denote confidence intervals and p-values denote significant differences relative to WT. (E) Ratios of observed versus expected number of enlarged endosomes for each mutant α-syn variant compared to WT (blue dotted line, observed/expected =1), indicating whether the mutant variants generate a disproportionately larger or lower number of enlarged endosomes compared to their total endosomal load. Significance was evaluated using Clopper-Pearson confidence intervals and two-sided exact binomial tests for p-values; black lines show confidence intervals at the three percentile thresholds (95^{th}, 97.5^{th}, 99^{th}), and p-values denote significant differences relative to WT.

Similar to the overall uptake efficiencies (Fig. 35), H50Q fibrils displayed the most rapid internalization, with pHrodo-positive puncta detectable as early as 4 h (Fig. 36A). In contrast, WT and A53T fibrils first showed detectable pHrodo puncta at 8 h, while A30P and E46K fibrils exhibited internalization only at later timepoints. Consistent with observations made for WT (Fig. 35A) [257], magnified confocal images at the 20 h timepoint showed that all mutant α-syn fibrils both associated with the plasma membrane and entered acidic endolysosomal compartments (Fig. 36B). Accumulation of fibrils within endolysosomal compartments was further supported by spatial distribution of the pHrodo-positive puncta, which were predominantly located in the perinuclear region, a characteristic site of lysosomes [336,337].

Surprisingly, the confocal images also revealed variant-dependent differences in endosomal enlargement, an established marker of endolysosomal dysfunction [338-340], aligning with the emerging link between lysosomal impairment and PD [341]. This observation prompted me to quantify the pHrodo-positive acidic compartments and visualize the size profiles for each variant using a cumulative distribution plot (Fig. 36C), which revealed that E46K showed a markedly lower propensity to induce endosomal enlargement than any other variant. To determine whether mutant fibrils generated a higher or lower proportion of enlarged endosomes than WT fibrils, I calculated odds ratios (ORs) for each variant, reflecting the likelihood that pHrodo-positive compartments surpassed the 95^{th}, 97.5^{th}, and 99^{th} percentile size thresholds of WT (Fig. 36D). Furthermore, because the fibril variants differed in the total number of pHrodo-positive acidic compartments they generated, I also calculated an observed over expected ratio of enlarged endosomes, using WT as the reference baseline, to determine whether each α-syn variant generated disproportionately more or fewer enlarged endosomes relative to its overall endosomal count (Fig. 36E). In both analyses, the blue dotted lines represent the WT baseline (OR = 1, observed/expected = 1). These analyses showed that A30P, H50Q and A53T modestly increased the prevalence of enlarged endosomes, whereas E46K reduced it.

Taken together, the data in Figures 35 and 36 demonstrate that the intrinsic properties of each α-syn fibril variant not only shape their uptake efficiency but also critically influence downstream endolysosomal behavior within the cell. This is notable because even though entry into the endolysosomal pathway represents a first step of prion-like propagation, an equally important requirement is the subsequent escape of fibrils from endosomes to seed endogenous α-syn in the cytosol. Previous studies have shown that α-syn fibrils can compromise lysosomal membrane integrity [342,343], thereby enhancing the seeding of endogenous α-syn [18]. This connection suggests that the endosomal enlargement observed

here, an established marker of endolysosomal dysfunction, may represent a contributing factor to fibril escape and cytosolic seeding.

6.4.2. α-synuclein variant-specific properties drive species-dependent seeding

The next question was whether the α-syn fibril variants also differ in their ability to seed endogenous α-syn monomers, representing the subsequent step in prion-like propagation beyond mere uptake. To address this, we used mouse (C57BL/6) and rat (Wistar Han) cortical neuronal cultures, which were incubated with varying concentrations of sonicated, unlabeled fibrils for 7 days, followed by immunocytochemical staining of cell nuclei (Hoechst), dendritic networks (MAP2), neuronal cell bodies (NeuN), and phosphorylated α-syn (pS129). High-content confocal microscopy and image-based quantification were used to assess cellular integrity and seeding outcomes. Because phosphorylation is the predominant post-translational modification of α-syn found in Lewy bodies in both humans [344,345] and animal models [346,347], and the added fibrils were not phosphorylated, the detected pS129-positive inclusions exclusively reflect newly formed aggregates rather than the exogenously applied fibrils. In addition to using primary neuronal mouse cultures, the most widely employed model for studying α-syn seeding [348,349], the study explored propagation behaviors in primary rat neuronal cultures to assess potential species-dependent differences in α-syn seeding. Rat neurons are common models in neuroscience which have some morphological advantages such as thicker dendrites and larger somas, as well as functional advantages such as more mature electrophysiological properties [350,351].

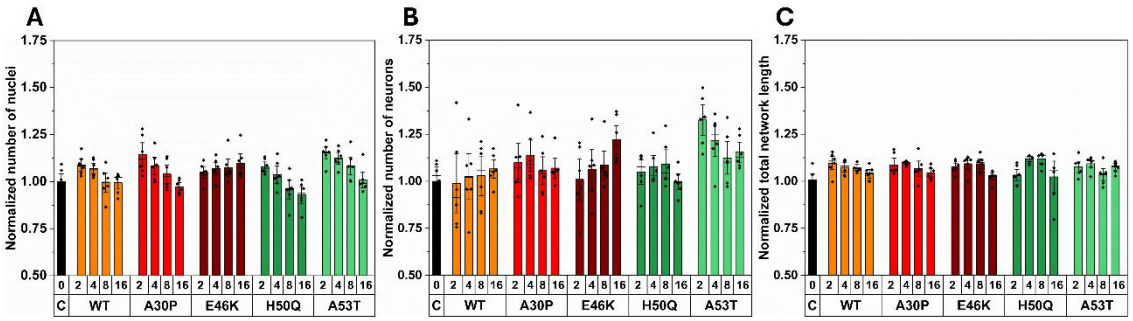

Figure 37. *Cellular integrity of nuclei, neuronal cell bodies and dendritic networks shown for one mouse replicate. (A-C) Image-based quantification of cell viability, including counts of Hoechst-labeled nuclei (A), NeuN-positive neurons (B), and MAP2-defined dendritic network length (C). All counts were normalized to untreated controls.*

To evaluate whether fibril treatment affected cellular integrity, I quantified cell viability by measuring total nuclei counts (Fig. 37A), neuron counts (Fig. 37B), and total dendritic network length (Fig. 37C). No notable loss of cellular integrity was observed, a pattern which was also conserved in rat neuronal cultures. However, clear differences in seeding outcomes emerged, both across the individual α-syn fibril variants and between species, indicating distinct variant-specific effects and species-dependent seeding responses (Fig. 38).

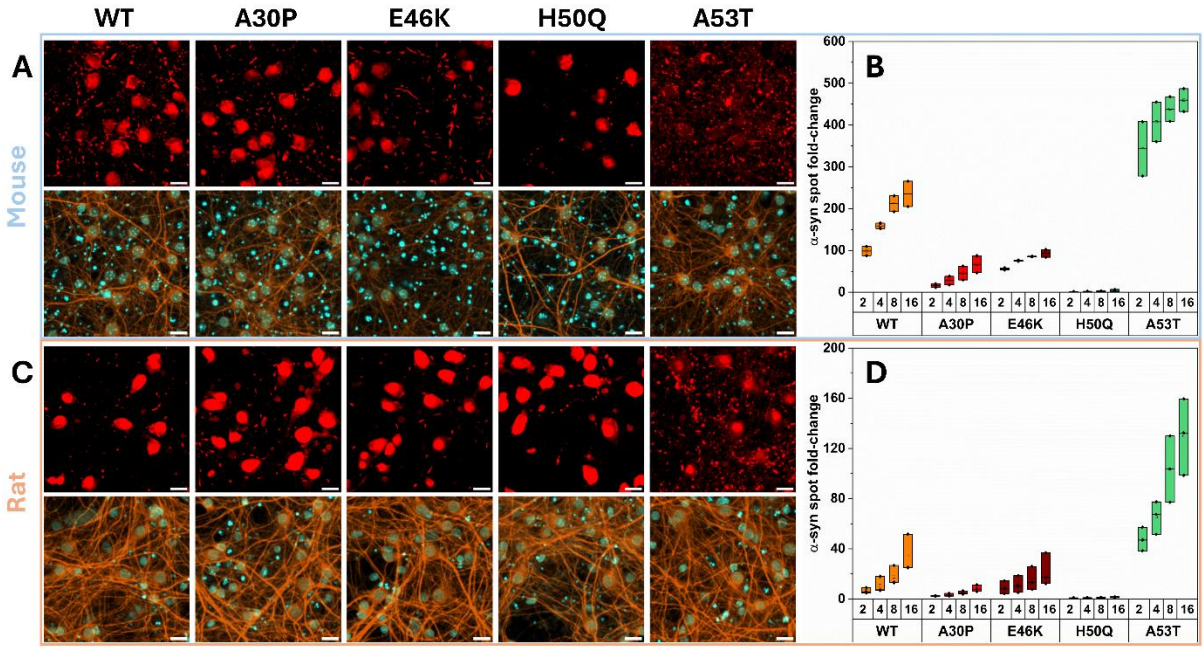

Figure 38. *Variant-specific seeding of α-syn pathology in primary mouse and rat neurons. Comparison of prion-like seeding triggered by WT and familial α-syn variants (A30P, E46K, H50Q, A53T), assessed in primary neuronal cultures from mouse (C57BL/6) and rat (Wistar Han) after 7 days of exposure to PFFs. (A, C) High-resolution confocal images of fixed mouse (A) and rat (C) neuronal cultures treated with 16 µg/ml WT or mutant α-syn PFFs show the appearance of cytosolic pS129-positive inclusions (upper panels) alongside Hoechst-labeled nuclei and MAP2-labeled dendritic networks (lower panels). The larger rounded pS129-positive staining reflects nuclear cross-reactivity rather than true cytosolic aggregate formation. Scale bars: 20 µm. (B, D) Quantification of pS129-positive puncta relative to untreated controls across increasing fibril concentrations (2-16 µg/ml) in mouse (B) and rat (D) cultures. Box plots depict the interquartile range (25-75%), median (horizontal line), mean (open square), and individual outliers (filled diamonds). Sample sizes: mouse N = 2, n = 6; rat N = 3, n = 6.*

The dendritic architecture differed substantially between mouse (Fig. 38A) and rat (Fig. 38B) cultures, aligning with prior observations that rat neurons develop thicker dendrites [350,351]. Within each species (mouse and rat), the variant-dependent hierarchy of seeding potency was conserved. A53T induced the strongest accumulation of pS129-positive inclusions, followed by WT, whereas H50Q produced minimal or no seeding above baseline endogenous α-syn levels (Fig. 38B, D). Similar variant-dependent seeding hierarchies have been reported *in vitro* for both self-seeding [312,317] (**paper II**) and cross-seeding [181,352] reactions. In contrast, this trend diverges from non-seeded aggregation kinetics, where familial mutants typically display accelerated fibril formation compared to WT [178,315]. Notably, across all fibril treatments, rat neuronal cultures displayed a lower magnitude of pS129 fold increase compared to mouse cultures, indicating species-dependent differences in seeding response.

The pronounced seeding potency of A53T likely reflects, in part, its sequence complementarity to endogenous mouse and rat α-syn, which naturally harbor the A53T substitution [353]. However, it also largely aligns with findings presented in **paper III**, where A53T displayed high permissiveness to both self- and cross-seed, suggesting that this fibril variant possesses an intrinsically high capacity for templating. Consistent with this, the comparatively weak seeding efficiencies of H50Q and, to a lesser extent, E46K, are in line with their behavior in the cross-seeding assays described in **paper III**, where heterologous templating progressed slowly due to each variant's strong preference for propagating its own fibril architecture, even at a high kinetic cost. The differences in seeding magnitude between mouse and rat neuronal cultures may stem from the single amino-acid difference in their endogenous α-syn sequences at residue 121 which is also distinct from the human sequence (G121 in mouse, S121 in rat, D121 in human) [354]. This position is known to influence C-terminal truncation and aggregation of α-syn [355,356], providing a plausible molecular basis for the species-dependent variation in seeding responses. However, mouse and rat neuronal cultures also differ in several biological processes that could influence their respective seeding responses, including protein clearance pathways, proteostasis capacity, neuronal maturation rate, and baseline α-syn expression levels [350,351,357,358].

A key observation emerging from the comparison of uptake (Fig. 35) and seeding efficiencies (Fig. 38) is that these parameters did not always correlate. Examining the two most prominent cases, H50Q and A53T, demonstrates that H50Q exhibited high uptake yet minimal seeding, whereas A53T showed only moderate uptake but high seeding efficiency. The dissociation between uptake and seeding likely arises from mechanisms beyond simple fibril internalization, involving variant-specific biophysical features and differences in how the fibril variants accumulate and persist within the endolysosomal system. For example, the H50Q substitution removes α-syn's only residue that can change its charge within the endolysosomal pH range, likely altering how the fibrils engage lysobisphosphatidic acid-rich late endosomal membranes [359]. This could reduce escape from endolysosomal compartments and account for the poor seeding efficiency of H50Q relative to A53T, despite substantial endolysosomal buildup. Furthermore, protein charge has also been shown to play an important role in the aggregation of H50Q, where non-polar (alanine), polar (glutatmine) or negatively charged (aspartic acid) residues reduced the aggregation propensity, whereas introducing a positively charged residue (arginine) enhances it [180]. This highlights that the charge at position 50 might be functionally important over the endosomal pH range.

6.4.3. α-synuclein variant-specific properties determine inclusion morphology

The final question I asked after observing substantial differences in uptake and seeding among the α-syn fibril variants was whether these disparities would also manifest in morphological differences of the resulting inclusions, and whether such morphological features might differ between mouse and rat neuronal cultures. To address this, I quantified inclusion morphology by measuring their size and shape using image-based analysis (Fig. 39).

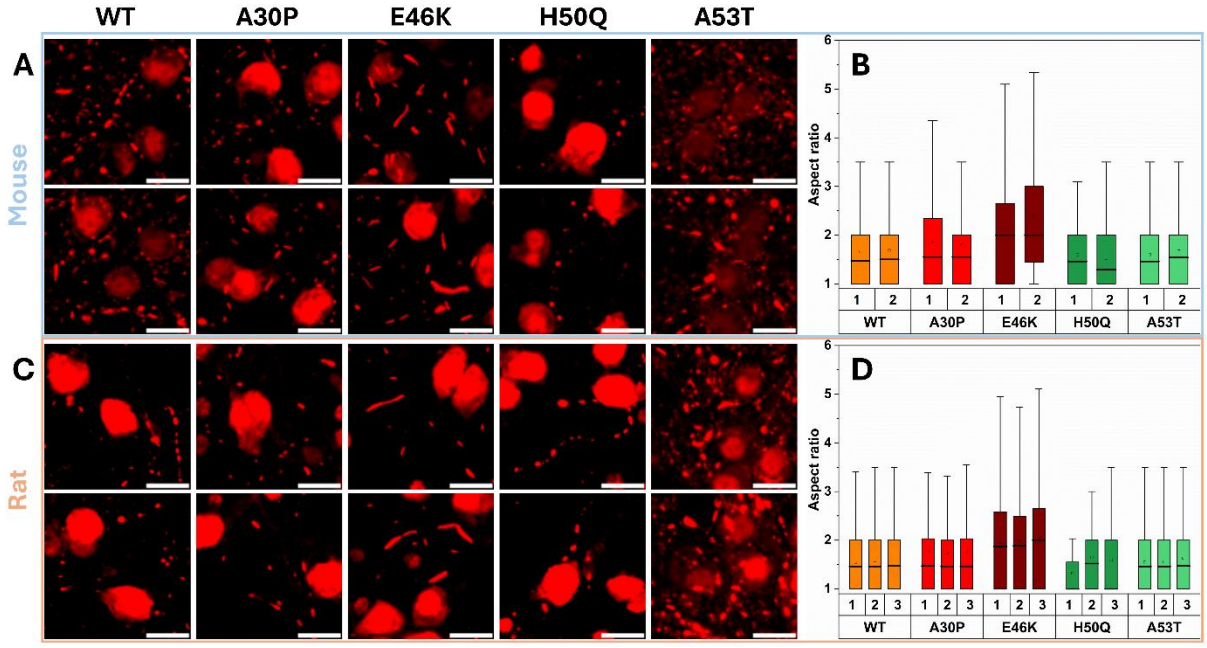

Figure 39. *Morphological variation of α-syn inclusions seeded by wild-type and mutant fibrils. Morphological characterization of the pS129-positive cytosolic inclusions identified in Fig. 38. (A, C) Confocal micrographs of pS129-positive inclusions in mouse (A) and rat (C) primary neuronal cultures, with two zoomed-in fields of view shown for each α-syn variant to illustrate inclusion abundance and structural appearance. Scale bars: 20 µm. (B, D) Quantification of inclusion morphology based on aspect ratio (longest/shortest axis). Box plots depict the interquartile range (25-75%), with medians indicated by horizontal lines, means by open squares, and outliers by filled diamonds. Aspect-ratio measurements were obtained from two biological replicates for mouse and three for rat, with nine fields of view analyzed per replicate and α-syn variant.*

Inclusion morphology was broadly comparable between mouse (Fig. 39A) and rat (Fig. 39C) neuronal cultures, spanning small, near-spherical inclusions to more elongated structures, however some α-syn variant specific inclusion morphologies were observed. The most pronounced morphological differences were observed for E46K, which predominantly generated large, elongated inclusions. This trend is consistent with its slightly elevated aspect ratios in both mouse (Fig. 39B) and rat (Fig. 39D) neuronal cultures. These findings align with earlier work showing that α-syn inclusions can adopt a wide range of morphologies [164,212,348], and that the structural features of the seeding assemblies play a decisive role in shaping the architecture of the aggregates that ultimately form [360-362]. Furthermore, these results, together with the conserved seeding hierarchy observed for mouse and rat neuronal cultures in Figure 38, support the idea that intrinsic properties of the fibril seeds, rather than species-specific cellular factors, primarily determine both seeding efficiency and structural characteristics of the resulting α-syn inclusions.

In summary, I have shown that wild-type and mutant α-syn fibrils engage the prion-like propagation pathway in distinct manners. The variants differed not only in how efficiently they were internalized, but also in how they were processed within the endolysosomal system, how readily they induced endosomal enlargement, and how effectively they initiated seeded aggregation. These variant-specific behaviors ultimately produced inclusions with characteristic morphological signatures, demonstrating that the structural identity of the seed

influences every stage from entry to aggregate formation. Rather than a single step dictating prion-like spread, our results show that propagation efficiency arises from the cumulative effect of several mechanisms, each of which is modulated differently by the individual α-syn variants. This explains why high uptake does not necessarily translate into strong seeding activity and underscores the multifaceted nature of amyloid propagation in neurons. Notably, several defining features previously observed *in vitro* in **papers I-III**, such as the influence of protein charge on fibril behavior, the variant-specific differences in aggregation propensity and the ability to cross-seed other α-syn variants, were likewise evident *in vivo*. This conservation across experimental systems indicates that these behaviors stem from intrinsic fibril properties rather than the biological environment. In light of the distinct α-syn strains identified in Parkinson's disease and related synucleinopathies, the findings further support the idea that structural polymorphism is a central driver of the variability and progression of α-syn associated neurodegeneration, making it a promising target for future development of therapeutics.

7. Concluding Remarks

To this day, Parkinson's disease (PD) and related synucleinopathies continue to be devastating neurodegenerative disorders with widespread impact on millions of people and their families worldwide. In the past several decades, major advances have been made to understand the molecular mechanisms that determine PD onset and propagation. This has firmly established α-syn as a key contributor to disease development. Despite these advances, the understanding of the initial events that cause α-syn to misfold and aggregate are still incomplete, and our knowledge of how the resulting aggregates contribute to initiating and propagating pathology remains insufficient, resulting in that we still have no means of halting disease progression. More than 50 years after its first introduction, L-dopa remains the most widely used symptomatic treatment of PD, yet the recent emergence of an antibody-based therapy against Aβ to combat Alzheimer's disease highlights the therapeutic potential of targeting amyloid fibrils.

In this thesis, I address some of these knowledge gaps by demonstrating that α-syn fibril formation and the resulting structural outcomes are shaped by both physiochemical (environmental) and mechanistic factors, and that responses to these factors are highly variant-dependent. I further demonstrate that variant-specific differences in aggregate formation critically influence cell-to-cell propagation, encompassing internalization, cellular processing, endogenous α-syn seeding, and the formation of larger inclusion bodies. Together, my findings provide important insights into how α-syn pathology spreads and highlight the significance of structure-function relationships for understanding the mechanisms that determine actions of amyloid fibrils, an area that may offer valuable targets for future therapeutic strategies.

At its core, my thesis investigates how physiochemical, mechanistical and structural factors shape α-syn fibril formation and how these variant-specific properties influence prion-like propagation. **Paper I** laid the foundation for this work by demonstrating that α-syn formation is highly sensitive to physiochemical conditions, establishing how these early determinants can shape aggregation kinetics and fibril structure, features that later prove crucial for downstream cellular processing and prion-like propagation. I demonstrate in **Paper I** that the most physiologically abundant monovalent cations, Na^+ and K^+, have distinct and opposing effects on WT α-syn aggregation kinetics, with Na^+ accelerating fibril formation, whereas K^+ progressively slows it with increasing concentration. The fact that these effects were confined to the lag phase highlights their strong influence on primary nucleation. I further show that these cations also influence structural outcomes, with Na^+ promoting more flexible fibrils and K^+ producing more rigid ones. My findings expand current knowledge by showing that, although the roles of anions [148] and multivalent cations [287] are well established as modulators of α-syn fibril formation, monovalent cations, which have been comparatively understudied, can also significantly influence fibril aggregation kinetics and structural outcomes, highlighting their relevance in both physiological and experimental context. Finally, the observation that monovalent cations modulate fibril flexibility and rigidity, thereby influencing fibril clustering, may offer new insights into the formation of Lewy bodies, which are characterized by densely packed α-syn fibrils formed in a K^+ rich environment [5].

Building on this foundation, in **paper II** I asked how another comparatively understudied mechanism, fragmentation, influences α-syn aggregation kinetics and structural outcomes. To address this, I modified the conventional ThT aggregation assay used in **paper I** by incorporating an ultrasonication step at the plateau phase, generating repeated rounds of fragmentation and re-aggregation. This new approach simulates the prolonged course of PD, during which fibrils are likely to undergo multiple cycles of breakage and regrowth, and represent a methodological contribution to the amyloid biophysics field. Using this framework, I extended the analysis to include pathological mutants (A30P, E46K, H50Q, A53T), enabling direct comparison of how fragmentation affects fibrils that differ both in structure and aggregation kinetics. I found that A30P, E46K, and A53T, three mutants notably associated with early-onset PD, showed progressively increased ThT fluorescence following fragmentation and re-growth, despite exhibiting no change in fibril mass. Such changes in ThT fluorescence can only be ascribed to differences in ThT binding and quantum yields [302] which are, in turn, heavily dependent on fibril architecture [303,304]. My results indicate that these variants evolve their structures and, furthermore, suggest that high polymorphic flexibility of fibrils may be important to drive early disease initiation and rapid progression, possibly by enabling rapid adaption to the intracellular environment [363], facilitating secondary nucleation [320], and/or by increasing the likelihood of forming pathogenic conformers capable of efficient intracellular spread [364]. Moreover, the key finding in **paper II** that fibril fragmentation can accelerate such conversion, gives this mechanism a more central role than previously acknowledged, prompting further studies under conditions that more faithfully mimic the cellular environment, where proteolytic enzymes [310] and chaperones [309] can increase the occurrence of fibril fragmentation events compared to their relative sparseness *in vitro*. Moreover, **paper II** provides the first evidence that α-syn fibrils can structurally evolve over time, and the comparative analysis of WT and mutant α-syn demonstrates that the propensity for such evolution is variant-specific. This advances current understanding of α-syn aggregation, complementing recent work linking fibril structure to distinct diseases [21], as well as extending the concept of structural evolution of amyloid fibrils first proposed in work on IAPP [22] and tau [23] fibrils. Such observations have important implications both in a biological context and for the development of effective PD therapeutics. The fibril structures observed in post-mortem patient tissue likely represent late-stage, highly matured assemblies, rather than the early-stage species that initiate pathology. As a result, therapeutics designed to target post-mortem fibril structures might face a fundamental challenge in that they may not effectively engage the early pathogenic assemblies that drive disease onset and progression. This distinction highlights the need to consider structural evolution, and earlier or more transient polymorphs, when developing therapeutics aimed at specific structural features of amyloid fibrils.

Having established in **paper II** that α-syn fibril composition is highly heterogenous, that fibril structures can evolve over time, and that these properties are strongly variant-specific, I next asked whether I could resolve and distinguish these structural differences without large-scale cryo-EM assisted structure determination. To this end, I leveraged the photophysical properties of ThT through ThT fluorescence lifetime analysis (**paper III)**. Using this approach, I demonstrated that α-syn fibril polymorphs generated through both self- and cross-seeding could be phenotyped based on their specific ThT fluorescence lifetime fingerprints, which, due to the tight binding of ThT to the amyloid fibril core, can be interpreted as direct reflections of underlying structural differences. **Paper III** represents a methodological

advance in that it establishes ThT fluorescence lifetime analysis as a time- and cost-effective method for phenotyping and comparing large fibril datasets generated from self- and cross-seeding, providing complementary structural information alongside established techniques such as cryo-EM [21,141] and AFM [365]. Furthermore, using fluorescence lifetime analysis coupled with kinetic analysis I was able to gain deeper knowledge regarding the differences in fluorescence intensity and kinetics that I observed in **paper II.** Across the cross-seeding experiments, fluorescence-lifetime combined with kinetics analyses revealed variant-specific differences in how different α-syn variants propagate structure. Some variants, such as E46K and H50Q, showed a strong tendency to propagate their native self-seeding structure, both when acting as seeds and when their monomers were seeded by other variants. However, this faithfulness to propagate their native self-seeded structures was accompanied by a substantial kinetic cost. WT and A30P monomers were more permissive and readily adopted the conformation of the incoming seed. In contrast, A53T showed an intermediate behavior, as a seed it preserved selected structural features, while as a monomer it largely maintained its native A53T structural fingerprint even when seeded by other variants. Moreover, several cross-seeding combinations notably produced 'hybrid' fibrils with lifetime signatures partially resembling both the parent seed and the preferred fibril conformation of the monomer, whereas others appeared to result in entirely new polymorphs, typically emerging under conditions of rapid assembly suggesting less faithful structural replication. Through these results, I showed that cross-seeding can lead to faithful templating, monomer-driven restructuring, or de novo polymorph formation, highlighting the diverse and dynamic structural landscape of α-syn fibrils. Overall, I provide valuable insights into that α-syn variants differ markedly in how they transmit or remodel structure during cross-seeding, emphasizing that variant-specific structural interplay may be an important contributor to progression of familial PD. A valuable next step, combining the observations in both **paper II** and **paper III**, would be to directly align the fluorescence-lifetime signatures with cryo-EM resolved fibril architectures, enabling the construction of an integrated lifetime-structure map for rough bulk-readouts of structural compositions within a sample.

Whereas **papers I-III** focused on fibril formation and structural outcomes from an *in vitro* biophysical perspective, in **paper IV** I shifted the focus to the cellular environment, investigating how these variant-specific properties manifest *in vivo*. The key question was how distinct aggregation kinetics and fibril architectures of the various α-syn variants observed in **papers I-III** connect to prion-like propagation, encompassing internalization, intracellular processing, endogenous α-syn seeding, and the development of larger inclusion bodies. Using flow cytometry to quantify fibril uptake in SH-SY5Y neuroblastoma cells, I found that internalization efficiency varied markedly between α-syn variants, indicating that cellular entry is strongly influenced by intrinsic fibril properties such as structure. Confocal imaging further revealed pronounced endosomal enlargement across most α-syn variants, a phenotype previously associated with endosomal dysfunction [338-340] and, to the best of my knowledge, previously only reported for WT α-syn fibrils [366]. Notably, these effects were more prominent for familial variants than for WT, aligning with the growing recognition of lysosomal impairment in PD [341] and suggesting a mechanistic link to the more aggressive early-onset forms of disease. Furthermore, I showed through confocal microscopy of mouse and rat neuronal cultures treated with the different α-syn variants that these variant-specific behaviors extended beyond uptake and endosomal responses to additional steps in the prion-like propagation pathway. Endogenous α-syn seeding was highly variant-dependent,

with substantial differences in seeding-efficiency noted across all α-syn variants. An important observation was also that cellular uptake efficiency did not necessarily correlate with a high seeding efficiency. Instead, these cellular outcomes in several instances mirrored the biophysical trends observed in **paper III**. Variants such as E46K and H50Q, which exhibited slow and kinetically costly aggregation due to preference of propagating their own structures during cross-seeding, produced comparatively few aggregates in both mouse and rat neurons. In contrast, A53T, characterized by rapid and permissive aggregation *in vitro*, generated the highest number of α-syn aggregates across both model systems. Importantly, these variant-specific patterns were conserved across species, albeit with different magnitudes, demonstrating that the efficiency of endogenous α-syn recruitment is tightly linked to intrinsic fibril properties, such as structure and kinetic accessibility. Lastly, a final observation was that the formation of larger, Lewy body-like inclusions and their resulting morphologies were dependent on the α-syn seed variant. Although this observation aligns with previous reports of morphologically diverse α-syn inclusions [164,212,348] and its dependence on the nature of the α-syn seed [360-362], my work provides the first large-scale side-by-side comparison of four of the most common familial PD variants. In conclusion, **Paper IV** thereby provides the first systematic comparison of WT and familial α-syn mutants (A30P, E46K, H50Q, A53T), showing variant specific effects across multiple stages of prion-like propagation, including internalization, endosomal responses, endogenous α-syn seeding, and the formation of inclusion bodies. This contributes to the growing body of literature which links structural polymorphism to disease function [21].

In summary, my thesis provides new mechanistic insight into α-syn aggregation and its propagation in PD, highlighting fibril assembly pathways and the resulting fibril structure as important targets for future therapeutic strategies.

8. Acknowledgements

After 5 years as a PhD student, this thesis marks the end of a long and challenging, yet also fun and educational journey. Along the way, I have been fortunate to receive support, encouragement, and inspiration from many people, and I would like to express my sincere gratitude to you all. This work would not have been possible without your help.

First and foremost, I want to thank my supervisor **Elin K. Esbjörner**. Without your support and encouragement, I would not have been able to complete this thesis. You have inspired me throughout my PhD, and our scientific discussions have sparked many interesting ideas, experiments, and ways of analyzing data. Your passion, curiosity, and dedication as a researcher have been truly motivating, and I have learned a great deal from watching how you approach science. Beyond the research itself, I'm deeply grateful for your kindness and for always showing understanding in every situation.

Furthermore, I want to thank my examiner, **Fredrik Westerlund**, and my co-supervisor, **Pernilla Wittung-Stafshede**, for all your support and encouragement throughout my PhD. Your input has always been valuable for my work.

To all the current members of the Esbjörner group. **Vesa Halipi**, we started our PhD journey on the same day, and it has truly been a blessing to have you as my colleague and friend. Thank you for all the help with my projects, for the motivational talks, and for the positive energy you bring into every situation. **Andrea Ramnath**, thank you for helping me with the confocal microscopy parts of my project and for tackling the more challenging analysis with such patience. It has been a lot of fun working with you, and even when things became complicated, you always maintained a positive attitude which kept me motivated. **Ranjeet Kumar**, thank you for teaching and helping me with protein purification. You've saved me countless times with your vast knowledge, and I'm grateful for your constant positive attitude and willingness to help. **Viktoria de Carvalho** and **Elin Persson**, thank you for bringing a lot of good energy into the group. Your creativity and craftiness have been inspirational, and I have truly appreciated the enthusiasm you contribute to the lab environment. **Jyoti Swami**, I appreciate the friendly attitude you bring to the group.

To all the previous members of the Esbjörner group which I've been fortunate to work with. **David Bernson**, thank you for being my supervisor during my master's thesis and for having the patience to teach me everything about protein purification and aggregation. The foundation you helped me build during that time became essential for my PhD, and I'm truly grateful for your guidance and support. **Marziyeh Ghaeidamini**, you have been so much fun to work with. Thank you for all the help and support you've given me in my projects, for all the laughs we've shared, and for all the times you let me annoy (and scare) you. My PhD journey would not have gone nearly as smoothly without you. **Nima Sasanian**, thank you for all the help you gave me both during my master's and throughout my PhD. I've always appreciated your support, your willingness to share your knowledge, and of course all the great tennis sessions we've had. **Emelie Wesén**, **Karin Norling**, **Daniel van Leeuwen** and **Quentin Lubart**, for all the help you provided and how you made me feel so welcome in the group. Your friendliness has meant a lot during my time here.

To all colleagues from the other research groups at the division of Molecular Bioscience. **Loise Råberg** and **Eve Pavlova** for all the fun parties, after-works, trips, laughs and shots we've shared. You truly made the PhD experience so much more enjoyable. **Jonatan Norborg** and **Johanna Fredriksson**, thank you for all the fun times throughout both our bachelor's and master's studies, as well as during the PhD. We've shared both the "suffering" and the unforgettable moments, and we've created memories that will stay with me for life. And to all the other people at Molecular Bioscience, thank you for making this such a welcoming and enjoyable workplace.

To my current and former office mates. **Radhika Nambannor Kunnath**, **Florian Morati,** and **Carl Möller**, thank you for all the interesting and fun discussions, and for all the help and support you've given me over the years. Sharing an office with you has made this journey much more enjoyable.

To **Gizem Erensoy,** our wonderful research engineer at Molecular Biosciences. I first met you during your time as a PostDoc in Alexandra's group, where your kindness and openness stood out immediately. Since becoming the division research engineer, you have become an essential part of everybody's work. Thank you for all that you do.

To all the bachelor's and master's students I've had the pleasure of supervising, as well as those who have contributed to my projects. **Jeremias Brunbauer, Andreas Gannholm, Mikaela Sjögren, Olivia Borg, and Elin Allgén**, thank you for your hard work, curiosity, and enthusiasm.

To my collaborators at GU. **Andreas Törnell** and **Anna Martner**, even though we haven't managed to finish the project (yet), it has been both fun and inspiring to collaborate with you and to gain insights from an immunology perspective. I hope the groundwork we've laid will grow into some exciting papers in the future.

To my collaborators at the department of Physics at Chalmers, especially **Kajsa Ahlgren** and **Jan Swenson**, for the fun collaboration regarding sugars and lysozyme fibrils. This provided valuable insights into amyloid fibrils from a physics perspective which I'm grateful for having been a part of.

To my collaborators from the Stubelius group, especially **Ula von Mentzer** and **Alexandra Stubelius**, for the interesting collaboration regarding nanoparticles and their implication in inflammation and drug delivery. This project provided me with insights in a completely different field which I'm truly grateful for.

To the team at Cellectricon, especially **Lotta Agholme**, **Andrea Lovincic Babic and Maitrayee Sinha**. Thank you for your unwavering support with the mouse and rat studies in my project. It has truly been a pleasure working with all of you.

To the wonderful administrative team at LIFE. **Anne-Lise Kramer** and **Gunilla Bankel Andersson**, thank you for always responding so quickly and helping with anything that came up. Your efficiency, kindness, and reliability have made an enormous difference. This place wouldn't run as smoothly as it does without you.

Above all, I want to thank the most important people in my life. **Pappa** for always supporting me throughout my life, in both the rough times and the good ones. You are a loving and endlessly caring father. I'm truly grateful for everything you've done and still do for me. **Mamma**, even though you are no longer with us, not a single day passes without me thinking of you. You will always live on in loving memory. You were together with pappa, a cornerstone in my life, and the support and love you gave me will be cherished forever. Your brave journey with MSA also inspired this thesis, born from my wish to better understand the disease you fought so courageously. To the **extended family**, thank you for always being so welcoming and for making me feel at home with you. And especially to you **Ellen**. My love for you is endless and I can't imagine my life without you. On the days when I was stressed or discouraged because things weren't working out the way I hoped, you were always there to cheer me up.

9. Bibliography

[1] Y. Luo, L. Qiao, M. Li, X. Wen, W. Zhang, X. Li, Global, Regional, National Epidemiology and Trends of Parkinson's Disease from 1990 to 2021: Findings from the Global Burden of Disease Study 2021, Frontiers in Aging Neuroscience 16 (2025) 1498756.
[2] D. Su, Y. Cui, C. He, P. Yin, R. Bai, J. Zhu, J.S. Lam, J. Zhang, R. Yan, X. Zheng, Projections for Prevalence of Parkinson's Disease and Its Driving Factors in 195 Countries and Territories to 2050: Modelling Study of Global Burden of Disease Study 2021, BMJ 388 (2025).
[3] M.C. Gonzalez, I. Dalen, J. Maple-Grødem, O.-B. Tysnes, G. Alves, Parkinson's Disease Clinical Milestones and Mortality, npj Parkinson's Disease 8 (2022) 58.
[4] J.H. Won, S.J. Byun, B.-M. Oh, S.J. Park, H.G. Seo, Risk and Mortality of Aspiration Pneumonia in Parkinson's Disease: A Nationwide Database Study, Scientific Reports 11 (2021) 6597.
[5] M.B. Fares, S. Jagannath, H.A. Lashuel, Reverse Engineering Lewy Bodies: How Far Have We Come and How Far Can We Go?, Nature Reviews Neuroscience 22 (2021) 111-131.
[6] J. Parkinson, An Essay on the Shaking Palsy, The Journal of Neuropsychiatry and Clinical Neurosciences 14 (2002) 223-236.
[7] F.H. Lewy, Paralysis Agitans. I. Pathologische Anatomie, Handbuch der Neurologie 3 (1912) 920-958.
[8] C. Trétiakoff, Contribution a L'etude De L'anatomie Pathologique Du Locus Niger De Soemmering Avec Quelques Deduction Relatives a La Pathogenie Des Troubles Du Tonus Musculaire Et De La Maladie De Parkinson, Theses de Paris (1919).
[9] M.G. Spillantini, M.L. Schmidt, V.M.-Y. Lee, J.Q. Trojanowski, R. Jakes, M. Goedert, A-Synuclein in Lewy Bodies, Nature 388 (1997) 839-840.
[10] M.G. Spillantini, R.A. Crowther, R. Jakes, M. Hasegawa, M. Goedert, A-Synuclein in Filamentous Inclusions of Lewy Bodies from Parkinson's Disease and Dementia with Lewy Bodies, Proceedings of the National Academy of Sciences 95 (1998) 6469-6473.
[11] H. Braak, K. Del Tredici, U. Rüb, R.A. De Vos, E.N.J. Steur, E. Braak, Staging of Brain Pathology Related to Sporadic Parkinson's Disease, Neurobiology of Aging 24 (2003) 197-211.
[12] J.H. Kordower, Y. Chu, R.A. Hauser, T.B. Freeman, C.W. Olanow, Lewy Body–Like Pathology in Long-Term Embryonic Nigral Transplants in Parkinson's Disease, Nature Medicine 14 (2008) 504-506.
[13] B.I. Giasson, K. Uryu, J.Q. Trojanowski, V.M.-Y. Lee, Mutant and Wild Type Human A-Synucleins Assemble into Elongated Filaments with Distinct Morphologies in Vitro, Journal of Biological Chemistry 274 (1999) 7619-7622.
[14] K.A. Conway, J.D. Harper, P.T. Lansbury, Fibrils Formed in Vitro from A-Synuclein and Two Mutant Forms Linked to Parkinson's Disease Are Typical Amyloid, Biochemistry 39 (2000) 2552-2563.
[15] A.K. Buell, C. Galvagnion, R. Gaspar, E. Sparr, M. Vendruscolo, T.P. Knowles, S. Linse, C.M. Dobson, Solution Conditions Determine the Relative Importance of Nucleation and Growth Processes in A-Synuclein Aggregation, Proceedings of the National Academy of Sciences 111 (2014) 7671-7676.
[16] R. Gaspar, G. Meisl, A.K. Buell, L. Young, C.F. Kaminski, T.P. Knowles, E. Sparr, S. Linse, Secondary Nucleation of Monomers on Fibril Surface Dominates A-Synuclein Aggregation and Provides Autocatalytic Amyloid Amplification, Quarterly Reviews of Biophysics 50 (2017) e6.
[17] P. Desplats, H.-J. Lee, E.-J. Bae, C. Patrick, E. Rockenstein, L. Crews, B. Spencer, E. Masliah, S.-J. Lee, Inclusion Formation and Neuronal Cell Death through Neuron-to-Neuron

Transmission of A-Synuclein, Proceedings of the National Academy of Sciences 106 (2009) 13010-13015.
[18] R.J. Karpowicz Jr, C.M. Haney, T.S. Mihaila, R.M. Sandler, E.J. Petersson, V.M.-Y. Lee, Selective Imaging of Internalized Proteopathic A-Synuclein Seeds in Primary Neurons Reveals Mechanistic Insight into Transmission of Synucleinopathies, Journal of Biological Chemistry 292 (2017) 13482-13497.
[19] R. Guerrero-Ferreira, N.M. Taylor, D. Mona, P. Ringler, M.E. Lauer, R. Riek, M. Britschgi, H. Stahlberg, Cryo-Em Structure of Alpha-Synuclein Fibrils, Elife 7 (2018) e36402.
[20] R. Guerrero-Ferreira, N.M. Taylor, A.-A. Arteni, P. Kumari, D. Mona, P. Ringler, M. Britschgi, M.E. Lauer, A. Makky, J. Verasdonck, Two New Polymorphic Structures of Human Full-Length Alpha-Synuclein Fibrils Solved by Cryo-Electron Microscopy, Elife 8 (2019) e48907.
[21] S.H. Scheres, B. Ryskeldi-Falcon, M. Goedert, Molecular Pathology of Neurodegenerative Diseases by Cryo-Em of Amyloids, Nature 621 (2023) 701-710.
[22] M. Wilkinson, Y. Xu, D. Thacker, A.I. Taylor, D.G. Fisher, R.U. Gallardo, S.E. Radford, N.A. Ranson, Structural Evolution of Fibril Polymorphs during Amyloid Assembly, Cell 186 (2023) 5798-5811. e5726.
[23] S. Lövestam, D. Li, J.L. Wagstaff, A. Kotecha, D. Kimanius, S.H. McLaughlin, A.G. Murzin, S.M. Freund, M. Goedert, S.H. Scheres, Disease-Specific Tau Filaments Assemble Via Polymorphic Intermediates, Nature 625 (2024) 119-125.
[24] A. Carlsson, M. Lindqvist, T. Magnusson, 3, 4-Dihydroxyphenylalanine and 5-Hydroxytryptophan as Reserpine Antagonists, Nature 180 (1957) 1200-1200.
[25] W. Poewe, A. Antonini, J.C. Zijlmans, P.R. Burkhard, F. Vingerhoets, Levodopa in the Treatment of Parkinson's Disease: An Old Drug Still Going Strong, Clinical Interventions in Aging (2010) 229-238.
[26] C.H. Van Dyck, C.J. Swanson, P. Aisen, R.J. Bateman, C. Chen, M. Gee, M. Kanekiyo, D. Li, L. Reyderman, S. Cohen, Lecanemab in Early Alzheimer's Disease, New England Journal of Medicine 388 (2023) 9-21.
[27] O. Arias-Carrión, M. Guerra-Crespo, F.J. Padilla-Godínez, L.O. Soto-Rojas, E. Manjarrez, A-Synuclein Pathology in Synucleinopathies: Mechanisms, Biomarkers, and Therapeutic Challenges, International Journal of Molecular Sciences 26 (2025) 5405.
[28] R. Bajracharya, A.C. Caruso, L.J. Vella, R.M. Nisbet, Current and Emerging Strategies for Enhancing Antibody Delivery to the Brain, Pharmaceutics 13 (2021) 2014.
[29] E.A. Ponomarenko, E.V. Poverennaya, E.V. Ilgisonis, M.A. Pyatnitskiy, A.T. Kopylov, V.G. Zgoda, A.V. Lisitsa, A.I. Archakov, The Size of the Human Proteome: The Width and Depth, International Journal of Analytical Chemistry 2016 (2016) 7436849.
[30] D. Whitford, Proteins: Structure and Function, John Wiley & Sons2013.
[31] R. Elkon, R. Agami, Characterization of Noncoding Regulatory DNA in the Human Genome, Nature Biotechnology 35 (2017) 732-746.
[32] G.L. Holliday, J.B. Mitchell, J.M. Thornton, Understanding the Functional Roles of Amino Acid Residues in Enzyme Catalysis, Journal of Molecular Biology 390 (2009) 560-577.
[33] Y. Zou, Y. Liu, X. Wu, S.M. Shell, Functions of Human Replication Protein a (Rpa): From DNA Replication to DNA Damage and Stress Responses, Journal of Cellular Physiology 208 (2006) 267-273.
[34] J. Xu, G.-P. Shi, Vascular Wall Extracellular Matrix Proteins and Vascular Diseases, Biochimica et Biophysica Acta (BBA)-Molecular Basis of Disease 1842 (2014) 2106-2119.

[35] M.A. Hediger, M.F. Romero, J.-B. Peng, A. Rolfs, H. Takanaga, E.A. Bruford, The Abcs of Solute Carriers: Physiological, Pathological and Therapeutic Implications of Human Membrane Transport Proteins: Introduction, Pflügers Archiv 447 (2004) 465-468.
[36] P. Lea, B. Miflin, Amino Acid Metabolism, Ann Rev Plant Physiol 28 (1977) 299-329.
[37] M.J. Lopez, S.S. Mohiuddin, Biochemistry, Essential Amino Acids, Statpearls [Internet], StatPearls Publishing2024.
[38] C.D. Georgiou, Functional Properties of Amino Acid Side Chains as Biomarkers of Extraterrestrial Life, Astrobiology 18 (2018) 1479-1496.
[39] K.A. Piez, Primary Structure, Biochemistry of Collagen, Springer1976, pp. 1-44.
[40] J.T. Pelton, L.R. McLean, Spectroscopic Methods for Analysis of Protein Secondary Structure, Analytical Biochemistry 277 (2000) 167-176.
[41] D. Barlow, J. Thornton, Helix Geometry in Proteins, Journal of Molecular Biology 201 (1988) 601-619.
[42] J.S. Nowick, Chemical Models of Protein B-Sheets, Accounts of Chemical Research 32 (1999) 287-296.
[43] V.A. Adhav, K. Saikrishnan, The Realm of Unconventional Noncovalent Interactions in Proteins: Their Significance in Structure and Function, Acs Omega 8 (2023) 22268-22284.
[44] I. Rehman, C.C. Kerndt, S. Botelho, Biochemistry, Tertiary Protein Structure, Statpearls [Internet], StatPearls Publishing2024.
[45] L.M. Veenhoff, E.H. Heuberger, B. Poolman, Quaternary Structure and Function of Transport Proteins, Trends in Biochemical Sciences 27 (2002) 242-249.
[46] S.W. Englander, T.R. Sosnick, L.C. Mayne, M. Shtilerman, P.X. Qi, Y. Bai, Fast and Slow Folding in Cytochrome C, Accounts of Chemical Research 31 (1998) 737-744.
[47] R. Ballew, J. Sabelko, M. Gruebele, Direct Observation of Fast Protein Folding: The Initial Collapse of Apomyoglobin, Proceedings of the National Academy of Sciences 93 (1996) 5759-5764.
[48] J.D. Bryngelson, J.N. Onuchic, N.D. Socci, P.G. Wolynes, Funnels, Pathways, and the Energy Landscape of Protein Folding: A Synthesis, Proteins: Structure, Function, and Bioinformatics 21 (1995) 167-195.
[49] J.N. Onuchic, Z. Luthey-Schulten, P.G. Wolynes, Theory of Protein Folding: The Energy Landscape Perspective, Annual Review of Physical Chemistry 48 (1997) 545-600.
[50] K. Kamagata, M. Arai, K. Kuwajima, Unification of the Folding Mechanisms of Non-Two-State and Two-State Proteins, Journal of Molecular Biology 339 (2004) 951-965.
[51] D. Barrick, R.L. Baldwin, The Molten Globule Intermediate of Apomyoglobin and the Process of Protein Folding, Protein Science 2 (1993) 869-876.
[52] O.B. Ptitsyn, Protein Folding: Hypotheses and Experiments, Journal of Protein Chemistry 6 (1987) 273-293.
[53] S.W. Englander, L. Mayne, The Nature of Protein Folding Pathways, Proceedings of the National Academy of Sciences 111 (2014) 15873-15880.
[54] M.S. Hipp, P. Kasturi, F.U. Hartl, The Proteostasis Network and Its Decline in Ageing, Nature Reviews Molecular Cell Biology 20 (2019) 421-435.
[55] R.J. Ellis, S.M. Van der Vies, Molecular Chaperones, Annual Review of Biochemistry 60 (1991) 321-347.
[56] B. Wilkinson, H.F. Gilbert, Protein Disulfide Isomerase, Biochimica et Biophysica Acta (BBA)-Proteins and Proteomics 1699 (2004) 35-44.
[57] D. Nandi, P. Tahiliani, A. Kumar, D. Chandu, The Ubiquitin-Proteasome System, Journal of Biosciences 31 (2006) 137-155.
[58] M.S. Hipp, S.-H. Park, F.U. Hartl, Proteostasis Impairment in Protein-Misfolding and-Aggregation Diseases, Trends in Cell Biology 24 (2014) 506-514.

[59] M.H. Polymeropoulos, C. Lavedan, E. Leroy, S.E. Ide, A. Dehejia, A. Dutra, B. Pike, H. Root, J. Rubenstein, R. Boyer, Mutation in the A-Synuclein Gene Identified in Families with Parkinson's Disease, Science 276 (1997) 2045-2047.
[60] L. Puspita, S.Y. Chung, J.-w. Shim, Oxidative Stress and Cellular Pathologies in Parkinson's Disease, Molecular Brain 10 (2017) 53.
[61] D.A. Di Monte, M. Lavasani, A.B. Manning-Bog, Environmental Factors in Parkinson's Disease, Neurotoxicology 23 (2002) 487-502.
[62] C.L. Masters, R. Bateman, K. Blennow, C.C. Rowe, R.A. Sperling, J.L. Cummings, Alzheimer's Disease, Nature Reviews Disease Primers 1 (2015) 15056.
[63] L.V. Kalia, A.E. Lang, Parkinson's Disease, The Lancet 386 (2015) 896-912.
[64] M.C. Kiernan, S. Vucic, B.C. Cheah, M.R. Turner, A. Eisen, O. Hardiman, J.R. Burrell, M.C. Zoing, Amyotrophic Lateral Sclerosis, The Lancet 377 (2011) 942-955.
[65] F. Chiti, C.M. Dobson, Protein Misfolding, Amyloid Formation, and Human Disease: A Summary of Progress over the Last Decade, Annual Review of Biochemistry 86 (2017) 27-68.
[66] P. Hammarström, F. Schneider, J.W. Kelly, Trans-Suppression of Misfolding in an Amyloid Disease, Science 293 (2001) 2459-2462.
[67] J.R. Kumita, S. Poon, G.L. Caddy, C.L. Hagan, M. Dumoulin, J.J. Yerbury, E.M. Stewart, C.V. Robinson, M.R. Wilson, C.M. Dobson, The Extracellular Chaperone Clusterin Potently Inhibits Human Lysozyme Amyloid Formation by Interacting with Prefibrillar Species, Journal of Molecular Biology 369 (2007) 157-167.
[68] T. Ong, B.W. Ramsey, Cystic Fibrosis: A Review, Jama 329 (2023) 1859-1871.
[69] E. Kelly, C.M. Greene, T.P. Carroll, N.G. McElvaney, S.J. O'Neill, Alpha-1 Antitrypsin Deficiency, Respiratory Medicine CME 4 (2011) 1-8.
[70] T.P. Knowles, M. Vendruscolo, C.M. Dobson, The Amyloid State and Its Association with Protein Misfolding Diseases, Nature Reviews Molecular Cell Biology 15 (2014) 384-396.
[71] A. Relini, S. Torrassa, R. Ferrando, R. Rolandi, S. Campioni, F. Chiti, A. Gliozzi, Detection of Populations of Amyloid-Like Protofibrils with Different Physical Properties, Biophysical Journal 98 (2010) 1277-1284.
[72] F. Chiti, C.M. Dobson, Protein Misfolding, Functional Amyloid, and Human Disease, Annual Review of Biochemistry 75 (2006) 333-366.
[73] M.S. Dueholm, S.V. Petersen, M. Sønderkær, P. Larsen, G. Christiansen, K.L. Hein, J.J. Enghild, J.L. Nielsen, K.L. Nielsen, P.H. Nielsen, Functional Amyloid in Pseudomonas, Molecular Microbiology 77 (2010) 1009-1020.
[74] D. Otzen, R. Riek, Functional Amyloids, Cold Spring Harbor Perspectives in Biology 11 (2019) a033860.
[75] P.C. Ke, R. Zhou, L.C. Serpell, R. Riek, T.P. Knowles, H.A. Lashuel, E. Gazit, I.W. Hamley, T.P. Davis, M. Fändrich, Half a Century of Amyloids: Past, Present and Future, Chemical Society Reviews 49 (2020) 5473-5509.
[76] M. Calamai, F. Chiti, C.M. Dobson, Amyloid Fibril Formation Can Proceed from Different Conformations of a Partially Unfolded Protein, Biophysical Journal 89 (2005) 4201-4210.
[77] N. Louros, J. Schymkowitz, F. Rousseau, Mechanisms and Pathology of Protein Misfolding and Aggregation, Nature Reviews Molecular Cell Biology 24 (2023) 912-933.
[78] H.F. Zein, I. Alam, P. Asanithi, T. Sutthibutpong, Molecular Dynamics Study on the Effects of Charged Amino Acid Distribution under Low Ph Condition to the Unfolding of Hen Egg White Lysozyme and Formation of Beta Strands, PloS One 17 (2022) e0249742.

[79] L. Frey, J. Zhou, G. Cereghetti, M.E. Weber, D. Rhyner, A. Pokharna, L. Wenchel, H. Kadavath, Y. Cao, B.H. Meier, A Structural Rationale for Reversible Vs Irreversible Amyloid Fibril Formation from a Single Protein, Nature Communications 15 (2024) 8448.
[80] C. Galvagnion, F.R. Marlet, S. Cerri, A.H. Schapira, F. Blandini, D.A. Di Monte, Sphingolipid Changes in Parkinson L444p Gba Mutation Fibroblasts Promote A-Synuclein Aggregation, Brain 145 (2022) 1038-1051.
[81] F. Havemeister, M. Ghaeidamini, E.K. Esbjörner, Monovalent Cations Have Different Effects on the Assembly Kinetics and Morphology of A-Synuclein Amyloid Fibrils, Biochemical and Biophysical Research Communications 679 (2023) 31-36.
[82] O. Coskuner-Weber, O. Mirzanli, V.N. Uversky, Intrinsically Disordered Proteins and Proteins with Intrinsically Disordered Regions in Neurodegenerative Diseases, Biophysical Reviews 14 (2022) 679-707.
[83] T. Pálmadóttir, J. Getachew, L. Ortigosa-Pascual, E. Axell, J. Wei, U. Olsson, T.P. Knowles, S. Linse, On the Reversibility of Amyloid Fibril Formation, Biophysics Reviews 6 (2025).
[84] M. Törnquist, T.C. Michaels, K. Sanagavarapu, X. Yang, G. Meisl, S.I. Cohen, T.P. Knowles, S. Linse, Secondary Nucleation in Amyloid Formation, Chemical Communications 54 (2018) 8667-8684.
[85] S. Campioni, G. Carret, S. Jordens, L.c. Nicoud, R. Mezzenga, R. Riek, The Presence of an Air–Water Interface Affects Formation and Elongation of A-Synuclein Fibrils, Journal of the American Chemical Society 136 (2014) 2866-2875.
[86] J.D. Camino, P. Gracia, N. Cremades, The Role of Water in the Primary Nucleation of Protein Amyloid Aggregation, Biophysical Chemistry 269 (2021) 106520.
[87] W.-F. Xue, A.L. Hellewell, E.W. Hewitt, S.E. Radford, Fibril Fragmentation in Amyloid Assembly and Cytotoxicity: When Size Matters, Prion 4 (2010) 20-25.
[88] T. Ikenoue, Y.H. Lee, J. Kardos, M. Saiki, H. Yagi, Y. Kawata, Y. Goto, Cold Denaturation of A-Synuclein Amyloid Fibrils, Angewandte Chemie International Edition 53 (2014) 7799-7804.
[89] J. Kardos, A. Micsonai, H. Pál-Gábor, É. Petrik, L. Gráf, J. Kovács, Y.-H. Lee, H. Naiki, Y. Goto, Reversible Heat-Induced Dissociation of B2-Microglobulin Amyloid Fibrils, Biochemistry 50 (2011) 3211-3220.
[90] D.R. Boyer, B. Li, C. Sun, W. Fan, K. Zhou, M.P. Hughes, M.R. Sawaya, L. Jiang, D.S. Eisenberg, The A-Synuclein Hereditary Mutation E46k Unlocks a More Stable, Pathogenic Fibril Structure, Proceedings of the National Academy of Sciences 117 (2020) 3592-3602.
[91] M.M. Schneider, S. Gautam, T.W. Herling, E. Andrzejewska, G. Krainer, A.M. Miller, V.A. Trinkaus, Q.A. Peter, F.S. Ruggeri, M. Vendruscolo, The Hsc70 Disaggregation Machinery Removes Monomer Units Directly from A-Synuclein Fibril Ends, Nature Communications 12 (2021) 5999.
[92] P. Arosio, T.P. Knowles, S. Linse, On the Lag Phase in Amyloid Fibril Formation, Physical Chemistry Chemical Physics 17 (2015) 7606-7618.
[93] S.I. Cohen, M. Vendruscolo, C.M. Dobson, T.P. Knowles, From Macroscopic Measurements to Microscopic Mechanisms of Protein Aggregation, Journal of Molecular Biology 421 (2012) 160-171.
[94] S. Linse, Toward the Equilibrium and Kinetics of Amyloid Peptide Self-Assembly, Current Opinion in Structural Biology 70 (2021) 87-98.
[95] S.I. Cohen, M. Vendruscolo, C.M. Dobson, T.P. Knowles, Nucleated Polymerization with Secondary Pathways. Iii. Equilibrium Behavior and Oligomer Populations, The Journal of Chemical Physics 135 (2011).
[96] D. Eisenberg, M. Jucker, The Amyloid State of Proteins in Human Diseases, Cell 148 (2012) 1188-1203.

[97] A. Alzheimer, Über Eigenartige Krankheitsfälle Des Späteren Alters, Zeitschrift für die gesamte Neurologie und Psychiatrie 4 (1911) 356-385.
[98] P. Ladewig, Double-Refringence of the Amyloid-Congo-Red-Complex in Histological Sections, Nature 156 (1945) 81-82.
[99] A.S. Cohen, E. Calkins, Electron Microscopic Observations on a Fibrous Component in Amyloid of Diverse Origins, Nature 183 (1959) 1202-1203.
[100] M. Kidd, Paired Helical Filaments in Electron Microscopy of Alzheimer's Disease, Nature 197 (1963) 192-193.
[101] E. Eanes, G. Glenner, X-Ray Diffraction Studies on Amyloid Filaments, Journal of Histochemistry & Cytochemistry 16 (1968) 673-677.
[102] G.G. Glenner, C.W. Wong, Alzheimer's Disease: Initial Report of the Purification and Characterization of a Novel Cerebrovascular Amyloid Protein, Biochemical and Biophysical Research Communications 120 (1984) 885-890.
[103] R. Nelson, M.R. Sawaya, M. Balbirnie, A.Ø. Madsen, C. Riekel, R. Grothe, D. Eisenberg, Structure of the Cross-B Spine of Amyloid-Like Fibrils, Nature 435 (2005) 773-778.
[104] A.T. Petkova, Y. Ishii, J.J. Balbach, O.N. Antzutkin, R.D. Leapman, F. Delaglio, R. Tycko, A Structural Model for Alzheimer's B-Amyloid Fibrils Based on Experimental Constraints from Solid State Nmr, Proceedings of the National Academy of Sciences 99 (2002) 16742-16747.
[105] A.W. Fitzpatrick, B. Falcon, S. He, A.G. Murzin, G. Murshudov, H.J. Garringer, R.A. Crowther, B. Ghetti, M. Goedert, S.H. Scheres, Cryo-Em Structures of Tau Filaments from Alzheimer’s Disease, Nature 547 (2017) 185-190.
[106] A.W. Fitzpatrick, G.T. Debelouchina, M.J. Bayro, D.K. Clare, M.A. Caporini, V.S. Bajaj, C.P. Jaroniec, L. Wang, V. Ladizhansky, S.A. Müller, Atomic Structure and Hierarchical Assembly of a Cross-B Amyloid Fibril, Proceedings of the National Academy of Sciences 110 (2013) 5468-5473.
[107] K. Liu, Y. Tao, Q. Zhao, W. Xia, X. Li, S. Zhang, Y. Yao, H. Xiang, C. Han, L. Tan, Binding Adaptability of Chemical Ligands to Polymorphic A-Synuclein Amyloid Fibrils, Proceedings of the National Academy of Sciences 121 (2024) e2321633121.
[108] Y. Han, J. Li, W. Xia, Q. Li, Z. Sun, W. Zeng, Y. Hu, K.C. Luk, C. Liu, S. Xiang, Fibril Fuzzy Coat Is Important for A-Synuclein Pathological Transmission Activity, Neuron 113 (2025) 1723-1740. e1727.
[109] D.R. Boyer, B. Li, C. Sun, W. Fan, M.R. Sawaya, L. Jiang, D.S. Eisenberg, Structures of Fibrils Formed by A-Synuclein Hereditary Disease Mutant H50q Reveal New Polymorphs, Nature Structural & Molecular Biology 26 (2019) 1044-1052.
[110] C.S. Goldsbury, G.J. Cooper, K.N. Goldie, S.A. Müller, E.L. Saafi, W. Gruijters, M.P. Misur, A. Engel, U. Aebi, J. Kistler, Polymorphic Fibrillar Assembly of Human Amylin, Journal of Structural Biology 119 (1997) 17-27.
[111] A.T. Petkova, R.D. Leapman, Z. Guo, W.-M. Yau, M.P. Mattson, R. Tycko, Self-Propagating, Molecular-Level Polymorphism in Alzheimer's B-Amyloid Fibrils, Science 307 (2005) 262-265.
[112] Y. Yang, Y. Shi, M. Schweighauser, X. Zhang, A. Kotecha, A.G. Murzin, H.J. Garringer, P.W. Cullinane, Y. Saito, T. Foroud, Structures of A-Synuclein Filaments from Human Brains with Lewy Pathology, Nature 610 (2022) 791-795.
[113] M. Schweighauser, Y. Shi, A. Tarutani, F. Kametani, A.G. Murzin, B. Ghetti, T. Matsubara, T. Tomita, T. Ando, K. Hasegawa, Structures of A-Synuclein Filaments from Multiple System Atrophy, Nature 585 (2020) 464-469.
[114] M. Kollmer, W. Close, L. Funk, J. Rasmussen, A. Bsoul, A. Schierhorn, M. Schmidt, C.J. Sigurdson, M. Jucker, M. Fändrich, Cryo-Em Structure and Polymorphism of Aβ

Amyloid Fibrils Purified from Alzheimer's Brain Tissue, Nature Communications 10 (2019) 4760.
[115] Y. Yang, D. Arseni, W. Zhang, M. Huang, S. Lövestam, M. Schweighauser, A. Kotecha, A.G. Murzin, S.Y. Peak-Chew, J. Macdonald, Cryo-Em Structures of Amyloid-B 42 Filaments from Human Brains, Science 375 (2022) 167-172.
[116] D. Arseni, M. Hasegawa, A.G. Murzin, F. Kametani, M. Arai, M. Yoshida, B. Ryskeldi-Falcon, Structure of Pathological Tdp-43 Filaments from Als with Ftld, Nature 601 (2022) 139-143.
[117] D. Arseni, R. Chen, A.G. Murzin, S.Y. Peak-Chew, H.J. Garringer, K.L. Newell, F. Kametani, A.C. Robinson, R. Vidal, B. Ghetti, Tdp-43 Forms Amyloid Filaments with a Distinct Fold in Type a Ftld-Tdp, Nature 620 (2023) 898-903.
[118] T. Ban, K. Yamaguchi, Y. Goto, Direct Observation of Amyloid Fibril Growth, Propagation, and Adaptation, Accounts of Chemical Research 39 (2006) 663-670.
[119] A. Peduzzo, S. Linse, A.K. Buell, The Properties of A-Synuclein Secondary Nuclei Are Dominated by the Solution Conditions Rather Than the Seed Fibril Strain, ACS Chemical Neuroscience 11 (2020) 909-918.
[120] S. Lövestam, M. Schweighauser, T. Matsubara, S. Murayama, T. Tomita, T. Ando, K. Hasegawa, M. Yoshida, A. Tarutani, M. Hasegawa, Seeded Assembly in Vitro Does Not Replicate the Structures of A-Synuclein Filaments from Multiple System Atrophy, FEBS Open Bio 11 (2021) 999-1013.
[121] X. Periole, T. Huber, A. Bonito-Oliva, K.C. Aberg, P.C. Van Der Wel, T.P. Sakmar, S.J. Marrink, Energetics Underlying Twist Polymorphisms in Amyloid Fibrils, The Journal of Physical Chemistry B 122 (2018) 1081-1091.
[122] B.R. Bloem, M.S. Okun, C. Klein, Parkinson's Disease, The Lancet 397 (2021) 2284-2303.
[123] C. Blauwendraat, K. Heilbron, C.L. Vallerga, S. Bandres-Ciga, R. Von Coelln, L. Pihlstrøm, J. Simón-Sánchez, C. Schulte, M. Sharma, L. Krohn, Parkinson's Disease Age at Onset Genome-Wide Association Study: Defining Heritability, Genetic Loci, and A-Synuclein Mechanisms, Movement Disorders 34 (2019) 866-875.
[124] S.-Y. Lim, C. Klein, Parkinson's Disease Is Predominantly a Genetic Disease, Journal of Parkinson's disease 14 (2024) 467-482.
[125] A. Anwar, S. Saleem, A. Akhtar, S. Ashraf, M.F. Ahmed, Juvenile Parkinson Disease, Cureus 11 (2019).
[126] A. Ascherio, M.A. Schwarzschild, The Epidemiology of Parkinson's Disease: Risk Factors and Prevention, The Lancet Neurology 15 (2016) 1257-1272.
[127] S. Bandres-Ciga, M. Diez-Fairen, J.J. Kim, A.B. Singleton, Genetics of Parkinson's Disease: An Introspection of Its Journey Towards Precision Medicine, Neurobiology of Disease 137 (2020) 104782.
[128] S. Latif, M. Jahangeer, D.M. Razia, M. Ashiq, A. Ghaffar, M. Akram, A. El Allam, A. Bouyahya, L. Garipova, M.A. Shariati, Dopamine in Parkinson's Disease, Clinica Chimica Acta 522 (2021) 114-126.
[129] J.M. Fearnley, A.J. Lees, Ageing and Parkinson's Disease: Substantia Nigra Regional Selectivity, Brain 114 (1991) 2283-2301.
[130] A.C. Whitfield, B.T. Moore, R.N. Daniels, Classics in Chemical Neuroscience: Levodopa, ACS Chemical Neuroscience 5 (2014) 1192-1197.
[131] S.M. Brooker, G.E. Naylor, D. Krainc, Cell Biology of Parkinson's Disease: Mechanisms of Synaptic, Lysosomal, and Mitochondrial Dysfunction, Current Opinion in Neurobiology 85 (2024) 102841.
[132] P. Calabresi, A. Mechelli, G. Natale, L. Volpicelli-Daley, G. Di Lazzaro, V. Ghiglieri, Alpha-Synuclein in Parkinson's Disease and Other Synucleinopathies: From Overt

Neurodegeneration Back to Early Synaptic Dysfunction, Cell Death & Disease 14 (2023) 176.
[133] F.N. Emamzadeh, Alpha-Synuclein Structure, Functions, and Interactions, Journal of Research in Medical Sciences 21 (2016) 29.
[134] M. Sharma, J. Burré, A-Synuclein in Synaptic Function and Dysfunction, Trends in Neurosciences 46 (2023) 153-166.
[135] J. Burré, The Synaptic Function of A-Synuclein, Journal of Parkinson's disease 5 (2015) 699-713.
[136] V. Gao, J.A. Briano, L.E. Komer, J. Burré, Functional and Pathological Effects of A-Synuclein on Synaptic Snare Complexes, Journal of Molecular Biology 435 (2023) 167714.
[137] L. Wang, U. Das, D.A. Scott, Y. Tang, P.J. McLean, S. Roy, A-Synuclein Multimers Cluster Synaptic Vesicles and Attenuate Recycling, Current Biology 24 (2014) 2319-2326.
[138] J. Sun, L. Wang, H. Bao, S. Premi, U. Das, E.R. Chapman, S. Roy, Functional Cooperation of A-Synuclein and Vamp2 in Synaptic Vesicle Recycling, Proceedings of the National Academy of Sciences 116 (2019) 11113-11115.
[139] W.K. Man, B. Tahirbegi, M.D. Vrettas, S. Preet, L. Ying, M. Vendruscolo, A. De Simone, G. Fusco, The Docking of Synaptic Vesicles on the Presynaptic Membrane Induced by A-Synuclein Is Modulated by Lipid Composition, Nature Communications 12 (2021) 927.
[140] A. Agarwal, A. Chandran, F. Raza, I.-M. Ungureanu, C. Hilcenko, K. Stott, N.A. Bright, N. Morone, A.J. Warren, J. Lautenschläger, Vamp2 Regulates Phase Separation of A-Synuclein, Nature Cell Biology 26 (2024) 1296-1308.
[141] M.R. Sawaya, M.P. Hughes, J.A. Rodriguez, R. Riek, D.S. Eisenberg, The Expanding Amyloid Family: Structure, Stability, Function, and Pathogenesis, Cell 184 (2021) 4857-4873.
[142] J. Lautenschläger, A.D. Stephens, G. Fusco, F. Ströhl, N. Curry, M. Zacharopoulou, C.H. Michel, R. Laine, N. Nespovitaya, M. Fantham, C-Terminal Calcium Binding of A-Synuclein Modulates Synaptic Vesicle Interaction, Nature Communications 9 (2018) 712.
[143] W. Hoyer, D. Cherny, V. Subramaniam, T.M. Jovin, Impact of the Acidic C-Terminal Region Comprising Amino Acids 109− 140 on A-Synuclein Aggregation in Vitro, Biochemistry 43 (2004) 16233-16242.
[144] F. Jia, A. Fellner, K.R. Kumar, Monogenic Parkinson's Disease: Genotype, Phenotype, Pathophysiology, and Genetic Testing, Genes 13 (2022) 471.
[145] C.M. Lill, Genetics of Parkinson's Disease, Molecular and Cellular Probes 30 (2016) 386-396.
[146] W. Scott, L. Yamaoka, J. Stajich, B. Scott, J. Vance, A. Roses, M. Pericak-Vance, R. Watts, M. Nance, J. Hubble, The [Alpha]-Synuclein Gene Is Not a Major Risk Factor in Familial Parkinson Disease, Neurogenetics 2 (1999) 191.
[147] A.D. Stephens, M. Zacharopoulou, R. Moons, G. Fusco, N. Seetaloo, A. Chiki, P.J. Woodhams, I. Mela, H.A. Lashuel, J.J. Phillips, Extent of N-Terminus Exposure of Monomeric Alpha-Synuclein Determines Its Aggregation Propensity, Nature Communications 11 (2020) 1-15.
[148] L.A. Munishkina, J. Henriques, V.N. Uversky, A.L. Fink, Role of Protein− Water Interactions and Electrostatics in A-Synuclein Fibril Formation, Biochemistry 43 (2004) 3289-3300.
[149] K. Afitska, A. Fucikova, V.V. Shvadchak, D.A. Yushchenko, A-Synuclein Aggregation at Low Concentrations, Biochimica et Biophysica Acta (BBA)-Proteins and Proteomics 1867 (2019) 701-709.
[150] A. Tarutani, G. Suzuki, A. Shimozawa, T. Nonaka, H. Akiyama, S.-i. Hisanaga, M. Hasegawa, The Effect of Fragmented Pathogenic A-Synuclein Seeds on Prion-Like Propagation, Journal of Biological Chemistry 291 (2016) 18675-18688.

[151] C. Galvagnion, A.K. Buell, G. Meisl, T.C. Michaels, M. Vendruscolo, T.P. Knowles, C.M. Dobson, Lipid Vesicles Trigger A-Synuclein Aggregation by Stimulating Primary Nucleation, Nature Chemical Biology 11 (2015) 229-234.
[152] Y. Li, C. Yang, S. Wang, D. Yang, Y. Zhang, L. Xu, L. Ma, J. Zheng, R.B. Petersen, L. Zheng, Copper and Iron Ions Accelerate the Prion-Like Propagation of A-Synuclein: A Vicious Cycle in Parkinson's Disease, International Journal of Biological Macromolecules 163 (2020) 562-573.
[153] V.N. Uversky, J. Li, A.L. Fink, Evidence for a Partially Folded Intermediate in A-Synuclein Fibril Formation, Journal of Biological Chemistry 276 (2001) 10737-10744.
[154] V.V. Shvadchak, K. Afitska, D.A. Yushchenko, Inhibition of A-Synuclein Amyloid Fibril Elongation by Blocking Fibril Ends, Angewandte Chemie International Edition 57 (2018) 5690-5694.
[155] S.I. Cohen, S. Linse, L.M. Luheshi, E. Hellstrand, D.A. White, L. Rajah, D.E. Otzen, M. Vendruscolo, C.M. Dobson, T.P. Knowles, Proliferation of Amyloid-B42 Aggregates Occurs through a Secondary Nucleation Mechanism, Proceedings of the National Academy of Sciences 110 (2013) 9758-9763.
[156] A.J. Dear, G. Meisl, J. Hu, T.P. Knowles, S. Linse, Kinetics of Seeded Protein Aggregation: Theory and Application, arXiv preprint arXiv:2503.20941 (2025).
[157] C.K. Xu, G. Meisl, E.A. Andrzejewska, G. Krainer, A.J. Dear, M. Castellana-Cruz, S. Turi, I.A. Edu, G. Vivacqua, R.P. Jacquat, A-Synuclein Oligomers Form by Secondary Nucleation, Nature Communications 15 (2024) 7083.
[158] X. Gao, M. Carroni, C. Nussbaum-Krammer, A. Mogk, N.B. Nillegoda, A. Szlachcic, D.L. Guilbride, H.R. Saibil, M.P. Mayer, B. Bukau, Human Hsp70 Disaggregase Reverses Parkinson's-Linked A-Synuclein Amyloid Fibrils, Molecular Cell 59 (2015) 781-793.
[159] Y. Nakagawa, H.C.-H. Shen, Y. Komi, S. Sugiyama, T. Kurinomaru, Y. Tomabechi, E. Krayukhina, K. Okamoto, T. Yokoyama, M. Shirouzu, Amyloid Conformation-Dependent Disaggregation in a Reconstituted Yeast Prion System, Nature Chemical Biology 18 (2022) 321-331.
[160] W.-F. Xue, A.L. Hellewell, W.S. Gosal, S.W. Homans, E.W. Hewitt, S.E. Radford, Fibril Fragmentation Enhances Amyloid Cytotoxicity*♦, Journal of Biological Chemistry 284 (2009) 34272-34282.
[161] S. Sanami, T.J. Purton, D.P. Smith, M.F. Tuite, W.-F. Xue, Comparative Analysis of the Relative Fragmentation Stabilities of Polymorphic Alpha-Synuclein Amyloid Fibrils, Biomolecules 12 (2022) 630.
[162] D. Emin, Y.P. Zhang, E. Lobanova, A. Miller, X. Li, Z. Xia, H. Dakin, D.I. Sideris, J.Y. Lam, R.T. Ranasinghe, Small Soluble A-Synuclein Aggregates Are the Toxic Species in Parkinson's Disease, Nature Communications 13 (2022) 5512.
[163] X.-y. Du, X.-x. Xie, R.-t. Liu, The Role of A-Synuclein Oligomers in Parkinson's Disease, International Journal of Molecular Sciences 21 (2020) 8645.
[164] W. Peelaerts, L. Bousset, A. Van der Perren, A. Moskalyuk, R. Pulizzi, M. Giugliano, C. Van den Haute, R. Melki, V. Baekelandt, A-Synuclein Strains Cause Distinct Synucleinopathies after Local and Systemic Administration, Nature 522 (2015) 340-344.
[165] A. Tarutani, T. Arai, S. Murayama, S.-i. Hisanaga, M. Hasegawa, Potent Prion-Like Behaviors of Pathogenic A-Synuclein and Evaluation of Inactivation Methods, Acta Neuropathologica Communications 6 (2018) 29.
[166] R. Bell, M. Castellana-Cruz, A. Nene, R.J. Thrush, C.K. Xu, J.R. Kumita, M. Vendruscolo, Effects of N-Terminal Acetylation on the Aggregation of Disease-Related A-Synuclein Variants, Journal of Molecular Biology 435 (2023) 167825.
[167] Y. Zhang, Y. Wang, Y. Liu, G. Wei, F. Ding, Y. Sun, Molecular Insights into the Misfolding and Dimerization Dynamics of the Full-Length A-Synuclein from Atomistic

Discrete Molecular Dynamics Simulations, ACS Chemical Neuroscience 13 (2022) 3126-3137.
[168] K.A. Conway, S.-J. Lee, J.-C. Rochet, T.T. Ding, R.E. Williamson, P.T. Lansbury Jr, Acceleration of Oligomerization, Not Fibrillization, Is a Shared Property of Both A-Synuclein Mutations Linked to Early-Onset Parkinson's Disease: Implications for Pathogenesis and Therapy, Proceedings of the National Academy of Sciences 97 (2000) 571-576.
[169] L.R. Lemkau, G. Comellas, K.D. Kloepper, W.S. Woods, J.M. George, C.M. Rienstra, Mutant Protein A30p A-Synuclein Adopts Wild-Type Fibril Structure, Despite Slower Fibrillation Kinetics, Journal of Biological Chemistry 287 (2012) 11526-11532.
[170] J. Li, V.N. Uversky, A.L. Fink, Effect of Familial Parkinson's Disease Point Mutations A30p and A53t on the Structural Properties, Aggregation, and Fibrillation of Human A-Synuclein, Biochemistry 40 (2001) 11604-11613.
[171] S. Devi, D.K. Garg, R. Bhat, A30p and A30g Mutations in A-Synuclein Promote Metastable Long-Lived Aggregates with Distinct Structural Responses to Egcg, Biochemistry 64 (2025) 4513-4528.
[172] R.A. Fredenburg, C. Rospigliosi, R.K. Meray, J.C. Kessler, H.A. Lashuel, D. Eliezer, P.T. Lansbury, The Impact of the E46k Mutation on the Properties of A-Synuclein in Its Monomeric and Oligomeric States, Biochemistry 46 (2007) 7107-7118.
[173] O. Khalaf, B. Fauvet, A. Oueslati, I. Dikiy, A.-L. Mahul-Mellier, F.S. Ruggeri, M.K. Mbefo, F. Vercruysse, G. Dietler, S.-J. Lee, The H50q Mutation Enhances A-Synuclein Aggregation, Secretion, and Toxicity, Journal of Biological Chemistry 289 (2014) 21856-21876.
[174] H. Long, W. Zheng, Y. Liu, Y. Sun, K. Zhao, Z. Liu, W. Xia, S. Lv, Z. Liu, D. Li, Wild-Type A-Synuclein Inherits the Structure and Exacerbated Neuropathology of E46k Mutant Fibril Strain by Cross-Seeding, Proceedings of the National Academy of Sciences 118 (2021) e2012435118.
[175] J. Lu, F. Sun, H. Ma, H. Qing, Y. Deng, Comparison between A-Synuclein Wild-Type and A53t Mutation in a Progressive Parkinson's Disease Model, Biochemical and Biophysical Research Communications 464 (2015) 988-993.
[176] Y. Sun, S. Hou, K. Zhao, H. Long, Z. Liu, J. Gao, Y. Zhang, X.-D. Su, D. Li, C. Liu, Cryo-Em Structure of Full-Length A-Synuclein Amyloid Fibril with Parkinson’s Disease Familial A53t Mutation, Cell Research 30 (2020) 360-362.
[177] Y. Li, C. Zhao, F. Luo, Z. Liu, X. Gui, Z. Luo, X. Zhang, D. Li, C. Liu, X. Li, Amyloid Fibril Structure of A-Synuclein Determined by Cryo-Electron Microscopy, Cell Research 28 (2018) 897-903.
[178] T. Ohgita, N. Namba, H. Kono, T. Shimanouchi, H. Saito, Mechanisms of Enhanced Aggregation and Fibril Formation of Parkinson’s Disease-Related Variants of A-Synuclein, Scientific Reports 12 (2022) 6770.
[179] J. Huang, R. Ahmed, M. Akimoto, K. Martinez Pomier, G. Melacini, Early-Onset Parkinson Mutation Remodels Monomer–Fibril Interactions to Allosterically Amplify Synuclein’s Amyloid Cascade, JACS Au 3 (2023) 3485-3493.
[180] Y.-C. Chi, G.S. Armstrong, D.N. Jones, E.Z. Eisenmesser, C.-W. Liu, Residue Histidine 50 Plays a Key Role in Protecting A-Synuclein from Aggregation at Physiological Ph, Journal of Biological Chemistry 289 (2014) 15474-15481.
[181] P. Flagmeier, G. Meisl, M. Vendruscolo, T.P. Knowles, C.M. Dobson, A.K. Buell, C. Galvagnion, Mutations Associated with Familial Parkinson’s Disease Alter the Initiation and Amplification Steps of A-Synuclein Aggregation, Proceedings of the National Academy of Sciences 113 (2016) 10328-10333.

[182] G.A. de Oliveira, J.L. Silva, Alpha-Synuclein Stepwise Aggregation Reveals Features of an Early Onset Mutation in Parkinson's Disease, Communications Biology 2 (2019) 374.
[183] K. Zhao, Y. Li, Z. Liu, H. Long, C. Zhao, F. Luo, Y. Sun, Y. Tao, X.-d. Su, D. Li, Parkinson's Disease Associated Mutation E46k of A-Synuclein Triggers the Formation of a Distinct Fibril Structure, Nature Communications 11 (2020) 2643.
[184] R. Porcari, C. Proukakis, C.A. Waudby, B. Bolognesi, P.P. Mangione, J.F. Paton, S. Mullin, L.D. Cabrita, A. Penco, A. Relini, The H50q Mutation Induces a 10-Fold Decrease in the Solubility of A-Synuclein, Journal of Biological Chemistry 290 (2015) 2395-2404.
[185] B.A. Hijaz, L.A. Volpicelli-Daley, Initiation and Propagation of A-Synuclein Aggregation in the Nervous System, Molecular Neurodegeneration 15 (2020) 19.
[186] A.B. Singleton, M. Farrer, J. Johnson, A. Singleton, S. Hague, J. Kachergus, M. Hulihan, T. Peuralinna, A. Dutra, R. Nussbaum, A-Synuclein Locus Triplication Causes Parkinson's Disease, Science 302 (2003) 841-841.
[187] J. Kachergus, M. Munz, E.-M. Larsson, B. Schule, J. Langston, F. Middleton, O. Ross, M. Hulihan, Phenotypic Variation in a Large Swedish Pedigree Due to Snca Duplication and Triplication, Neurology 68 (2007) 916-922.
[188] I. Martin, J.W. Kim, V.L. Dawson, T.M. Dawson, Lrrk2 Pathobiology in Parkinson's Disease, Journal of Neurochemistry 131 (2014) 554-565.
[189] S.-H. Kuo, I. Tasset, M.M. Cheng, A. Diaz, M.-K. Pan, O.J. Lieberman, S.J. Hutten, R.N. Alcalay, S. Kim, P. Ximénez-Embún, Mutant Glucocerebrosidase Impairs A-Synuclein Degradation by Blockade of Chaperone-Mediated Autophagy, Science Advances 8 (2022) eabm6393.
[190] M. Atias, Y. Tevet, J. Sun, A. Stavsky, S. Tal, J. Kahn, S. Roy, D. Gitler, Synapsins Regulate A-Synuclein Functions, Proceedings of the National Academy of Sciences 116 (2019) 11116-11118.
[191] Y. Nakata, T. Yasuda, M. Fukaya, S. Yamamori, M. Itakura, T. Nihira, H. Hayakawa, A. Kawanami, M. Kataoka, M. Nagai, Accumulation of A-Synuclein Triggered by Presynaptic Dysfunction, Journal of Neuroscience 32 (2012) 17186-17196.
[192] S. Chandra, G. Gallardo, R. Fernández-Chacón, O.M. Schlüter, T.C. Südhof, A-Synuclein Cooperates with Cspα in Preventing Neurodegeneration, Cell 123 (2005) 383-396.
[193] D. Li, K. Liu, D. Li, A. Brunger, C. Li, J. Burré, J. Diao, A-Synuclein Condensation in Synaptic Vesicle Function and Synucleinopathies, Trends in Cell Biology (2025).
[194] T.L. Lewis Jr, S.-K. Kwon, A. Lee, R. Shaw, F. Polleux, Mff-Dependent Mitochondrial Fission Regulates Presynaptic Release and Axon Branching by Limiting Axonal Mitochondria Size, Nature Communications 9 (2018) 5008.
[195] M.T. Henrich, W.H. Oertel, D.J. Surmeier, F.F. Geibl, Mitochondrial Dysfunction in Parkinson's Disease–a Key Disease Hallmark with Therapeutic Potential, Molecular Neurodegeneration 18 (2023) 83.
[196] P.R. Angelova, A.Y. Abramov, Role of Mitochondrial Ros in the Brain: From Physiology to Neurodegeneration, FEBS Letters 592 (2018) 692-702.
[197] S.J. Won, R. Fong, N. Butler, J. Sanchez, Y. Zhang, C. Wong, O. Tambou Nzoutchoum, A. Huynh, J. Pan, R.A. Swanson, Neuronal Oxidative Stress Promotes A-Synuclein Aggregation in Vivo, Antioxidants 11 (2022) 2466.
[198] X. Wang, K. Becker, N. Levine, M. Zhang, A.P. Lieberman, D.J. Moore, J. Ma, Pathogenic Alpha-Synuclein Aggregates Preferentially Bind to Mitochondria and Affect Cellular Respiration, Acta Neuropathologica Communications 7 (2019) 41.
[199] J. Burré, M. Sharma, T.C. Südhof, A-Synuclein Assembles into Higher-Order Multimers Upon Membrane Binding to Promote Snare Complex Formation, Proceedings of the National Academy of Sciences 111 (2014) E4274-E4283.

[200] Z. Lv, M. Hashemi, S. Banerjee, K. Zagorski, J.-C. Rochet, Y.L. Lyubchenko, Assembly of A-Synuclein Aggregates on Phospholipid Bilayers, Biochimica et Biophysica Acta (BBA)-Proteins and Proteomics 1867 (2019) 802-812.
[201] C. Galvagnion, J.W. Brown, M.M. Ouberai, P. Flagmeier, M. Vendruscolo, A.K. Buell, E. Sparr, C.M. Dobson, Chemical Properties of Lipids Strongly Affect the Kinetics of the Membrane-Induced Aggregation of A-Synuclein, Proceedings of the National Academy of Sciences 113 (2016) 7065-7070.
[202] J. Burré, M. Sharma, T.C. Südhof, Definition of a Molecular Pathway Mediating A-Synuclein Neurotoxicity, Journal of Neuroscience 35 (2015) 5221-5232.
[203] E. Jo, N. Fuller, R.P. Rand, P. St George-Hyslop, P.E. Fraser, Defective Membrane Interactions of Familial Parkinson's Disease Mutant A30p A-Synuclein, Journal of Molecular Biology 315 (2002) 799-807.
[204] I.M. van der Wateren, T.P. Knowles, A.K. Buell, C.M. Dobson, C. Galvagnion, C-Terminal Truncation of A-Synuclein Promotes Amyloid Fibril Amplification at Physiological Ph, Chemical Science 9 (2018) 5506-5516.
[205] S. Sahoo, A.A. Padhy, V. Kumari, P. Mishra, Role of Ubiquitin–Proteasome and Autophagy-Lysosome Pathways in A-Synuclein Aggregate Clearance, Molecular Neurobiology 59 (2022) 5379-5407.
[206] I. Kawahata, D.I. Finkelstein, K. Fukunaga, Pathogenic Impact of A-Synuclein Phosphorylation and Its Kinases in A-Synucleinopathies, International Journal of Molecular Sciences 23 (2022) 6216.
[207] H. Braak, U. Rüb, W. Gai, K. Del Tredici, Idiopathic Parkinson's Disease: Possible Routes by Which Vulnerable Neuronal Types May Be Subject to Neuroinvasion by an Unknown Pathogen, Journal of Neural Transmission 110 (2003) 517-536.
[208] L.A. Volpicelli-Daley, Effects of A-Synuclein on Axonal Transport, Neurobiology of Disease 105 (2017) 321-327.
[209] L.A. Volpicelli-Daley, K.L. Gamble, C.E. Schultheiss, D.M. Riddle, A.B. West, V.M.-Y. Lee, Formation of A-Synuclein Lewy Neurite–Like Aggregates in Axons Impedes the Transport of Distinct Endosomes, Molecular Biology of the Cell 25 (2014) 4010-4023.
[210] M.K. Borland, P.A. Trimmer, J.D. Rubinstein, P.M. Keeney, K. Mohanakumar, L. Liu, J.P. Bennett Jr, Chronic, Low-Dose Rotenone Reproduces Lewy Neurites Found in Early Stages of Parkinson's Disease, Reduces Mitochondrial Movement and Slowly Kills Differentiated Sh-Sy5y Neural Cells, Molecular Neurodegeneration 3 (2008) 21.
[211] D.L. Fischer, M. Menard, O.Z. Abdelaziz, N.M. Kanaan, V.G. Cobbs, R.E. Kennedy, G.E. Serrano, T.G. Beach, L.A. Volpicelli-Daley, Distinct Subcellular Localization of Tau and Alpha-Synuclein in Lewy Body Disease, Acta Neuropathologica Communications 13 (2025) 14.
[212] A.-L. Mahul-Mellier, J. Burtscher, N. Maharjan, L. Weerens, M. Croisier, F. Kuttler, M. Leleu, G.W. Knott, H.A. Lashuel, The Process of Lewy Body Formation, Rather Than Simply A-Synuclein Fibrillization, Is One of the Major Drivers of Neurodegeneration, Proceedings of the National Academy of Sciences 117 (2020) 4971-4982.
[213] H. Sekiya, T. Matsubara, M.A. DeTure, D.W. Dickson, Neuropathology of Lewy Body Dementia: Lewy-Related Pathology, A-Synuclein Oligomers, and Comorbid Pathologies, Molecular Neurodegeneration 20 (2025) 117.
[214] S. Chartier, C. Duyckaerts, Is Lewy Pathology in the Human Nervous System Chiefly an Indicator of Neuronal Protection or of Toxicity?, Cell and Tissue Research 373 (2018) 149-160.
[215] J. Cummings, L. Apostolova, G. Rabinovici, A. Atri, P. Aisen, S. Greenberg, S. Hendrix, D. Selkoe, M. Weiner, R. Petersen, Lecanemab: Appropriate Use Recommendations, The Journal of Prevention of Alzheimer's Disease 10 (2023) 362-377.

[216] G. Albertini, M. Zielonka, M.-L. Cuypers, A. Snellinx, C. Xu, S. Poovathingal, M. Wojno, K. Davie, V. van Lieshout, K. Craessaerts, The Alzheimer's Therapeutic Lecanemab Attenuates Aβ Pathology by Inducing an Amyloid-Clearing Program in Microglia, Nature Neuroscience (2025) 1-11.
[217] K. McFarthing, S. Buff, G. Rafaloff, B. Fiske, L. Mursaleen, R. Fuest, R.K. Wyse, S.R. Stott, Parkinson's Disease Drug Therapies in the Clinical Trial Pipeline: 2023 Update, Journal of Parkinson's disease 13 (2023) 427-439.
[218] R.A. Hauser, A.J. Espay, A.L. Ellenbogen, H.H. Fernandez, S.H. Isaacson, P.A. LeWitt, W.G. Ondo, R. Pahwa, J. Schwarz, F. Stocchi, Ipx203 Vs Immediate-Release Carbidopa-Levodopa for the Treatment of Motor Fluctuations in Parkinson Disease: The Rise-Pd Randomized Clinical Trial, JAMA Neurology 80 (2023) 1062-1069.
[219] M.J. Soileau, J. Aldred, K. Budur, N. Fisseha, V.S. Fung, A. Jeong, T.E. Kimber, K. Klos, I. Litvan, D. O'Neill, Safety and Efficacy of Continuous Subcutaneous Foslevodopa-Foscarbidopa in Patients with Advanced Parkinson's Disease: A Randomised, Double-Blind, Active-Controlled, Phase 3 Trial, The Lancet Neurology 21 (2022) 1099-1109.
[220] A.J. Espay, F. Stocchi, R. Pahwa, A. Albanese, A. Ellenbogen, J.J. Ferreira, N. Giladi, T. Gurevich, S. Hassin-Baer, J. Hernandez-Vara, Safety and Efficacy of Continuous Subcutaneous Levodopa–Carbidopa Infusion (Nd0612) for Parkinson's Disease with Motor Fluctuations (Boundless): A Phase 3, Randomised, Double-Blind, Double-Dummy, Multicentre Trial, The Lancet Neurology 23 (2024) 465-476.
[221] C.W. Olanow, D. McIntyre, M. Matarazzo, M. Leinonen, A. McGarry, C. Kamp, J. Kennedy, M. Torti, R. Kruger, J.A. Obeso, Continuous Levodopa Delivery with an Intraoral Micropump System: An Open-Label Pharmacokinetics and Clinical Study, Movement Disorders 39 (2024) 945-954.
[222] R. Riesenberg, J. Werth, Y. Zhang, S. Duvvuri, D. Gray, Pf-06649751 Efficacy and Safety in Early Parkinson's Disease: A Randomized, Placebo-Controlled Trial, Therapeutic Advances in Neurological Disorders 13 (2020) 1756286420911296.
[223] A. Antonini, S. Waters, C. Sonesson, J. Landström, N. Waters, J. Tedroff, Results from Irl790c005—a Randomized, Double-Blind, Placebo-Controlled Phase Iib Study Evaluating the Efficacy of Mesdopetam on Daily on-Time without Troublesome Dyskinesia in Patients with Parkinson's Disease, MDS international congress, 2023.
[224] A. Van Laar, C. Christine, A. Merola, N. Phielipp, B. Elder, P. Larson, W.S. Sebastian, M. Fiandaca, A. Kells, K. Bankiewicz, Phase 1b Safety and Preliminary Efficacy of Bilateral Intraputaminal Delivery of Aav2 Gdnf (Ab-1005) in Participants with Mild or Moderate Parkinson's Disease (N2. 001), Neurology, Lippincott Williams & Wilkins Hagerstown, MD, 2024, pp. 6786.
[225] J.D. Heiss, C. Lungu, D.A. Hammoud, P. Herscovitch, D.J. Ehrlich, D.P. Argersinger, S. Sinharay, G. Scott, T. Wu, H.J. Federoff, Trial of Magnetic Resonance–Guided Putaminal Gene Therapy for Advanced Parkinson's Disease, Movement Disorders 34 (2019) 1073-1078.
[226] C. Henchcliffe, H. Sarva, A. Lozano, A. Fasano, S. Kalia, K.K.H. Yu, C. Brennan, W. Stemple, N. Abid, M. Yountz, Safety, Tolerability, and Clinical Assessment of Bemdaneprocel for Parkinson's Disease: 18-Month Results from a Phase 1 Study (P9-3.007), Neurology, Lippincott Williams & Wilkins Hagerstown, MD, 2024, pp. 3382.
[227] N.s.I.N. Drug, Parkinson's Ipsc Trial, Nature Biotechnology 41 (2023) 1179-1185.
[228] G. Pagano, K.I. Taylor, J. Anzures Cabrera, T. Simuni, K. Marek, R.B. Postuma, N. Pavese, F. Stocchi, K. Brockmann, H. Svoboda, Prasinezumab Slows Motor Progression in Rapidly Progressing Early-Stage Parkinson's Disease, Nature Medicine 30 (2024) 1096-1103.
[229] J.W. Smit, P. Basile, M.K. Prato, L. Detalle, F.X. Mathy, A. Schmidt, M. Lalla, M. Germani, C. Domange, A.L. Biere, Phase 1/1b Studies of Ucb0599, an Oral Inhibitor of

A-Synuclein Misfolding, Including a Randomized Study in Parkinson's Disease, Movement Disorders 37 (2022) 2045-2056.
[230] C. Fang, P. Hernandez, K. Liow, E. Damiano, H. Zetterberg, K. Blennow, D. Feng, M. Chen, M. Maccecchini, Buntanetap, a Novel Translational Inhibitor of Multiple Neurotoxic Proteins, Proves to Be Safe and Promising in Both Alzheimer's and Parkinson's Patients, The Journal of Prevention of Alzheimer's Disease 10 (2023) 25-33.
[231] J. Wagner, S. Ryazanov, A. Leonov, J. Levin, S. Shi, F. Schmidt, C. Prix, F. Pan-Montojo, U. Bertsch, G. Mitteregger-Kretzschmar, Anle138b: A Novel Oligomer Modulator for Disease-Modifying Therapy of Neurodegenerative Diseases Such as Prion and Parkinson's Disease, Acta Neuropathologica 125 (2013) 795-813.
[232] M. Reilly, R. Miller, M. Thomson, V. Patris, P. Ryle, L. McLoughlin, P. Mutch, P. Gilboy, C. Miller, M. Broekema, Randomized, Double-Blind, Placebo-Controlled, Dose-Escalating Phase I, Healthy Subjects Study of Intravenous Opn-305, a Humanized Anti-Tlr2 Antibody, Clinical Pharmacology & Therapeutics 94 (2013) 593-600.
[233] M.M. Rahman, C. Lendel, Extracellular Protein Components of Amyloid Plaques and Their Roles in Alzheimer's Disease Pathology, Molecular Neurodegeneration 16 (2021) 59.
[234] D. Jennings, S. Huntwork-Rodriguez, A.G. Henry, J.C. Sasaki, R. Meisner, D. Diaz, H. Solanoy, X. Wang, E. Negrou, V.V. Bondar, Preclinical and Clinical Evaluation of the Lrrk2 Inhibitor Dnl201 for Parkinson's Disease, Science Translational Medicine 14 (2022) eabj2658.
[235] J.M. den Heijer, A.C. Kruithof, M. Moerland, M. Walker, L. Dudgeon, C. Justman, I. Solomini, L. Splitalny, N. Leymarie, K. Khatri, A Phase 1b Trial in Gba1-Associated Parkinson's Disease of Bia-28-6156, a Glucocerebrosidase Activator, Movement Disorders 38 (2023) 1197-1208.
[236] A. Van der Perren, G. Gelders, A. Fenyi, L. Bousset, F. Brito, W. Peelaerts, C. Van den Haute, S. Gentleman, R. Melki, V. Baekelandt, The Structural Differences between Patient-Derived A-Synuclein Strains Dictate Characteristics of Parkinson's Disease, Multiple System Atrophy and Dementia with Lewy Bodies, Acta Neuropathologica 139 (2020) 977-1000.
[237] J.P. Kane, A. Surendranathan, A. Bentley, S.A. Barker, J.-P. Taylor, A.J. Thomas, L.M. Allan, R.J. McNally, P.W. James, I.G. McKeith, Clinical Prevalence of Lewy Body Dementia, Alzheimer's Research & Therapy 10 (2018) 19.
[238] P. Borghammer, N. Okkels, D. Weintraub, Parkinson's Disease and Dementia with Lewy Bodies: One and the Same, Journal of Parkinson's disease 14 (2024) 383-397.
[239] T.F. Outeiro, D.J. Koss, D. Erskine, L. Walker, M. Kurzawa-Akanbi, D. Burn, P. Donaghy, C. Morris, J.-P. Taylor, A. Thomas, Dementia with Lewy Bodies: An Update and Outlook, Molecular Neurodegeneration 14 (2019) 5.
[240] M.G. Spillantini, M. Goedert, The A-Synucleinopathies: Parkinson's Disease, Dementia with Lewy Bodies, and Multiple System Atrophy, Annals of the New York Academy of Sciences 920 (2000) 16-27.
[241] S. Kato, H. Nakamura, Cytoplasmic Argyrophilic Inclusions in Neurons of Pontine Nuclei in Patients with Olivopontocerebellar Atrophy: Immunohistochemical and Ultrastructural Studies, Acta Neuropathologica 79 (1990) 584-594.
[242] C. Peng, R.J. Gathagan, D.J. Covell, C. Medellin, A. Stieber, J.L. Robinson, B. Zhang, R.M. Pitkin, M.F. Olufemi, K.C. Luk, Cellular Milieu Imparts Distinct Pathological A-Synuclein Strains in A-Synucleinopathies, Nature 557 (2018) 558-563.
[243] A. Fanciulli, G.K. Wenning, Multiple-System Atrophy, New England Journal of Medicine 372 (2015) 249-263.
[244] M. Masuda-Suzukake, T. Nonaka, M. Hosokawa, T. Oikawa, T. Arai, H. Akiyama, D.M. Mann, M. Hasegawa, Prion-Like Spreading of Pathological A-Synuclein in Brain, Brain 136 (2013) 1128-1138.

[245] A.R. Castle, A.C. Gill, Physiological Functions of the Cellular Prion Protein, Frontiers in Molecular Biosciences 4 (2017) 19.
[246] M. Nuvolone, M. Hermann, S. Sorce, G. Russo, C. Tiberi, P. Schwarz, E. Minikel, D. Sanoudou, P. Pelczar, A. Aguzzi, Strictly Co-Isogenic C57bl/6j-Prnp−/− Mice: A Rigorous Resource for Prion Science, Journal of Experimental Medicine 213 (2016) 313-327.
[247] F. Llorens, P. Carulla, A. Villa, J.M. Torres, P. Fortes, I. Ferrer, J.A. del Rio, Prpc Regulates Epidermal Growth Factor Receptor Function and Cell Shape Dynamics in Neuro2a Cells, Journal of Neurochemistry 127 (2013) 124-138.
[248] R. Chiesa, The Elusive Role of the Prion Protein and the Mechanism of Toxicity in Prion Disease, PLoS Pathogens 11 (2015) e1004745.
[249] A. Jan, N.P. Gonçalves, C.B. Vaegter, P.H. Jensen, N. Ferreira, The Prion-Like Spreading of Alpha-Synuclein in Parkinson's Disease: Update on Models and Hypotheses, International Journal of Molecular Sciences 22 (2021) 8338.
[250] H. Braak, E. Ghebremedhin, U. Rüb, H. Bratzke, K. Del Tredici, Stages in the Development of Parkinson's Disease-Related Pathology, Cell and Tissue Research 318 (2004) 121-134.
[251] J.-Y. Li, E. Englund, J.L. Holton, D. Soulet, P. Hagell, A.J. Lees, T. Lashley, N.P. Quinn, S. Rehncrona, A. Björklund, Lewy Bodies in Grafted Neurons in Subjects with Parkinson's Disease Suggest Host-to-Graft Disease Propagation, Nature Medicine 14 (2008) 501-503.
[252] N.L. Rey, S. George, J.A. Steiner, Z. Madaj, K.C. Luk, J.Q. Trojanowski, V.M.-Y. Lee, P. Brundin, Spread of Aggregates after Olfactory Bulb Injection of A-Synuclein Fibrils Is Associated with Early Neuronal Loss and Is Reduced Long Term, Acta Neuropathologica 135 (2018) 65-83.
[253] A. Recasens, B. Dehay, J. Bové, I. Carballo-Carbajal, S. Dovero, A. Pérez-Villalba, P.O. Fernagut, J. Blesa, A. Parent, C. Perier, Lewy Body Extracts from Parkinson Disease Brains Trigger A-Synuclein Pathology and Neurodegeneration in Mice and Monkeys, Annals of Neurology 75 (2014) 351-362.
[254] K.C. Luk, V.M. Kehm, B. Zhang, P. O'Brien, J.Q. Trojanowski, V.M. Lee, Intracerebral Inoculation of Pathological A-Synuclein Initiates a Rapidly Progressive Neurodegenerative A-Synucleinopathy in Mice, Journal of Experimental Medicine 209 (2012) 975-986.
[255] K.L. Paumier, K.C. Luk, F.P. Manfredsson, N.M. Kanaan, J.W. Lipton, T.J. Collier, K. Steece-Collier, C.J. Kemp, S. Celano, E. Schulz, Intrastriatal Injection of Pre-Formed Mouse A-Synuclein Fibrils into Rats Triggers A-Synuclein Pathology and Bilateral Nigrostriatal Degeneration, Neurobiology of Disease 82 (2015) 185-199.
[256] S. Aulić, T.T.N. Le, F. Moda, S. Abounit, S. Corvaglia, L. Casalis, S. Gustincich, C. Zurzolo, F. Tagliavini, G. Legname, Defined A-Synuclein Prion-Like Molecular Assemblies Spreading in Cell Culture, BMC Neuroscience 15 (2014) 69.
[257] X. Zhang, E. Wesén, R. Kumar, D. Bernson, A. Gallud, A. Paul, P. Wittung-Stafshede, E.K. Esbjörner, Correlation between Cellular Uptake and Cytotoxicity of Fragmented A-Synuclein Amyloid Fibrils Suggests Intracellular Basis for Toxicity, ACS Chemical Neuroscience 11 (2020) 233-241.
[258] J.C. Watts, K. Giles, A. Oehler, L. Middleton, D.T. Dexter, S.M. Gentleman, S.J. DeArmond, S.B. Prusiner, Transmission of Multiple System Atrophy Prions to Transgenic Mice, Proceedings of the National Academy of Sciences 110 (2013) 19555-19560.
[259] K.A. Jellinger, G.K. Wenning, N. Stefanova, Is Multiple System Atrophy a Prion-Like Disorder?, International Journal of Molecular Sciences 22 (2021) 10093.
[260] N. Uemura, M.T. Uemura, K.C. Luk, V.M.-Y. Lee, J.Q. Trojanowski, Cell-to-Cell Transmission of Tau and A-Synuclein, Trends in Molecular Medicine 26 (2020) 936-952.

[261] H.-J. Lee, S. Patel, S.-J. Lee, Intravesicular Localization and Exocytosis of A-Synuclein and Its Aggregates, Journal of Neuroscience 25 (2005) 6016-6024.
[262] M.G. Stykel, K.M. Humphries, E. Kamski-Hennekam, B. Buchner-Duby, N. Porte-Trachsel, T. Ryan, C.L. Coackley, V.V. Bamm, G. Harauz, S.D. Ryan, A-Synuclein Mutation Impairs Processing of Endomembrane Compartments and Promotes Exocytosis and Seeding of A-Synuclein Pathology, Cell Reports 35 (2021).
[263] M. Guo, J. Wang, Y. Zhao, Y. Feng, S. Han, Q. Dong, M. Cui, K. Tieu, Microglial Exosomes Facilitate A-Synuclein Transmission in Parkinson's Disease, Brain 143 (2020) 1476-1497.
[264] B.B. Holmes, S.L. DeVos, N. Kfoury, M. Li, R. Jacks, K. Yanamandra, M.O. Ouidja, F.M. Brodsky, J. Marasa, D.P. Bagchi, Heparan Sulfate Proteoglycans Mediate Internalization and Propagation of Specific Proteopathic Seeds, Proceedings of the National Academy of Sciences 110 (2013) E3138-E3147.
[265] V. Grozdanov, K.M. Danzer, Release and Uptake of Pathologic Alpha-Synuclein, Cell and Tissue Research 373 (2018) 175-182.
[266] X. Mao, M.T. Ou, S.S. Karuppagounder, T.-I. Kam, X. Yin, Y. Xiong, P. Ge, G.E. Umanah, S. Brahmachari, J.-H. Shin, Pathological A-Synuclein Transmission Initiated by Binding Lymphocyte-Activation Gene 3, Science 353 (2016) aah3374.
[267] K.-M. Wu, Q.-H. Xu, Y.-Q. Liu, Y.-W. Feng, S.-D. Han, Y.-R. Zhang, S.-D. Chen, Y. Guo, B.-S. Wu, L.-Z. Ma, Neuronal Fam171a2 Mediates A-Synuclein Fibril Uptake and Drives Parkinson's Disease, Science 387 (2025) 892-900.
[268] I. Khan, P.S. Steeg, Endocytosis: A Pivotal Pathway for Regulating Metastasis, British Journal of Cancer 124 (2021) 66-75.
[269] K. Kakuda, K. Ikenaka, A. Kuma, J. Doi, C. Aguirre, N. Wang, T. Ajiki, C.-J. Choong, Y. Kimura, S.M.M. Badawy, Lysophagy Protects against Propagation of A-Synuclein Aggregation through Ruptured Lysosomal Vesicles, Proceedings of the National Academy of Sciences 121 (2024) e2312306120.
[270] P. Jiang, M. Gan, S.-H. Yen, P.J. McLean, D.W. Dickson, Impaired Endo-Lysosomal Membrane Integrity Accelerates the Seeding Progression of A-Synuclein Aggregates, Scientific Reports 7 (2017) 7690.
[271] S. Awa, G. Suzuki, M. Masuda-Suzukake, T. Nonaka, M. Saito, M. Hasegawa, Phosphorylation of Endogenous A-Synuclein Induced by Extracellular Seeds Initiates at the Pre-Synaptic Region and Spreads to the Cell Body, Scientific Reports 12 (2022) 1163.
[272] M.-B. Fares, B. Maco, A. Oueslati, E. Rockenstein, N. Ninkina, V.L. Buchman, E. Masliah, H.A. Lashuel, Induction of De Novo A-Synuclein Fibrillization in a Neuronal Model for Parkinson's Disease, Proceedings of the National Academy of Sciences 113 (2016) E912-E921.
[273] S. Abounit, C. Zurzolo, Wiring through Tunneling Nanotubes–from Electrical Signals to Organelle Transfer, Journal of Cell Science 125 (2012) 1089-1098.
[274] B.V. Dieriks, T.I. Park, C. Fourie, R.L. Faull, M. Dragunow, M.A. Curtis, A-Synuclein Transfer through Tunneling Nanotubes Occurs in Sh-Sy5y Cells and Primary Brain Pericytes from Parkinson's Disease Patients, Scientific Reports 7 (2017) 42984.
[275] M. Tardivel, S. Bégard, L. Bousset, S. Dujardin, A. Coens, R. Melki, L. Buée, M. Colin, Tunneling Nanotube (Tnt)-Mediated Neuron-to Neuron Transfer of Pathological Tau Protein Assemblies, Acta Neuropathologica Communications 4 (2016) 117.
[276] S. Abounit, L. Bousset, F. Loria, S. Zhu, F. de Chaumont, L. Pieri, J.C. Olivo-Marin, R. Melki, C. Zurzolo, Tunneling Nanotubes Spread Fibrillar A-Synuclein by Intercellular Trafficking of Lysosomes, The EMBO Journal 35 (2016) 2120-2138.

[277] L. Narhi, S.J. Wood, S. Steavenson, Y. Jiang, G.M. Wu, D. Anafi, S.A. Kaufman, F. Martin, K. Sitney, P. Denis, Both Familial Parkinson's Disease Mutations Accelerate A-Synuclein Aggregation, Journal of Biological Chemistry 274 (1999) 9843-9846.
[278] M. Biancalana, S. Koide, Molecular Mechanism of Thioflavin-T Binding to Amyloid Fibrils, Biochimica et Biophysica Acta (BBA)-Proteins and Proteomics 1804 (2010) 1405-1412.
[279] H. Levine III, Thioflavine T Interaction with Synthetic Alzheimer's Disease B-Amyloid Peptides: Detection of Amyloid Aggregation in Solution, Protein Science 2 (1993) 404-410.
[280] C. Xue, T.Y. Lin, D. Chang, Z. Guo, Thioflavin T as an Amyloid Dye: Fibril Quantification, Optimal Concentration and Effect on Aggregation, Royal Society Open Science 4 (2017).
[281] L. Giehm, D.E. Otzen, Strategies to Increase the Reproducibility of Protein Fibrillization in Plate Reader Assays, Analytical Biochemistry 400 (2010) 270-281.
[282] N.K. Polinski, L.A. Volpicelli-Daley, C.E. Sortwell, K.C. Luk, N. Cremades, L.M. Gottler, J. Froula, M.F. Duffy, V.M. Lee, T.N. Martinez, Best Practices for Generating and Using Alpha-Synuclein Pre-Formed Fibrils to Model Parkinson's Disease in Rodents, Journal of Parkinson's disease 8 (2018) 303-322.
[283] A.C.M. Ferreon, A.A. Deniz, A-Synuclein Multistate Folding Thermodynamics: Implications for Protein Misfolding and Aggregation, Biochemistry 46 (2007) 4499-4509.
[284] D. Nečas, P. Klapetek, Gwyddion: An Open-Source Software for Spm Data Analysis, Central European Journal of Physics 10 (2012) 181-188.
[285] I. Horcas, R. Fernández, J. Gomez-Rodriguez, J. Colchero, J. Gómez-Herrero, A.M. Baro, Wsxm: A Software for Scanning Probe Microscopy and a Tool for Nanotechnology, Review of Scientific Instruments 78 (2007).
[286] G. Lamour, J.B. Kirkegaard, H. Li, T.P. Knowles, J. Gsponer, Easyworm: An Open-Source Software Tool to Determine the Mechanical Properties of Worm-Like Chains, Source Code for Biology and Medicine 9 (2014) 16.
[287] V.N. Uversky, J. Li, A.L. Fink, Metal-Triggered Structural Transformations, Aggregation, and Fibrillation of Human A-Synuclein: A Possible Molecular Link between Parkinson′ S Disease and Heavy Metal Exposure, Journal of Biological Chemistry 276 (2001) 44284-44296.
[288] K. Klement, K. Wieligmann, J. Meinhardt, P. Hortschansky, W. Richter, M. Fändrich, Effect of Different Salt Ions on the Propensity of Aggregation and on the Structure of Alzheimer's Aβ (1-40) Amyloid Fibrils, Journal of Molecular Biology 373 (2007) 1321-1333.
[289] J.S. Pedersen, J.M. Flink, D. Dikov, D.E. Otzen, Sulfates Dramatically Stabilize a Salt-Dependent Type of Glucagon Fibrils, Biophysical Journal 90 (2006) 4181-4194.
[290] B. Raman, E. Chatani, M. Kihara, T. Ban, M. Sakai, K. Hasegawa, H. Naiki, C.M. Rao, Y. Goto, Critical Balance of Electrostatic and Hydrophobic Interactions Is Required for B2-Microglobulin Amyloid Fibril Growth and Stability, Biochemistry 44 (2005) 1288-1299.
[291] R. Gaspar, M. Lund, E. Sparr, S. Linse, Anomalous Salt Dependence Reveals an Interplay of Attractive and Repulsive Electrostatic Interactions in A-Synuclein Fibril Formation, QRB Discovery 1 (2020) e2.
[292] K. Suzuki, T. Miura, H. Takeuchi, Inhibitory Effect of Copper (Ii) on Zinc (Ii)-Induced Aggregation of Amyloid B-Peptide, Biochemical and Biophysical Research Communications 285 (2001) 991-996.
[293] O.V. Bocharova, L. Breydo, V.V. Salnikov, I.V. Baskakov, Copper (Ii) Inhibits in Vitro Conversion of Prion Protein into Amyloid Fibrils, Biochemistry 44 (2005) 6776-6787.
[294] E.F. Aziz, N. Ottosson, S. Eisebitt, W. Eberhardt, B. Jagoda-Cwiklik, R. Vácha, P. Jungwirth, B. Winter, Cation-Specific Interactions with Carboxylate in Amino Acid and

Acetate Aqueous Solutions: X-Ray Absorption and Ab Initio Calculations, The Journal of Physical Chemistry B 112 (2008) 12567-12570.
[295] K.D. Collins, G.W. Neilson, J.E. Enderby, Ions in Water: Characterizing the Forces That Control Chemical Processes and Biological Structure, Biophysical Chemistry 128 (2007) 95-104.
[296] A.M. Grant, M.C. Krecker, M.K. Gupta, P.B. Dennis, M.G. Crosby, V.V. Tsukruk, Marine Structural Protein Stability Induced by Hofmeister Salt Annealing and Enzymatic Cross-Linking, ACS Biomaterials Science & Engineering 6 (2020) 5519-5526.
[297] V. Yeh, J.M. Broering, A. Romanyuk, B. Chen, Y.O. Chernoff, A.S. Bommarius, The Hofmeister Effect on Amyloid Formation Using Yeast Prion Protein, Protein Science 19 (2010) 47-56.
[298] M. Weijers, K. Broersen, P.A. Barneveld, M.A. Cohen Stuart, R.J. Hamer, H.H. De Jongh, R.W. Visschers, Net Charge Affects Morphology and Visual Properties of Ovalbumin Aggregates, Biomacromolecules 9 (2008) 3165-3172.
[299] Y. Miller, B. Ma, R. Nussinov, Polymorphism in Alzheimer Aβ Amyloid Organization Reflects Conformational Selection in a Rugged Energy Landscape, Chemical Reviews 110 (2010) 4820-4838.
[300] N. Carulla, G.L. Caddy, D.R. Hall, J. Zurdo, M. Gairí, M. Feliz, E. Giralt, C.V. Robinson, C.M. Dobson, Molecular Recycling within Amyloid Fibrils, Nature 436 (2005) 554-558.
[301] D.M. Walsh, A. Lomakin, G.B. Benedek, M.M. Condron, D.B. Teplow, Amyloid B-Protein Fibrillogenesis: Detection of a Protofibrillar Intermediate, Journal of Biological Chemistry 272 (1997) 22364-22372.
[302] D.J. Lindberg, A. Wenger, E. Sundin, E. Wesén, F. Westerlund, E.K. Esbjörner, Binding of Thioflavin-T to Amyloid Fibrils Leads to Fluorescence Self-Quenching and Fibril Compaction, Biochemistry 56 (2017) 2170-2174.
[303] D.J. Lindberg, M.S. Wranne, M.G. Gatty, F. Westerlund, E.K. Esbjörner, Steady-State and Time-Resolved Thioflavin-T Fluorescence Can Report on Morphological Differences in Amyloid Fibrils Formed by Aβ (1-40) and Aβ (1-42), Biochemical and Biophysical Research Communications 458 (2015) 418-423.
[304] R. Cukalevski, X. Yang, G. Meisl, U. Weininger, K. Bernfur, B. Frohm, T.P. Knowles, S. Linse, The Aβ40 and Aβ42 Peptides Self-Assemble into Separate Homomolecular Fibrils in Binary Mixtures but Cross-React during Primary Nucleation, Chemical Science 6 (2015) 4215-4233.
[305] M. Vilar, H.-T. Chou, T. Lührs, S.K. Maji, D. Riek-Loher, R. Verel, G. Manning, H. Stahlberg, R. Riek, The Fold of A-Synuclein Fibrils, Proceedings of the National Academy of Sciences 105 (2008) 8637-8642.
[306] L. Bousset, L. Pieri, G. Ruiz-Arlandis, J. Gath, P.H. Jensen, B. Habenstein, K. Madiona, V. Olieric, A. Böckmann, B.H. Meier, Structural and Functional Characterization of Two Alpha-Synuclein Strains, Nature Communications 4 (2013) 1-13.
[307] J.F. Smith, T.P. Knowles, C.M. Dobson, C.E. MacPhee, M.E. Welland, Characterization of the Nanoscale Properties of Individual Amyloid Fibrils, Proceedings of the National Academy of Sciences 103 (2006) 15806-15811.
[308] M. Tanaka, S.R. Collins, B.H. Toyama, J.S. Weissman, The Physical Basis of How Prion Conformations Determine Strain Phenotypes, Nature 442 (2006) 585-589.
[309] J. Shorter, S. Lindquist, Hsp104 Catalyzes Formation and Elimination of Self-Replicating Sup35 Prion Conformers, Science 304 (2004) 1793-1797.
[310] M.I. Sulatsky, O.V. Stepanenko, O.V. Stepanenko, E.V. Mikhailova, A.I. Sulatskaya, From Protective Enzyme to Facilitator of Amyloid Propagation: Cathepsin D-Mediated

Amyloid Fibril Fragmentation, International Journal of Biological Macromolecules (2025) 140971.
[311] A.R.A. Ladiwala, J. Litt, R.S. Kane, D.S. Aucoin, S.O. Smith, S. Ranjan, J. Davis, W.E. Van Nostrand, P.M. Tessier, Conformational Differences between Two Amyloid B Oligomers of Similar Size and Dissimilar Toxicity, Journal of Biological Chemistry 287 (2012) 24765-24773.
[312] F. Havemeister, V. Halipi, M. Ghaeidamini, E.K. Esbjörner, Fragmentation-Induced Disassembly and Reaggregation of A-Synuclein Amyloid Fibrils, ACS Chemical Neuroscience (2026).
[313] V.I. Stsiapura, A.A. Maskevich, V.A. Kuzmitsky, V.N. Uversky, I.M. Kuznetsova, K.K. Turoverov, Thioflavin T as a Molecular Rotor: Fluorescent Properties of Thioflavin T in Solvents with Different Viscosity, The Journal of Physical Chemistry B 112 (2008) 15893-15902.
[314] A. Sidhu, J. Vaneyck, C. Blum, I. Segers-Nolten, V. Subramaniam, Polymorph-Specific Distribution of Binding Sites Determines Thioflavin-T Fluorescence Intensity in A-Synuclein Fibrils, Amyloid 25 (2018) 189-196.
[315] A. Sidhu, I. Segers-Nolten, V. Raussens, M.M. Claessens, V. Subramaniam, Distinct Mechanisms Determine A-Synuclein Fibril Morphology during Growth and Maturation, ACS Chemical Neuroscience 8 (2017) 538-547.
[316] S.B. Nielsen, F. Macchi, S. Raccosta, A.E. Langkilde, L. Giehm, A. Kyrsting, A.S.P. Svane, M. Manno, G. Christiansen, N.C. Nielsen, Wildtype and A30p Mutant Alpha-Synuclein Form Different Fibril Structures, PloS One 8 (2013) e67713.
[317] D.D. Dhavale, C. Tsai, D.P. Bagchi, L.A. Engel, J. Sarezky, P.T. Kotzbauer, A Sensitive Assay Reveals Structural Requirements for A-Synuclein Fibril Growth, Journal of Biological Chemistry 292 (2017) 9034-9050.
[318] S. Freire, M.H. de Araujo, W. Al-Soufi, M. Novo, Photophysical Study of Thioflavin T as Fluorescence Marker of Amyloid Fibrils, Dyes and Pigments 110 (2014) 97-105.
[319] P.K. Singh, A.K. Mora, S. Nath, Ultrafast Fluorescence Spectroscopy Reveals a Dominant Weakly-Emissive Population of Fibril Bound Thioflavin-T, Chemical Communications 51 (2015) 14042-14045.
[320] S. Mehra, L. Gadhe, R. Bera, A.S. Sawner, S.K. Maji, Structural and Functional Insights into A-Synuclein Fibril Polymorphism, Biomolecules 11 (2021) 1419.
[321] S. Hadi Alijanvand, A. Peduzzo, A.K. Buell, Secondary Nucleation and the Conservation of Structural Characteristics of Amyloid Fibril Strains, Frontiers in Molecular Biosciences 8 (2021) 669994.
[322] T. Watanabe-Nakayama, M. Nawa, H. Konno, N. Kodera, T. Ando, D.B. Teplow, K. Ono, Self-and Cross-Seeding on A-Synuclein Fibril Growth Kinetics and Structure Observed by High-Speed Atomic Force Microscopy, ACS Nano 14 (2020) 9979-9989.
[323] K.C. Luk, V. Kehm, J. Carroll, B. Zhang, P. O'brien, J.Q. Trojanowski, V.M.-Y. Lee, Pathological A-Synuclein Transmission Initiates Parkinson-Like Neurodegeneration in Nontransgenic Mice, Science 338 (2012) 949-953.
[324] E.C. Freundt, N. Maynard, E.K. Clancy, S. Roy, L. Bousset, Y. Sourigues, M. Covert, R. Melki, K. Kirkegaard, M. Brahic, Neuron-to-Neuron Transmission of A-Synuclein Fibrils through Axonal Transport, Annals of Neurology 72 (2012) 517-524.
[325] F. Clavaguera, T. Bolmont, R.A. Crowther, D. Abramowski, S. Frank, A. Probst, G. Fraser, A.K. Stalder, M. Beibel, M. Staufenbiel, Transmission and Spreading of Tauopathy in Transgenic Mouse Brain, Nature Cell Biology 11 (2009) 909-913.
[326] M. Meyer-Luehmann, J. Coomaraswamy, T. Bolmont, S. Kaeser, C. Schaefer, E. Kilger, A. Neuenschwander, D. Abramowski, P. Frey, A.L. Jaton, Exogenous Induction of

Cerebral B-Amyloidogenesis Is Governed by Agent and Host, Science 313 (2006) 1781-1784.
[327] P. Smethurst, J. Newcombe, C. Troakes, R. Simone, Y.-R. Chen, R. Patani, K. Sidle, In Vitro Prion-Like Behaviour of Tdp-43 in Als, Neurobiology of Disease 96 (2016) 236-247.
[328] J.I. Ayers, S.E. Fromholt, V.M. O'Neal, J.H. Diamond, D.R. Borchelt, Prion-Like Propagation of Mutant Sod1 Misfolding and Motor Neuron Disease Spread Along Neuroanatomical Pathways, Acta Neuropathologica 131 (2016) 103-114.
[329] I. Jeon, F. Cicchetti, G. Cisbani, S. Lee, E. Li, J. Bae, N. Lee, L. Li, W. Im, M. Kim, Human-to-Mouse Prion-Like Propagation of Mutant Huntingtin Protein, Acta Neuropathologica 132 (2016) 577-592.
[330] A. Mukherjee, D. Morales-Scheihing, N. Salvadores, I. Moreno-Gonzalez, C. Gonzalez, K. Taylor-Presse, N. Mendez, M. Shahnawaz, A.O. Gaber, O.M. Sabek, Induction of Iapp Amyloid Deposition and Associated Diabetic Abnormalities by a Prion-Like Mechanism, Journal of Experimental Medicine 214 (2017) 2591-2610.
[331] H.-J. Lee, J.-E. Suk, E.-J. Bae, J.-H. Lee, S.R. Paik, S.-J. Lee, Assembly-Dependent Endocytosis and Clearance of Extracellular a-Synuclein, The International Journal of Biochemistry & Cell Biology 40 (2008) 1835-1849.
[332] A.N. Shrivastava, L. Bousset, M. Renner, V. Redeker, J. Savistchenko, A. Triller, R. Melki, Differential Membrane Binding and Seeding of Distinct A-Synuclein Fibrillar Polymorphs, Biophysical Journal 118 (2020) 1301-1320.
[333] N.P. Marotta, J. Ara, N. Uemura, M.G. Lougee, E.S. Meymand, B. Zhang, E.J. Petersson, J.Q. Trojanowski, V.M.-Y. Lee, Alpha-Synuclein from Patient Lewy Bodies Exhibits Distinct Pathological Activity That Can Be Propagated in Vitro, Acta Neuropathologica Communications 9 (2021) 188.
[334] J. Huotari, A. Helenius, Endosome Maturation, The EMBO Journal 30 (2011) 3481.
[335] S. Zhang, Y.-Q. Liu, C. Jia, Y.-J. Lim, G. Feng, E. Xu, H. Long, Y. Kimura, Y. Tao, C. Zhao, Mechanistic Basis for Receptor-Mediated Pathological A-Synuclein Fibril Cell-to-Cell Transmission in Parkinson's Disease, Proceedings of the National Academy of Sciences 118 (2021) e2011196118.
[336] X. Li, N. Rydzewski, A. Hider, X. Zhang, J. Yang, W. Wang, Q. Gao, X. Cheng, H. Xu, A Molecular Mechanism to Regulate Lysosome Motility for Lysosome Positioning and Tubulation, Nature Cell Biology 18 (2016) 404-417.
[337] J. Pu, C.M. Guardia, T. Keren-Kaplan, J.S. Bonifacino, Mechanisms and Functions of Lysosome Positioning, Journal of Cell Science 129 (2016) 4329-4339.
[338] K. Willén, J.R. Edgar, T. Hasegawa, N. Tanaka, C.E. Futter, G.K. Gouras, Aβ Accumulation Causes Mvb Enlargement and Is Modelled by Dominant Negative Vps4a, Molecular Neurodegeneration 12 (2017) 61.
[339] S. Söllvander, E. Nikitidou, R. Brolin, L. Söderberg, D. Sehlin, L. Lannfelt, A. Erlandsson, Accumulation of Amyloid-B by Astrocytes Result in Enlarged Endosomes and Microvesicle-Induced Apoptosis of Neurons, Molecular Neurodegeneration 11 (2016) 38.
[340] J.-C. Cossec, J. Lavaur, D.E. Berman, I. Rivals, A. Hoischen, S. Stora, C. Ripoll, C. Mircher, Y. Grattau, J.-C. OlivoMarin, Trisomy for Synaptojanin1 in down Syndrome Is Functionally Linked to the Enlargement of Early Endosomes, Human Molecular Genetics 21 (2012) 3156-3172.
[341] A.D. Klein, J.R. Mazzulli, Is Parkinson's Disease a Lysosomal Disorder?, Oxford University Press, 2018.
[342] D. Freeman, R. Cedillos, S. Choyke, Z. Lukic, K. McGuire, S. Marvin, A.M. Burrage, S. Sudholt, A. Rana, C. O'Connor, Alpha-Synuclein Induces Lysosomal Rupture and Cathepsin Dependent Reactive Oxygen Species Following Endocytosis, PloS One 8 (2013) e62143.

[343] W.P. Flavin, L. Bousset, Z.C. Green, Y. Chu, S. Skarpathiotis, M.J. Chaney, J.H. Kordower, R. Melki, E.M. Campbell, Endocytic Vesicle Rupture Is a Conserved Mechanism of Cellular Invasion by Amyloid Proteins, Acta Neuropathologica 134 (2017) 629-653.
[344] J.F. Kellie, R.E. Higgs, J.W. Ryder, A. Major, T.G. Beach, C.H. Adler, K. Merchant, M.D. Knierman, Quantitative Measurement of Intact Alpha-Synuclein Proteoforms from Post-Mortem Control and Parkinson's Disease Brain Tissue by Intact Protein Mass Spectrometry, Scientific Reports 4 (2014) 5797.
[345] D.G. Walker, L.-F. Lue, C.H. Adler, H.A. Shill, J.N. Caviness, M.N. Sabbagh, H. Akiyama, G.E. Serrano, L.I. Sue, T.G. Beach, Changes in Properties of Serine 129 Phosphorylated A-Synuclein with Progression of Lewy-Type Histopathology in Human Brains, Experimental Neurology 240 (2013) 190-204.
[346] L. Chen, M.B. Feany, A-Synuclein Phosphorylation Controls Neurotoxicity and Inclusion Formation in a Drosophila Model of Parkinson Disease, Nature Neuroscience 8 (2005) 657-663.
[347] M. Yamada, T. Iwatsubo, Y. Mizuno, H. Mochizuki, Overexpression of A-Synuclein in Rat Substantia Nigra Results in Loss of Dopaminergic Neurons, Phosphorylation of A-Synuclein and Activation of Caspase-9: Resemblance to Pathogenetic Changes in Parkinson's Disease, Journal of Neurochemistry 91 (2004) 451-461.
[348] L.A. Volpicelli-Daley, K.C. Luk, T.P. Patel, S.A. Tanik, D.M. Riddle, A. Stieber, D.F. Meaney, J.Q. Trojanowski, V.M.-Y. Lee, Exogenous A-Synuclein Fibrils Induce Lewy Body Pathology Leading to Synaptic Dysfunction and Neuron Death, Neuron 72 (2011) 57-71.
[349] L.A. Volpicelli-Daley, K.C. Luk, V.M. Lee, Addition of Exogenous A-Synuclein Preformed Fibrils to Primary Neuronal Cultures to Seed Recruitment of Endogenous A-Synuclein to Lewy Body and Lewy Neurite–Like Aggregates, Nature Protocols 9 (2014) 2135-2146.
[350] P. Vitale, F. Librizzi, A.C. Vaiana, E. Capuana, M. Pezzoli, Y. Shi, A. Romani, M. Migliore, R. Migliore, Different Responses of Mice and Rats Hippocampus Ca1 Pyramidal Neurons to in Vitro and in Vivo-Like Inputs, Frontiers in Cellular Neuroscience 17 (2023) 1281932.
[351] B.N. Routh, D. Johnston, K. Harris, R.A. Chitwood, Anatomical and Electrophysiological Comparison of Ca1 Pyramidal Neurons of the Rat and Mouse, Journal of Neurophysiology 102 (2009) 2288-2302.
[352] A. Sidhu, I. Segers-Nolten, V. Subramaniam, Conformational Compatibility Is Essential for Heterologous Aggregation of A-Synuclein, ACS Chemical Neuroscience 7 (2016) 719-727.
[353] J.W. Howe, C.E. Sortwell, M.F. Duffy, C.J. Kemp, C.P. Russell, M. Kubik, P. Patel, K.C. Luk, O.M. El-Agnaf, J.R. Patterson, Preformed Fibrils Generated from Mouse Alpha-Synuclein Produce More Inclusion Pathology in Rats Than Fibrils Generated from Rat Alpha-Synuclein, Parkinsonism & Related Disorders 89 (2021) 41-47.
[354] C. Lavedan, The Synuclein Family, Genome Research 8 (1998) 871-880.
[355] N. Landeck, K.E. Strathearn, D. Ysselstein, K. Buck, S. Dutta, S. Banerjee, Z. Lv, J.D. Hulleman, J. Hindupur, L.-K. Lin, Two C-Terminal Sequence Variations Determine Differential Neurotoxicity between Human and Mouse A-Synuclein, Molecular Neurodegeneration 15 (2020) 49.
[356] L. Ma, C. Yang, X. Zhang, Y. Li, S. Wang, L. Zheng, K. Huang, C-Terminal Truncation Exacerbates the Aggregation and Cytotoxicity of A-Synuclein: A Vicious Cycle in Parkinson's Disease, Biochimica et Biophysica Acta (BBA)-Molecular Basis of Disease 1864 (2018) 3714-3725.
[357] P.J. Kahle, M. Neumann, L. Ozmen, V. Müller, H. Jacobsen, A. Schindzielorz, M. Okochi, U. Leimer, H. van der Putten, A. Probst, Subcellular Localization of Wild-Type and

Parkinson's Disease-Associated Mutant A-Synuclein in Human and Transgenic Mouse Brain, Journal of Neuroscience 20 (2000) 6365-6373.
[358] B. Boland, A. Kumar, S. Lee, F.M. Platt, J. Wegiel, W.H. Yu, R.A. Nixon, Autophagy Induction and Autophagosome Clearance in Neurons: Relationship to Autophagic Pathology in Alzheimer's Disease, Journal of Neuroscience 28 (2008) 6926-6937.
[359] T. Kobayashi, M.-H. Beuchat, M. Lindsay, S. Frias, R.D. Palmiter, H. Sakuraba, R.G. Parton, J. Gruenberg, Late Endosomal Membranes Rich in Lysobisphosphatidic Acid Regulate Cholesterol Transport, Nature Cell Biology 1 (1999) 113-118.
[360] A.-L. Mahul-Mellier, M.F. Altay, N. Maharjan, N. Ait-Bouziad, A. Chiki, S. Jagannath, G. Limorenko, S. Novello, J. Ricci, Y. Jasiqi, Differential Role of C-Terminal Truncations on Alpha-Synuclein Pathology and Lewy Body Formation, npj Parkinson's Disease 11 (2025) 261.
[361] A.N. Sacino, M.A. Thomas, C. Ceballos-Diaz, P.E. Cruz, A.M. Rosario, J. Lewis, B.I. Giasson, T.E. Golde, Conformational Templating of A-Synuclein Aggregates in Neuronal-Glial Cultures, Molecular Neurodegeneration 8 (2013) 17.
[362] E.A. Ostrakhovitch, E.-S. Song, J.E. Stegemann, M. McLeod, T.R. Yamasaki, Effect of Hydrogen Sulfide on Alpha-Synuclein Aggregation and Cell Viability, Scientific Reports 15 (2025) 15597.
[363] A.D. Stephens, M. Zacharopoulou, G.S.K. Schierle, The Cellular Environment Affects Monomeric A-Synuclein Structure, Trends in Biochemical Sciences 44 (2019) 453-466.
[364] R.W. So, J.C. Watts, A-Synuclein Conformational Strains as Drivers of Phenotypic Heterogeneity in Neurodegenerative Diseases, Journal of Molecular Biology 435 (2023) 168011.
[365] L.D. Aubrey, B.J. Blakeman, L. Lutter, C.J. Serpell, M.F. Tuite, L.C. Serpell, W.-F. Xue, Quantification of Amyloid Fibril Polymorphism by Nano-Morphometry Reveals the Individuality of Filament Assembly, Communications Chemistry 3 (2020) 125.
[366] A. Dilsizoglu Senol, M. Samarani, S. Syan, C.M. Guardia, T. Nonaka, N. Liv, P. Latour-Lambert, M. Hasegawa, J. Klumperman, J.S. Bonifacino, A-Synuclein Fibrils Subvert Lysosome Structure and Function for the Propagation of Protein Misfolding between Cells through Tunneling Nanotubes, PLoS Biology 19 (2021) e3001287.